THE UNIVERSITY OF MANITOBA

STATICAL BEHAVIOUR OF CROPPED-WEB JOINTS
FOR TRUSSES
WITH ROUND TUBULAR MEMBERS.

by

J. B. CIWKO

A Thesis
PRESENTED TO THE FACULTY OF GRADUATE STUDIES
IN PARTIAL FULFILLMENT OF THE REQUIREMENTS FOR THE DEGREE OF
MASTER OF SCIENCE
DEPARTMENT OF CIVIL ENGINEERING

WINNIPEG, MANITOBA
CANADA

OCTOBER 1980

STATICAL BEHAVIOUR OF CROPPED-WEB JOINTS
FOR TRUSSES
WITH ROUND TUBULAR MEMBERS

BY

JOSEPH BARRY MICHAEL CIWKO

A thesis submitted to the Faculty of Graduate Studies of the University of Manitoba in partial fulfillment of the requirements of the degree of

MASTER OF SCIENCE

ABSTRACT

The static behaviour of 61 isolated cropped-web tubular truss joints is described. The effects of various parameters on joint strength, flexibility and ductility are investigated and reported. A statistical approach is used to generate empirical equations for the estimation of the joint strength and the joint flexibility. The ultimate strengths of statically loaded cropped-web joints are comparable to those of similar profiled-web joints. Cropped-web joints with round chords are less flexible than similar cropped-web joints involving square chords. Recommendations for design and further research are provided.

ACKNOWLEDGEMENT

The guidance and patience of Dr. G. A. Morris for the duration of this study are gratefully acknowledged.

The author would like to thank Mr. J. Clark, Mr. E. Lemke, Mr. M. McVey, Mr. W. Wiles, Mr. D. Wiebe, and Mr. L. Wilkins for their invaluable time and assistance in the testing phase of this study.

Financial assistance was provided by the University of Manitoba and the Steel Company of Canada, Limited. Material for all test specimens was provided by the Steel Company of Canada, Limited.

Finally, the author would like to thank his parents and friends for their help and encouragement.

TABLE OF CONTENTS

Page

LIST OF TABLES

LIST OF FIGURES

Figure | Page

Figure Page

LIST OF SYMBOLS

b_o	Outside width of rectangular chord.
d_o, d_1, d_2	Outside diameters of the chord, compression web and tension web, respectively.
d	Diameter of compression web or tension web when equal in size.
e	Joint eccentricity.
E	Modulus of elasticity (200,000 MPa or 30,000 ksi)
f_c	Compression joint flexibility.
f_t	Tension joint flexibility.
g	Joint gap.
h_o	Outside depth of rectangular chord.
J_r	Factored joint resistance.
J_u	Ultimate joint load.
K	Effective length factor.
kips	1 kip = 1000 lbs.
kN	Kilo-newton.
L_o, L_1, L_2	Lengths of the chord, compression web and tension web, respectively.
m	Meter
mm	Millimeter.
N	Newton.
N_o, N_1, N_2	Axial loads in the chord, compression web and tension web, respectively.
N_{1b}	Buckling strength of the compression web.
N_{oe}, N_{1e}, N_{2e}	Axial yield loads of the chord, compression web and tension web, respectively.

N_{ou}, N_{1u}, N_{2u}	Axial ultimate loads of the chord, compression web and tension web, respectively.
O_v	Web overlap.
p	Length of the cropped edge of the tension web.
Pa	Pascal.
q	Overlap length of the compression web.
r	Radius of gyration of the compression web.
R_m	Mean resistance from tests.
R_n	Nominal resistance as expressed by the design criteria.
t_o, t_1, t_2	Wall thicknesses of the chord, compression web and tension web, respectively.
t	Wall thickness of the compression web or tension web when equal in size.
V_F	Coefficient of variation of the test/predicted results, the fabrication, or the manufacturing.
V_m	Coefficient of variation of the material yield strength.
V_P	Coefficient of variation of the professional assumptions.
α	Statistical significance level.
β	Safety index.
γ	Numerical factor equal to 0.55.
δ_1, δ_2	Chord deformation along the axes of the compression and tension webs, respectively.
Δ_j	Mid-span truss deflection due to joint deformation.
Δ_m	Mid-span truss deflection due to member deformation.
λ	Statistical confidence level.
ν_1	Number of independent variables used in a given run of the regression program.

ν_1	Degrees of freedom in a given run of the regression program.
σ_{oe}, σ_{1e}, σ_{2e}	Yield stresses of the chord, compression web and tension web, respectively.
σ_{ou}, σ_{1u}, σ_{2u}	Ultimate stresses of the chord, compression web and tension web, respectively.
ϕ	Capacity reduction factor.

CHAPTER I

INTRODUCTION

1.1) General

During the past 20 years, interest has increased in the use of hollow structural sections (HSS) in truss construction.

Hollow structural sections possess several strong advantages compared to conventional sections. They have high resistance to buckling and twisting. This generally results in weight savings in the order of 20 per cent. They expose less surface area than do conventional sections of similar weight and size. Thus they reduce the maintenance or protective covering required. The strength of a HSS member can be increased without changing its external dimensions, by filling it with grout or by selecting a section with a greater wall thickness. HSS members offer relatively small resistance to wind or wave action and, as well, they produce asthetically pleasing structures.

Although HSS are excellent in many respects, their primary drawback in trusses relates to the joints or connections. Figure 1.1 illustrates several forms of tubular truss joints. Complex profiling and difficulties in welding or bolting may be encountered at the joint, particularly when circular hollow sections (CHS) are involved. Improved welding techniques along with the advent of automatic profiling machines have reduced these problems to some extent, but still the fabrication costs of such joints remain high.

The use of gusset plates as an alternative to profiling has been

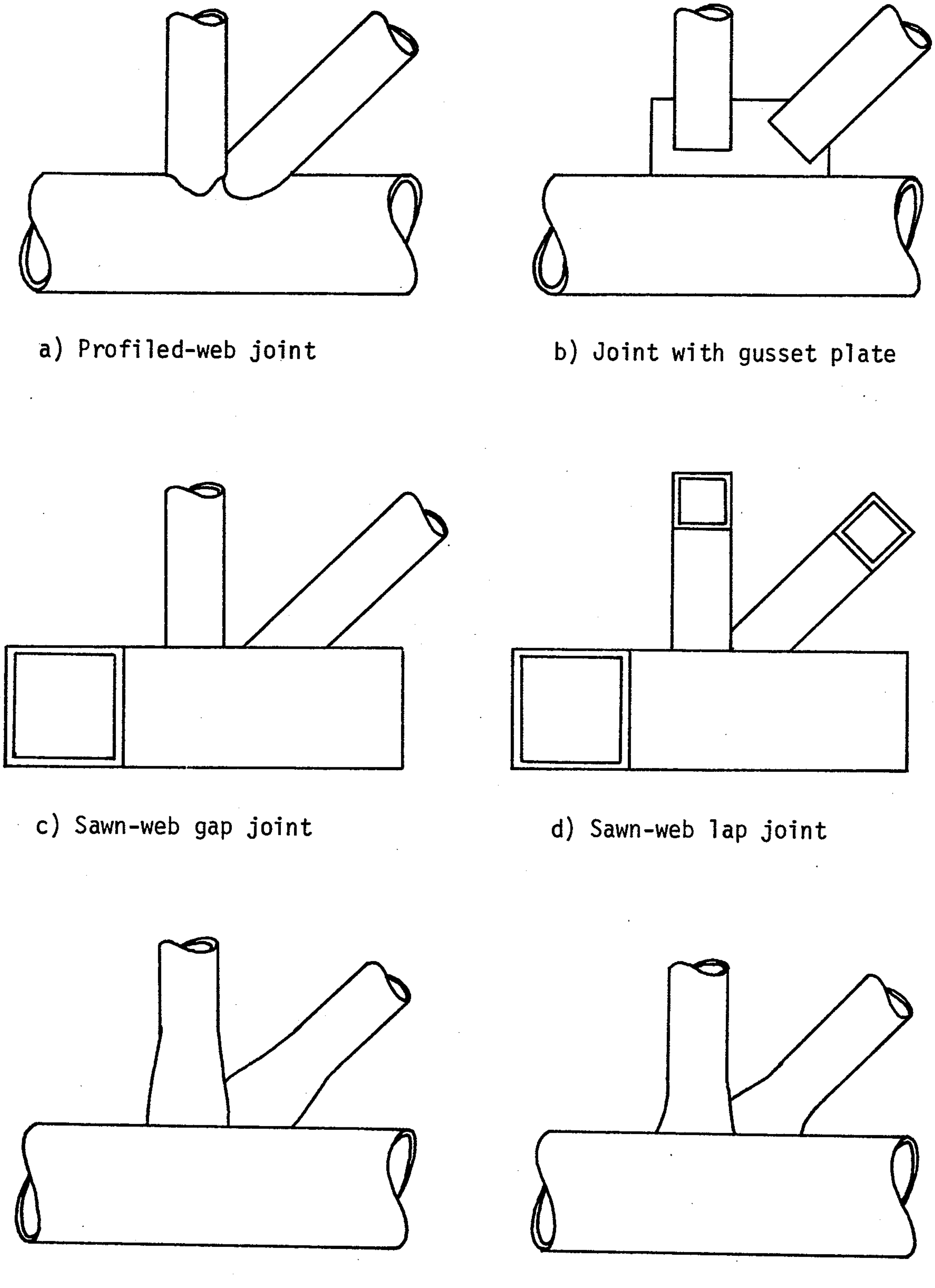

a) Profiled-web joint

b) Joint with gusset plate

c) Sawn-web gap joint

d) Sawn-web lap joint

e) Flattened-web joint

f) Cropped-web joint

Fig. 1.1 - Tubular truss joints.

investigated by several researchers. However, gusset plates have been found to be somewhat less effective than direct connections between members.

An economical alternative to member profiling is the process of end-flattening. It results in simplified welds and does not require additional material. Generally, this technique requires two steps for member preparation; namely, cutting and end-flattening. However, a more efficient form of end-flattening is end-cropping, a process of simultaneously cutting and flattening the member in one operation. Flattened member ends are particularly economical for joints between round tubular webs and round tubular chords, where profiling is otherwise unavoidable.

Because the behaviour of trusses with end-cropped webs has not been researched extensively, the use of such joints has been very limited. However, the available research indicates this type of member end preparation to be a safe, economical alternative to profiling, providing the loading is static.

1.2) Tubular Truss Joint Research

To date, research on tubular truss joints has covered several common truss geometries involving various web-chord combinations of circular, square, and rectangular hollow structural sections. Both isolated joint specimens and full scale trusses have been investigated and reasonably consistent results have been obtained. Furthermore, various techniques of web member end preparation have been investigated. Although the bulk of the research has been experimentally based, several attempts at theoretical investigations have been partially successful in duplicating the experimental results.

1.2.1) Joint Performance

To evaluate the behaviour of a joint, a measure of performance must be established. The most frequently used measure of joint performance is the ultimate strength, although joint stiffness and ductility have also been used. The latter, however, have generally eluded a common definition and they are more difficult to quantify.

For ease of comparison, researchers usually have expressed the ultimate strengths of tubular truss joints in non-dimensional form. The most common forms are joint efficiency and joint load factor. Joint efficiency has been defined as: the ratio of the failure load for the joint to (a) the ultimate strength of the tension web (Bouwkamp 1968), or (b) the yield strength of the first member to yield (Jamm et al. 1952, and Eastwood et al. 1970). Joint load factor has been defined as the ratio of the failure load for the joint to the design load of the compression or tension web (Eastwood et al. 1970).

Other parameters which have been used to express joint strength include the following:

a) $J_u/t_o\sigma_{oe}$, (Eastwood et al 1970), although it is not dimensionless.

b) $J_u/t_o^2\sigma_{oe}$, (Kurobane et al 1969, Togo 1969)

c) $J_u/t_o^{0.5}b_o^{1.5}\sigma_{oe}$, (Wardenier 1977)

d) $J_u/t_ob_o\sigma_{oe}$, (Thiensiripipat 1979).

In these expressions, J_u is the ultimate load perpendicular to the chord, t_o is the chord thickness, $d_o(b_o)$ is the chord diameter (width), and σ_{oe} is the chord yield strength. These forms have been more successful than joint efficiency or joint load factor in relating strength to the joint geometry and material characteristics.

The stiffness of a tubular truss joint has been defined as the slope of the approximately straight-line portion of the load-deformation diagram. Because the joint behaves non-linearly in many cases, the joint stiffness tends to be sensitive to the load level at which it is calculated. This tends to make it an unsatisfactory measure of performance. The joint stiffness has been used to estimate the approximate additional truss deflection due to joint deformation (Thiensiripipat 1979).

Joint ductility is a measure of the load-carrying capacity of a joint after initial yielding has occurred. It has been found that the favourable stress redistribution characteristics of tubular truss joints make them quite ductile (Anderson 1961 and Eastwood et al. 1970).

1.2.2) Parameters Affecting Performance

The three most significant of the several parameters which have been found to influence the performance of a tubular truss joint are the chord thickness to diameter (width) ratio, t_o/d_o or t_o/b_o, the web diameter (width) to chord diameter (width), d/d_o or d/b_o, and the web lap, $O_v=q/d_2$, or gap, $O_g=g/d_2$. The aforementioned parameters are illustrated in Figure 1.2.

Research has shown that joint strength and stiffness increase with an increase in the chord thickness to diameter (width) ratio, particularly for gap joints. This is because of the increased bending and

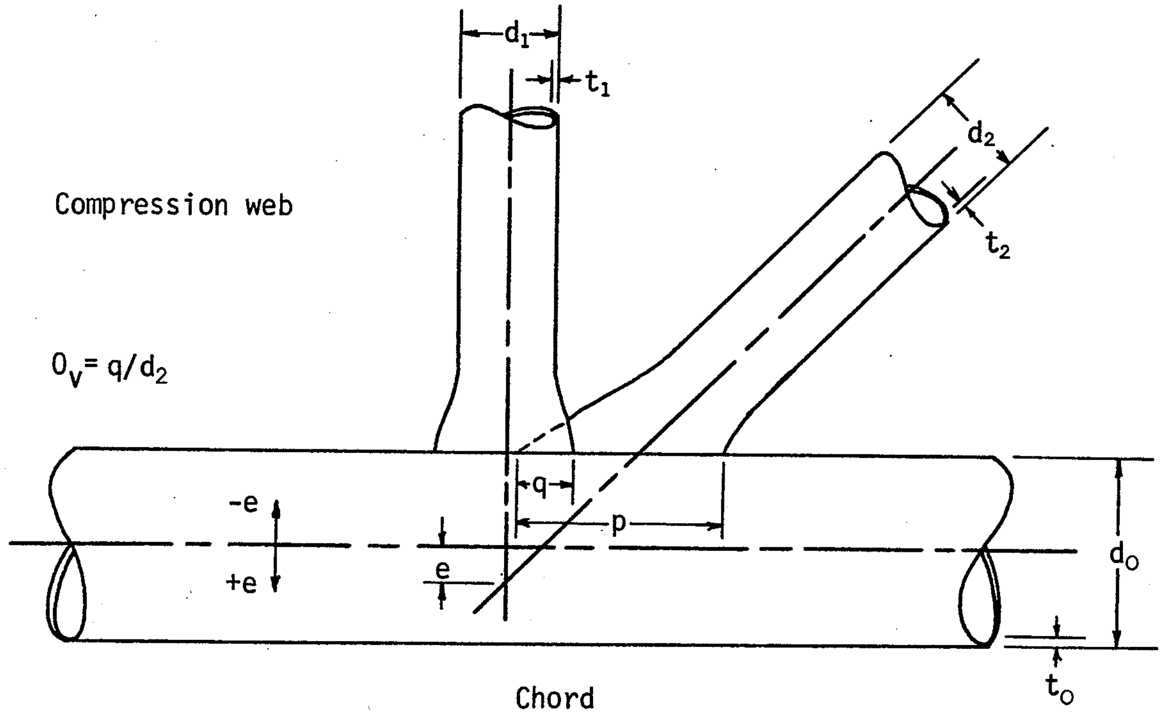

a) Overlap joint with circular chord.

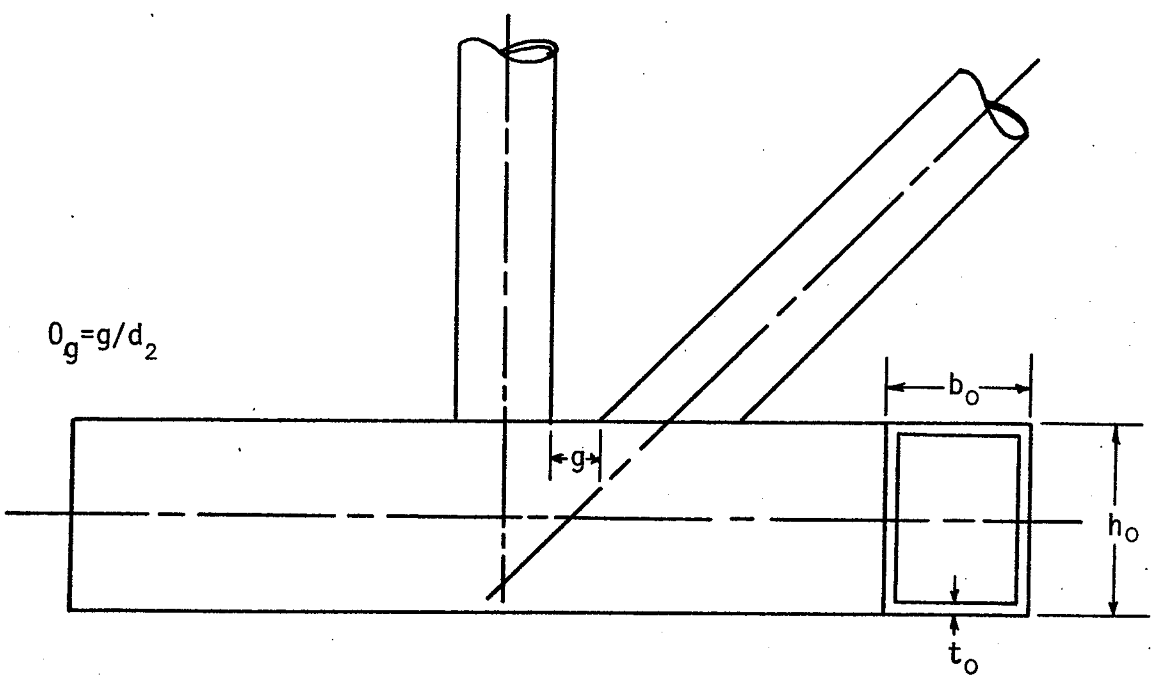

b) Gap joint with rectangular chord.

Fig. 1.2 - Joint properties.

load transfer capacity of the chord wall. There is also a decrease in joint ductility, since failure tends to occur in the members before yielding of the chord is achieved. The resulting load-deformation curves indicate a brittle type of failure.

An increase in the web diameter (width) to chord diameter (width) ratio has been found to improve the load distribution on the chord face and to reduce the rotational deformation of the joint. This results in an increase in strength and stiffness and a reduction in ductility. The reason is that, when the web to chord diameter (width) is large, more load is transferred to the side walls of the chord and thus the plastic deformation of the joint is reduced.

A web lap has been found to be more advantageous than a web gap. The former permits a direct transfer of web forces through the web interconnection. This results in increased joint strength and stiffness. A decrease in web gap or an increase in web lap usually produces an increase in strength and stiffness and a decrease in joint ductility. Gap joints have been found to be more ductile than lap joints.

Several investigators have used joint eccentricity, defined as the perpendicular distance the intersection of the web axis lies from the chord axis (see Figure 1.2a), as a joint parameter. This, however, gives an indication of the moment in the chord at and due to the joint, rather than a measure of the web interconnection. The latter influences the joint strength, stiffness, and ductility more significantly than eccentricity. Eastwood et al. (1970) indicated that the chord moments due to joint eccentricity could be accounted for using conventional design techniques. In addition, Jamm et al. (1952) stated that joint eccentricity would not be a problem provided the web axes intersected within the middle half of the chord diameter.

1.2.3) Failure Modes

The failure of a tubular truss joint usually has been assumed to coincide with the point of maximum load carrying capacity. Eastwood et al. (1970), however, arbitrarily defined it as corresponding to a rate of deformation in the loading ram of 0.45 inches per minute without any increase in load. The two definitions produce comparable ultimate loads, since deflection usually becomes excessive immediately before the maximum load is reached.

Various failure modes have been reported; however, the general mechanism of failure is as follows. The chord face undergoes deformation as a result of the web loading. This in turn subjects the webs to end moments which usually induce compression web buckling or tension web tearing in the heat affected zone near the web member interconnection.

Other failure modes which have been observed include tension web fracture, shearing through the web interconnection, chord wall tearing, and buckling of the chord member.

1.3) Objectives and Limitations

The objective of this study was to measure experimentally the static load-deformation behaviour of Pratt-type truss joints involving round chords and round cropped webs.

This study was limited to an experimental investigation of 61 isolated Pratt type joints. No analytical study was attempted. The tension and compression webs for any given joint specimen were of the same size. The maximum sizes of the members in the specimens were limited by the capacity of the loading assembly (889 kN, 200 kips). The influence of three geometric parameters; the chord thickness to diameter ratio (t_o/d_o), the web diameter to chord diameter ratio (d_1/d_o) and the web lap (O_v), on the load-deformation behaviour of the joints was investigated. All other parameters were kept as nearly constant as possible.

There was no preload applied to the chord. Previous investigators (Bouwkamp 1968, Mee 1969, Eastwood et al 1969) have indicated that chord preload did not significantly affect the ultimate loads of the joints. However, recent tests of end-cropped joints which have been incorporated into trusses (Ghosh 1979) suggest that large axial stresses in the chord do influence joint behaviour.

CHAPTER 2

TEST PROGRAM

In this chapter, the selection of geometry and joint parameters for the test specimens are discussed. In addition, the fabrication techniques, the specimen measurements, the test apparatus and the test procedure are described.

2.1) Specimen Design

A Pratt-type joint, shown in Figure 2.1, was chosen for the specimen geometry. It is widely employed and, more important, it produces the most severe case of loading on the chord face. Thus, design criteria developed for the Pratt joint may be conservatively applied to other joint geometries. Furthermore, several investigators in the past have used Pratt-type joints, thus facilitating comparison of results.

The specimen web and chord members were chosen to provide five different values for each of the parameters, t_o/d_o and d_1/d_o. In addition, three values of web lap were chosen for various combinations of t_o/d_o and d_1/d_o.

The joints were designed as isolated specimens modelling a Pratt-type truss, 1.83 m (6 feet) in depth, with the tension diagonals oriented at 45 degrees (see Figure 2.1). It was assumed that a statically loaded truss would deform with inflection points at the mid-lengths of the members, as indicated in Figure 2.2, if out of plane buckling were prevented. Thus, a typical specimen, shown in Figure 2.3,

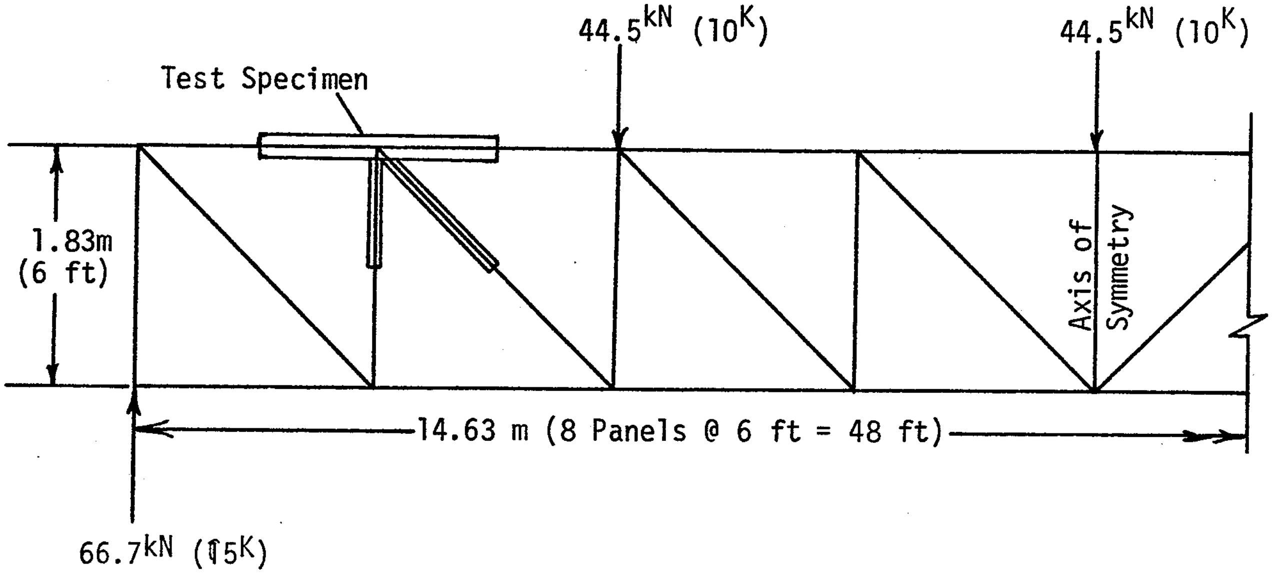

Fig. 2.1 - Pratt truss and test specimen.

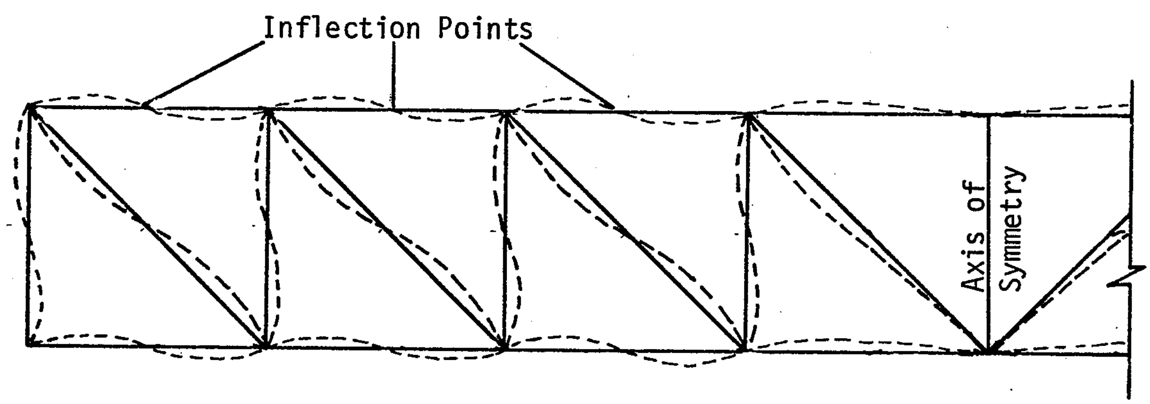

Fig. 2.2 - Assumed elastic deformation considering bending of members only.

As no prestress was applied to the chord, the specimen chord member was shortened, by the amount indicated with the broken line, to save on material.

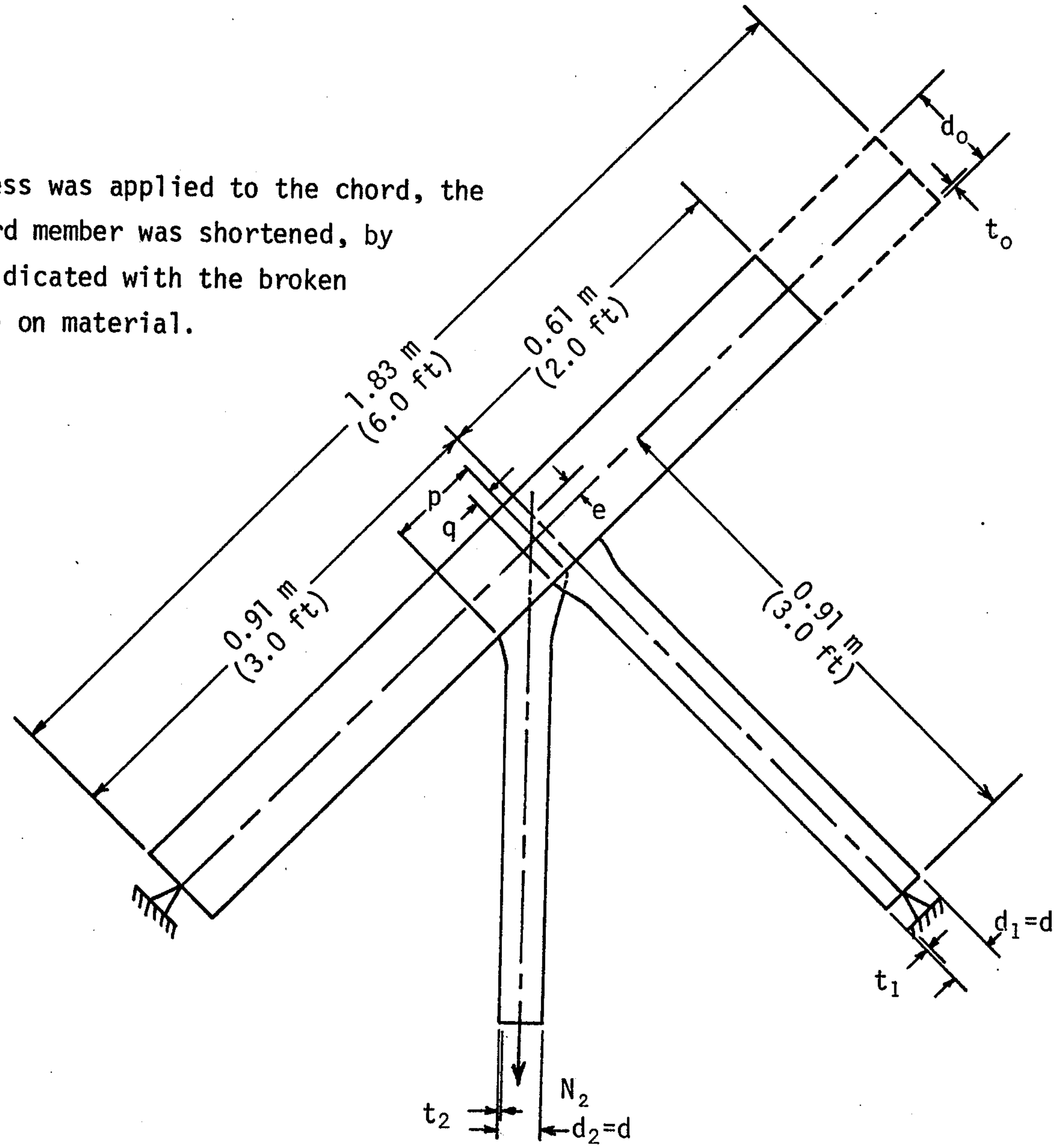

Fig. 2.3 - Typical test specimen.

had members extending from the joint in question halfway to the adjacent truss panel joints. The joint welds were designed in accordance with the member design loads in the prototype truss.

The specimen parameters (t_o/d_o, d_1/d_o, and O_v), the compression web slenderness ratio (L_1/r_1), the joint eccentricity to chord diameter ratio (e/d_o), and specified size of the web-chord fillet weld are indicated in table 2.1. Table 2.2 lists the specimen member sizes and material properties. Several specimens embody extreme values of t_o/d_o which would not be used in practice. However, these were included with the intention of assembling complete information concerning the influence of the t_o/d_o ratio on joint performance.

2.2) Specimen Designation

The specimen designation was derived from the three major parameters found to affect joint performance in tubular trusses. The designation is as follows. The first character is a digit, ranging from 1 to 6, referring to a specific t_o/d_o ratio. This is followed by an alphabetic character, D, E, F, G, or H, identifying an approximate d_1/d_o ratio. Finally, the last two characters are digits, either 00, 50, or 75, which represent the lap of the web members expressed as a percentage of the tension web diameter.

2.3) Fabrication

The cropping, cutting, fitting, and tack welding of all specimens were carried out in the Civil Engineering Laboratories at the University of Manitoba.

TABLE 2.1

SPECIMEN PROPERTIES

Specimen	t_o/d_o	d_1/d_o	L_1/r_1	0_v	e/d_o	Weld Size (in.)	(mm)
1D00	0.0174	0.355	90.0	0	0.149	1/4	6.35
1D50	0.0177	0.357	90.0	50	-0.032	1/4	6.35
1D75	0.0176	0.356	90.0	75	-0.122	1/4	6.35
2D00	0.0278	0.360	90.0	0	0.149	1/4	6.35
2D50	0.0277	0.359	90.0	50	-0.032	1/4	6.35
2D75	0.0279	0.359	90.0	75	-0.122	1/4	6.35
3D00	0.0403	0.359	90.0	0	0.149	1/4	6.35
3D50	0.0403	0.360	90.0	50	-0.032	1/4	6.35
3D75	0.0401	0.359	90.0	75	-0.122	1/4	6.35
4D00	0.0395	0.363	133	0	0.144	3/16	4.76
4D50	0.0419	0.363	133	50	-0.044	3/16	4.76
4D75	0.0391	0.363	133	75	-0.098	3/16	4.76
5D00	0.0496	0.364	133	0	0.144	3/16	4.76
5D50	0.0496	0.364	133	50	-0.044	3/16	4.76
5D75	0.0498	0.365	133	75	-0.098	3/16	4.76
6D00	0.0681	0.364	133	0	0.144	3/16	4.76
6D50	0.0690	0.365	133	50	-0.044	3/16	4.76
6D75	0.0698	0.366	133	75	-0.098	3/16	4.76
1E00	0.0176	0.430	75.0	0	0.270	5/16	7.94
1E50	0.0177	0.432	75.0	50	0.051	5/16	7.94
1E75	0.0178	0.432	75.0	75	-0.054	5/16	7.94
2E00	0.0279	0.434	75.0	0	0.270	5/16	7.94
2E50	0.0275	0.430	75.0	50	0.051	5/16	7.94
2E75	0.0276	0.434	75.0	75	-0.054	5/16	7.94
3E00	0.0404	0.434	75.0	0	0.270	5/16	7.94
3E50	0.0404	0.434	75.0	50	0.051	5/16	7.94
3E75	0.0402	0.435	75.0	75	-0.054	5/16	7.94
4E00	0.0397	0.424	113	0	0.256	3/16	4.76
4E50	0.0391	0.424	113	50	0.044	3/16	4.76
4E75	0.0392	0.423	113	75	-0.067	3/16	4.76
5E00	0.0501	0.426	113	0	0.256	3/16	4.76
5E50	0.0501	0.426	113	50	0.044	3/16	4.76
5E75	0.0504	0.425	113	75	-0.067	3/16	4.76
6E00	0.0692	0.425	113	0	0.256	3/16	4.76
6E50	0.0703	0.426	113	50	0.044	3/16	4.76
6E75	0.0701	0.424	113	75	-0.067	3/16	4.76

TABLE 2.1 (continued)

Specimen	t_o/d_o	d_1/d_o	L_1/r_1	O_v	e/d_o	Weld Size (in.)	(mm)
2F50	0.0279	0.530	60.5	50	0.209	5/16	7.94
2F75	0.0279	0.529	60.5	75	0.078	5/16	7.94
3F50	0.0399	0.529	60.5	50	0.209	5/16	7.94
3F75	0.0401	0.529	60.5	75	0.078	5/16	7.94
4F00	0.0391	0.525	90.0	0	0.456	1/4	6.35
4F50	0.0411	0.526	90.0	50	0.191	1/4	6.35
4F75	0.0417	0.529	90.0	75	0.060	1/4	6.35
5F50	0.0530	0.529	90.0	50	0.191	1/4	6.35
5F75	0.0526	0.528	90.0	75	0.060	1/4	6.35
6F50	0.0670	0.527	90.0	50	0.191	1/4	6.35
6F75	0.0667	0.528	90.0	75	0.060	1/4	6.35
4G00	0.0391	0.636	75.0	0	0.633	5/16	7.94
4G50	0.0389	0.637	75.0	50	0.313	5/16	7.94
4G75	0.0390	0.635	75.0	75	0.153	5/16	7.94
5G50	0.0531	0.637	75.0	50	0.313	5/16	7.94
5G75	0.0528	0.640	75.0	75	0.153	5/16	7.94
6G50	0.0690	0.639	75.0	50	0.313	5/16	7.94
6G75	0.0692	0.639	75.0	75	0.153	5/16	7.94
4H00	0.0410	0.781	60.5	0	0.933	5/16	7.94
4H50	0.0409	0.781	60.5	50	0.544	5/16	7.94
4H75	0.0416	0.780	60.5	75	0.351	5/16	7.94
5H50	0.0501	0.781	60.5	50	0.544	5/16	7.94
5H75	0.0495	0.781	60.5	75	0.351	5/16	7.94
6H50	0.0670	0.780	60.5	50	0.544	5/16	7.94
6H75	0.0665	0.781	60.5	75	0.351	5/16	7.94

Definition of symbols.

t_o = chord thickness.

d_o = chord diameter.

d_1 = compression web diameter.

L_1 = compression web length in prototype truss.

r_1 = radius of gyration of compression web.

O_v = web lap.

e = joint eccentricity.

TABLE 2.2

MEMBER SIZES AND PROPERTIES

Specimen	Chord				Compression Web			Tension Web				
	t_o (mm)	d_o (mm)	σ_{oe} (N/mm^2)	σ_{oe} (N/mm^2)	t_1 (mm)	d_1 (mm)	t_1/d_1	t_2 (mm)	d_2 (mm)	t_2/d_2	$\sigma_{1,2e}$ (N/mm^2)	$\sigma_{1,2u}$ (N/mm^2)
1D00	2.97	171	325	440	3.25	60.5	0.054	3.23	60.5	0.053	357	559
1D50	3.00	169	323	446	3.25	60.5	0.054	3.23	60.5	0.053	357	559
1D75	3.00	171	325	441	3.02	60.7	0.050	3.23	60.5	0.053	357	559
2D00	4.67	168	294	426	3.25	60.5	0.054	3.18	60.5	0.053	357	559
2D50	4.67	169	290	421	3.00	60.7	0.049	3.25	60.7	0.054	357	559
2D75	4.70	169	312	424	3.20	60.5	0.053	3.15	60.7	0.052	357	559
3D00	6.81	169	356	451	3.12	60.7	0.051	3.20	60.5	0.053	357	559
3D50	6.78	168	307	441	3.12	60.7	0.051	3.12	60.7	0.051	357	559
3D75	6.77	169	344	439	3.12	60.7	0.051	3.12	60.7	0.051	357	559
4D00	4.55	115	359	525	2.97	41.7	0.071	3.00	41.7	0.072	370	537
4D50	4.83	115	370	533	3.00	41.7	0.072	3.00	41.7	0.072	370	537
4D75	4.50	115	364	523	3.00	41.7	0.072	2.97	41.7	0.071	370	537
5D00	5.69	115	345	501	3.02	41.7	0.072	3.00	41.7	0.072	370	537
5D50	5.69	115	345	501	3.00	41.7	0.072	3.02	41.9	0.072	370	537
5D75	5.72	115	362	511	3.02	41.9	0.072	2.97	41.7	0.071	370	537
6D00	7.82	115	392	558	2.97	41.9	0.071	2.97	41.7	0.071	370	537
6D50	7.90	115	388	558	2.97	41.9	0.971	3.02	41.9	0.072	370	537
6D75	7.98	114	370	547	3.05	41.9	0.073	3.00	41.9	0.072	370	537
1E00	3.00	170	332	433	4.55	73.2	0.062	4.42	73.2	0.060	370	541
1E50	3.00	169	308	436	4.60	73.2	0.062	4.47	73.4	0.061	370	541
1E75	3.02	169	330	443	4.60	73.2	0.063	4.47	73.4	0.061	370	541
2E00	4.70	169	299	426	4.62	73.2	0.063	4.42	73.2	0.060	370	541
2E50	4.67	170	303	413	4.57	73.2	0.062	4.52	73.2	0.062	370	541
2E75	4.65	169	312	429	4.52	73.2	0.062	4.37	73.2	0.060	370	541
3E00	6.81	169	305	421	4.37	73.4	0.060	4.42	72.9	0.061	370	541
3E50	6.81	169	338	442	4.52	73.2	0.062	4.34	73.2	0.060	370	541
3E75	6.78	169	345	449	4.67	73.4	0.064	4.42	72.9	0.061	370	541
4E00	4.57	115	368	507	3.05	48.8	0.063	2.97	48.8	0.061	351	525
4E50	4.50	115	368	545	3.02	48.8	0.062	3.02	48.8	0.062	351	525
4E75	4.52	115	358	523	3.00	48.8	0.061	3.02	48.8	0.062	351	525
5E00	5.74	115	367	513	3.12	48.8	0.064	3.12	48.8	0.064	351	525
5E50	5.74	115	346	493	3.15	48.8	0.065	3.12	48.8	0.064	351	525
5E75	5.79	115	345	504	3.12	48.8	0.064	3.10	48.8	0.064	351	525

TABLE 2.2 (continued)

Specimen	Chord				Compression Web			Tension Web				
	t_o (mm)	d_o (mm)	σ_{oe} (N/mm^2)	σ_{ou} (N/mm^2)	t_1 (mm)	d_1 (mm)	t_1/d_1	t_2 (mm)	d_2 (mm)	t_2/d_2	$\sigma_{1,2e}$ (N/mm^2)	$\sigma_{1,2u}$ (N/mm^2)
6E00	7.92	115	409	578	3.10	48.8	0.064	3.05	48.8	0.063	351	525
6E50	8.05	115	380	548	3.18	48.8	0.065	3.10	48.8	0.064	351	525
6E75	8.05	115	385	554	2.97	48.8	0.061	3.02	48.8	0.062	351	525
2F50	4.70	168	300	420	3.84	89.3	0.043	3.81	89.4	0.043	404	537
2F75	4.70	169	300	420	3.84	89.2	0.043	3.81	89.4	0.043	406	536
3F50	6.73	169	345	443	3.84	89.2	0.043	3.76	89.4	0.042	404	537
3F75	6.76	169	345	443	3.81	89.3	0.043	3.79	89.4	0.042	400	531
4F00	4.50	115	371	541	3.18	60.5	0.053	3.18	60.7	0.052	354	518
4F50	4.72	115	353	539	3.43	60.5	0.057	3.15	60.5	0.052	359	528
4F75	4.78	115	353	539	3.45	60.6	0.057	3.18	60.7	0.052	358	529
5F50	6.07	115	369	544	3.40	60.6	0.056	3.18	60.5	0.053	358	529
5F75	6.02	115	369	544	3.43	60.5	0.057	3.18	60.5	0.053	358	529
6F50	7.67	115	389	563	3.43	60.3	0.057	3.18	60.5	0.053	360	531
6F75	7.65	115	389	563	3.38	60.5	0.056	3.18	60.5	0.053	358	529
4G00	4.50	115	371	541	4.32	73.1	0.059	4.37	73.4	0.060	397	535
4G50	4.47	115	371	541	4.27	73.3	0.058	4.50	73.4	0.061	406	538
4G75	4.50	115	371	541	4.32	73.2	0.059	4.39	73.4	0.060	406	538
5G50	6.10	115	369	544	4.47	73.1	0.061	4.42	73.2	0.060	387	530
5G75	6.05	115	369	544	4.47	73.3	0.061	4.39	73.4	0.060	396	534
6G50	7.90	115	383	555	4.52	73.2	0.067	4.27	73.2	0.058	396	534
6G75	7.93	115	376	548	4.52	73.2	0.062	4.27	73.2	0.058	396	534
4H00	4.70	115	353	539	3.91	89.5	0.044	3.79	89.7	0.042	385	523
4H50	4.70	115	353	539	3.94	89.6	0.044	3.84	89.7	0.043	390	529
4H75	4.78	115	353	539	3.94	89.6	0.044	3.79	89.4	0.042	392	528
5H50	5.74	115	369	511	3.94	89.5	0.044	3.81	89.2	0.043	390	529
5H75	5.66	115	369	511	3.94	89.5	0.044	3.84	89.7	0.043	392	528
6H50	7.70	115	389	563	3.91	89.5	0.044	3.79	89.4	0.042	390	529
6H75	7.62	115	385	546	3.91	89.5	0.044	3.81	89.4	0.043	392	520

Definition of symbols.

t_o = chord thickness.

d_o = chord diameter.

σ_{oe} = chord yield strength.

σ_{ou} = chord ultimate strength.

t_1 = compression web thickness.

d_1 = compression web diameter.

t_2 = tension web thickness.

d_2 = tension web diameter.

$\sigma_{1,2e}$ = web yield strength.

$\sigma_{1,2u}$ = web ultimate strength.

The web member cropping was accomplished using a "cropping" machine, illustrated in Figure 2.4, consisting of two V-shaped steel blades which simultaneously flattened and sheared the webs. Care was taken to position the seam of the web member at approximately 45 degrees to the direction of cropping in order to minimize the incidence of splitting along the seam. As a consequence, no seam splitting was observed throughout the cropping process.

The three members forming a specimen were carefully assembled in a jig, assuring that the chord seam was not on the face to which the webs were to be welded. The assembly was then tack welded as shown in Figures 2.6(a) and 2.6(b). Final welding was done by a certified welder.

In order to minimize specimen distortion during the final welding the welding sequence indicated in Figure 2.4 was employed.

2.4) Materials

The sections used for the web members and the 114 mm (4.5 in.) diameter chord members were hot formed and conformed to CSA Specification G40.21 Class H Grade 50W. The 168 mm (6.625 in.) diameter chord sections were cold formed, stress relieved, conforming to CSA Specification G40.21 Class H Grade 42W.

The chord and web yield strengths, σ_e, and ultimate strengths, σ_u were determined from tension tests. The measured values are presented in table 2.2.

2.5) Measurement of Strain and Deformation

Specimen measurements were accomplished using electric

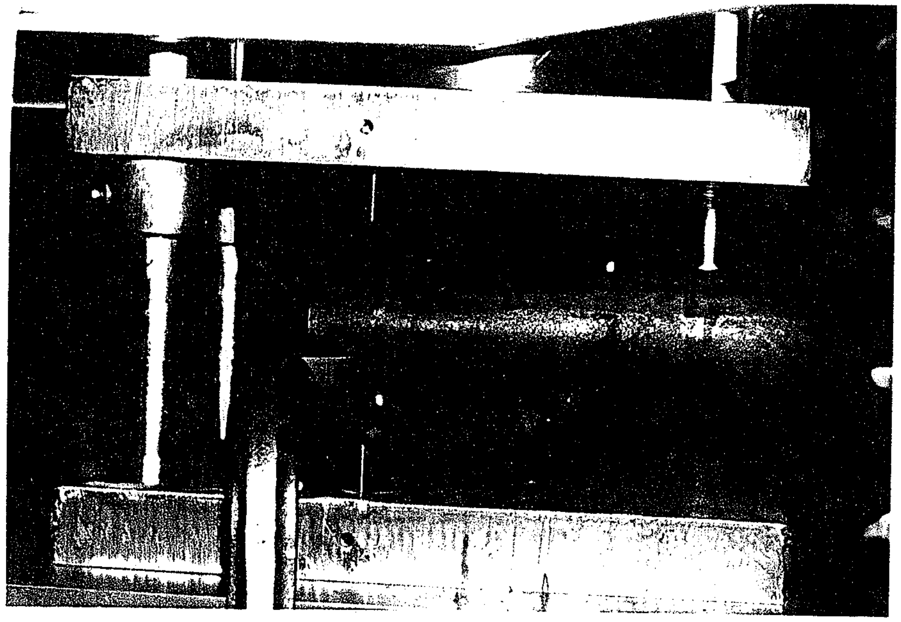

Fig. 2.4 - Cropping device.

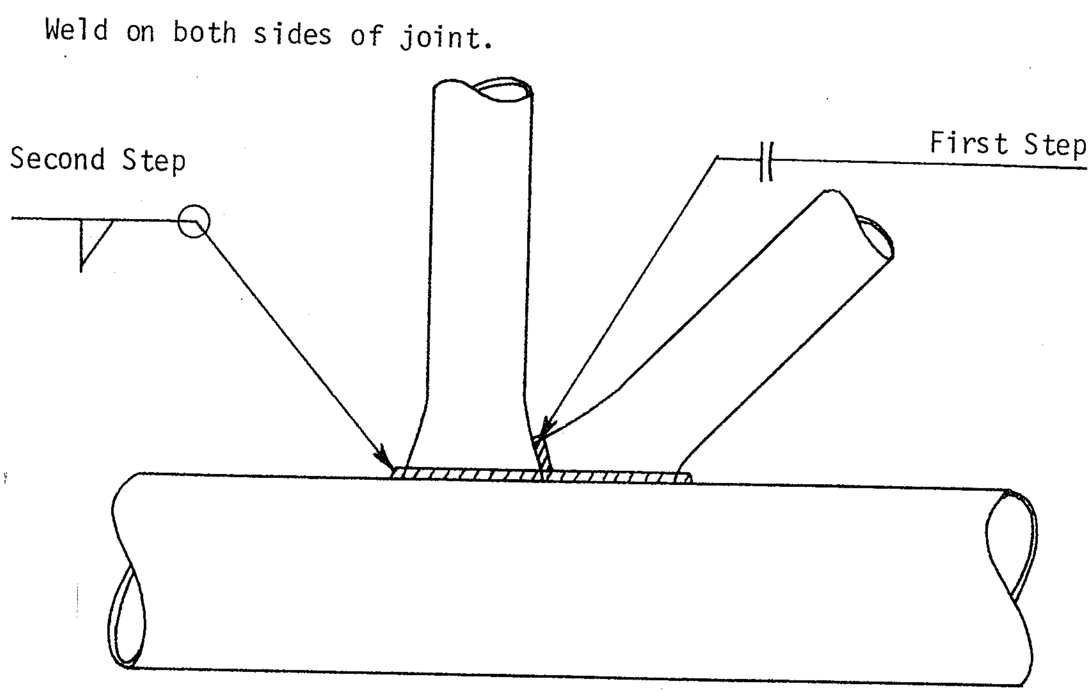

Fig. 2.5 - Welding sequence.

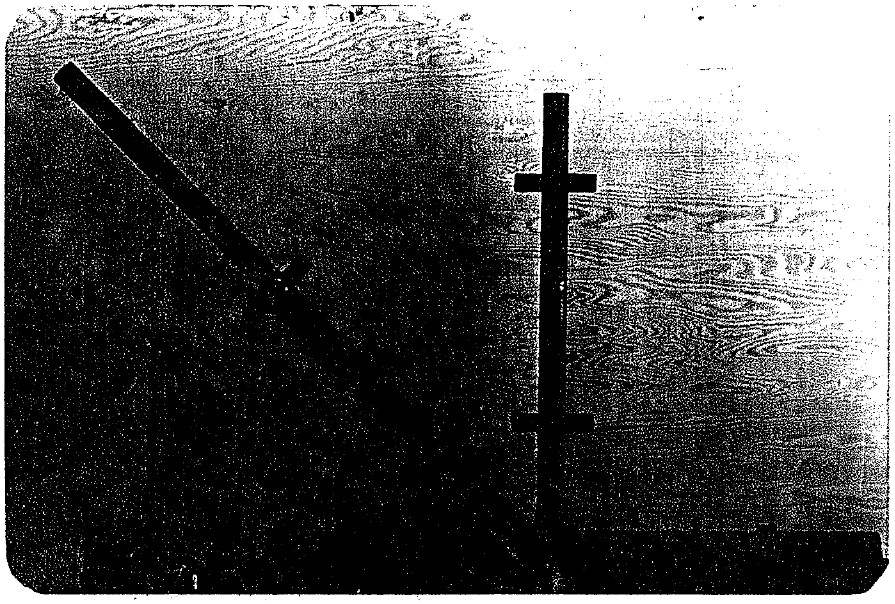

Fig. 2.6(a) - Jig used in specimen fabrication.

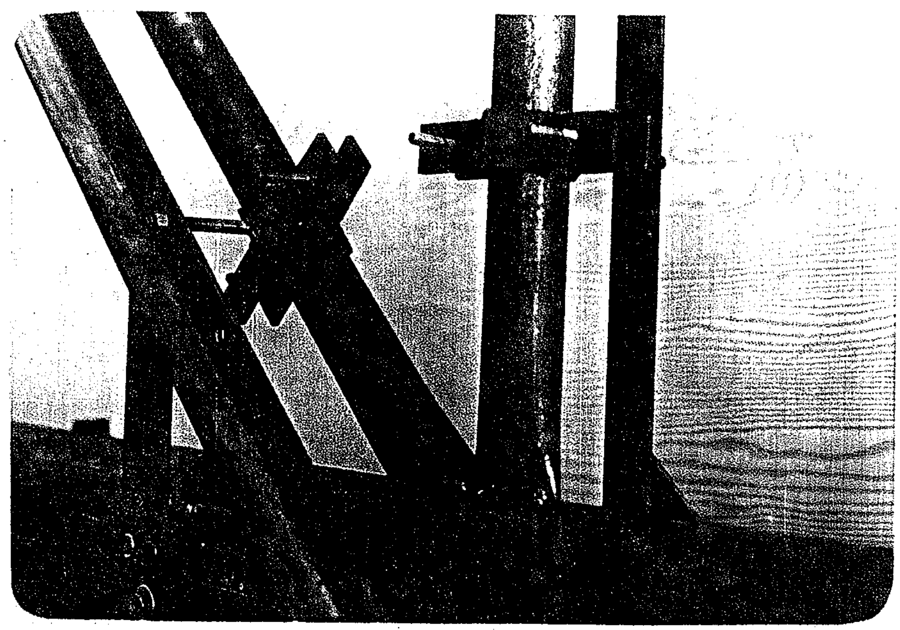

Fig. 2.6(b) - Tack welded specimen.

resistance strain gauges and linear voltage displacement transducers (LVDT).

It was decided that a minimum of eight gauges per specimen would be used, but it was also felt that additional strain information for sixteen of the specimens was required for a more complete comparison of the effects of the geometric parameters on joint performance. Thus, fifteen gauges were used on each of these specimens. In addition, a total of 22 gauges were used on specimen 4G50.

All strain gauges were type EA-06-250B6-120 manufactured by Micro-Measurements. The grid length was 6.35 mm (0.25 in.) with a strain limit of 5 per cent.

The strain gauge locations are indicated in Figure 2.7(a) and 2.7(b). Gauges 1 to 4, which measured longitudinal compression web strains, were used to check the member load and to indicate compression web bending. Inplane longitudinal compression web strains were measured near the joint (an area of high stress concentrations) by gauges 5 and 6. Gauges 7 and 8 measured circumferential chord strains at the base of the joint, in the crotches between the webs and the chord. For cropped-web joints these were found to be areas of maximum stress.

The specimens with fifteen gauges had, in addition, gauge 9 located in a plane perpendicular to, and at the same cross-section as, gauges 5 and 6. It was used to measure the longitudinal compression web strain near the joint. Gauges 10, 11 and 12 were similarly located on the tension web, to obtain information concerning the longitudinal tension web strain distribution in this area. Gauges 13, 14 and 15 were located on the chord face as close to the base of the weld as

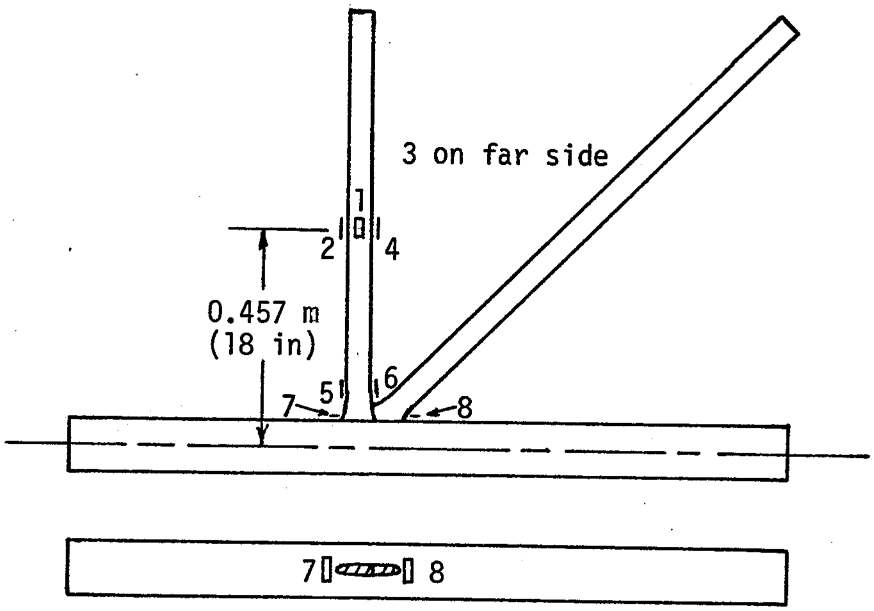

Specimen with eight gauges.

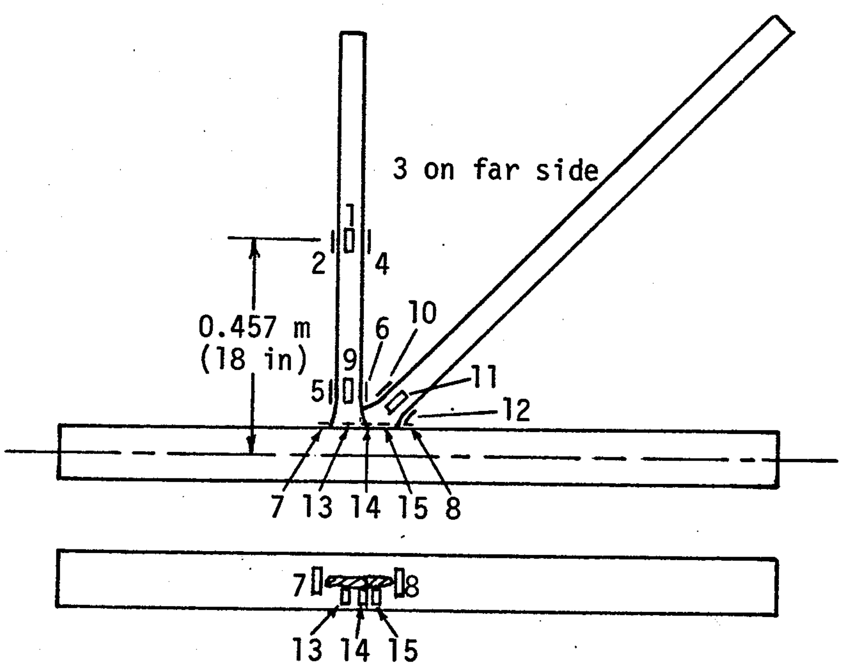

Specimen with fifteen gauges.

Fig. 2.7(a) - Strain gauge locations.

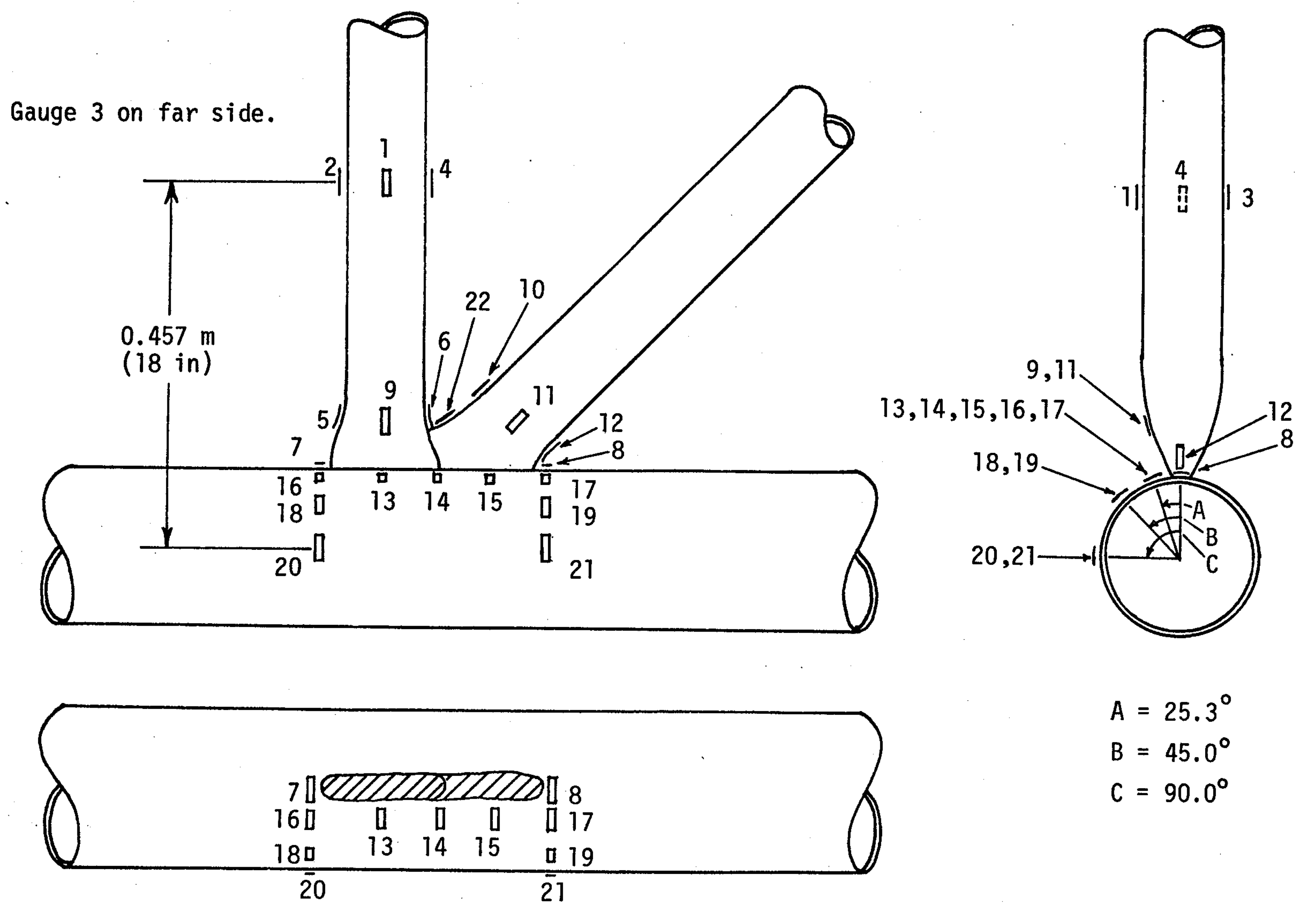

Fig. 2.7(b) - Strain gauge locations - Specimen 4G50.

possible, to measure the circumferential chord strains in this area.

Specimen 4G50 employed a further six gauges to measure circumferential chord strains at various locations near the joint as indicated in Figure 2.7(b). A seventh additional gauge was located on the tension web next to the web interconnection to measure the longitudinal strains in this area.

Eleven LVDT's were used on each specimen. Seven of these measured chord face deformation directly beneath the joint. Four measured compression web displacement in the plane of the specimen. Transducers were Hewlett Packard series, model 7DCDT, with a stroke of 12.7 mm (0.5 in.) and an accuracy of $\pm$0.025 mm (0.001 in.).

The typical transducer assembly, which included a mounting frame, is illustrated in Figure 2.8. Figure 2.9 indicates the transducer locations. Those transducers which measured chord face deformation were mounted opposite the joint, as shown in Figure 2.10. Brass rods connected to the stainless steel cores of the transducers passed through the mounting bolts through the chord wall, and extended to the interior of the loaded chord face. To measure the compression web displacement, four transducers were mounted on an aluminum datum arm. The datum arm was rigidly fixed to the load frame.

To aid observation of specimen yielding, a white wash was applied to each specimen.

2.6) Testing Procedure

All specimens were tested in the loading frame shown in Figure 2.11. The chord and compression web were pin supported on cylindrical

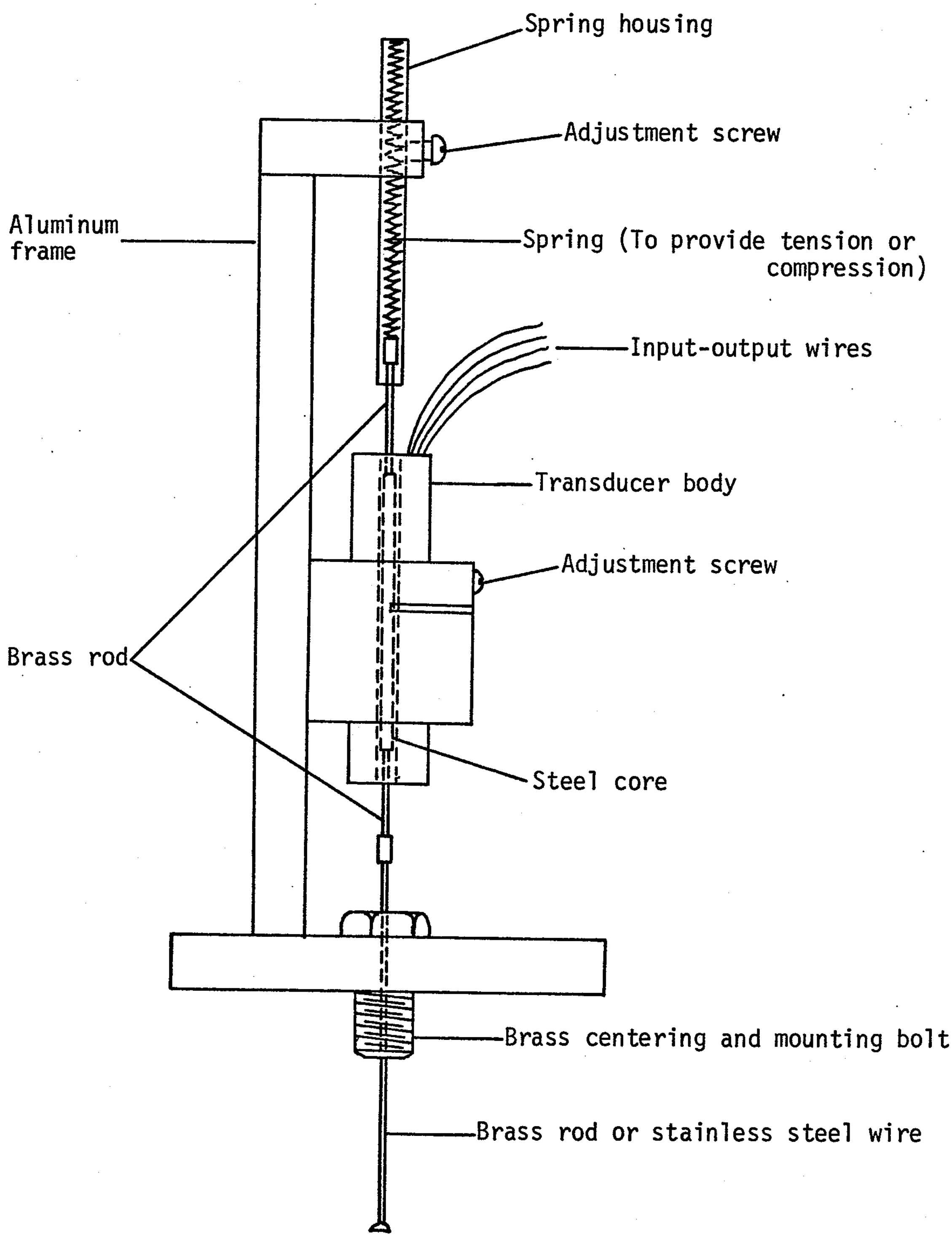

Fig. 2.8 - Transducer assembly.

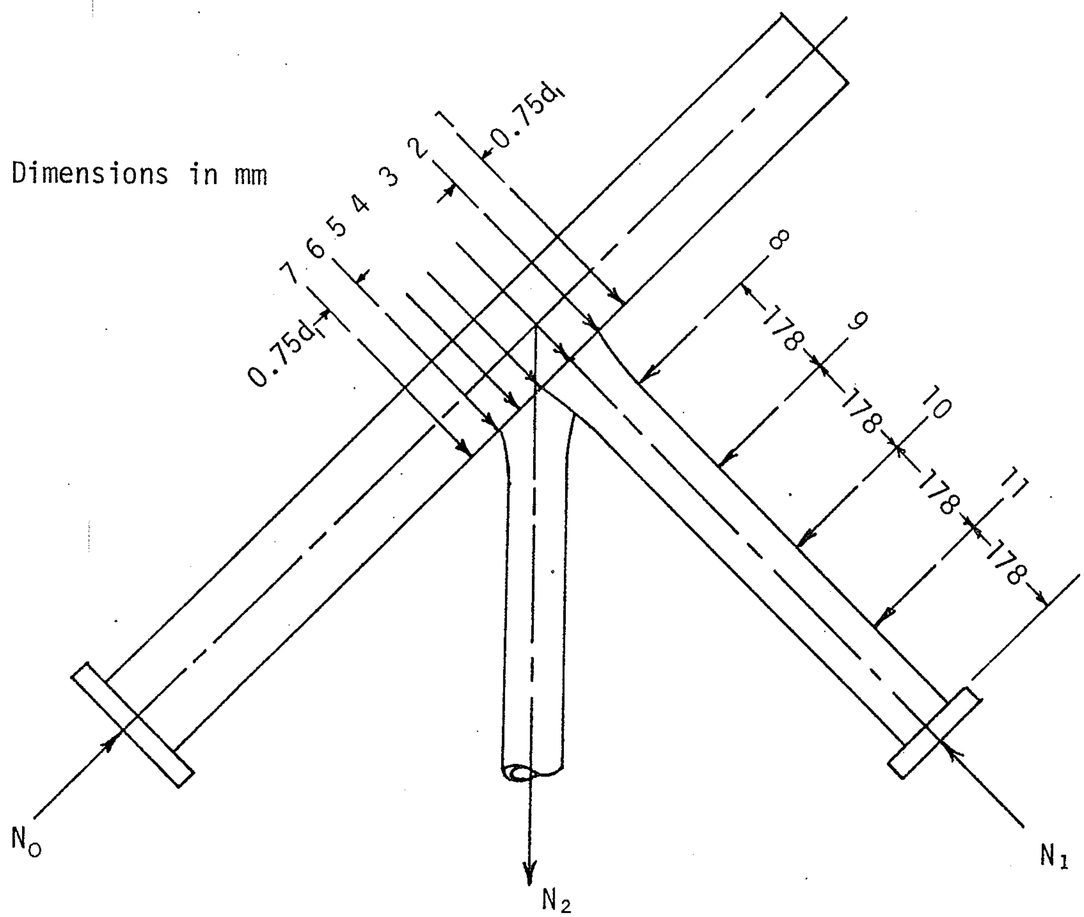

Fig. 2.9 - Transducer locations.

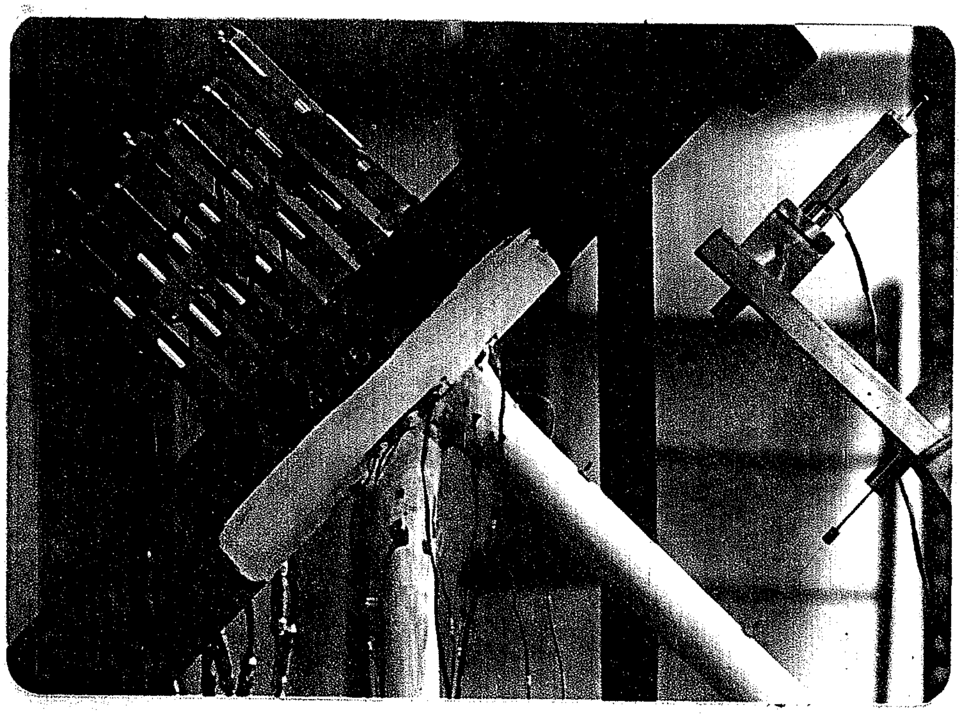

Fig. 2.10 - Mounted transducers.

bearings which precluded out-of-plane buckling of the compression web. Pin supports of this type simulate the in-plane conditions in a relatively stiff truss.

The specimens were loaded via the tension web through a pin type connection, by a 889 kN (200 kip) capacity, manually operated hydraulic loading jack. A 889 kN (200 kip) capacity load cell, located between the tension web and the jack, measured the specimen load (see Figure 2.11).

Initially, the load was applied in appropriate predetermined increments. After each increment, a complete set of readings were automatically recorded by the data acquisition system. However, after the onset of yielding readings were taken at frequent, manually selected loading increments. The loading was continued until specimen buckling or fracture rendered any increase in load impossible.

2.7) Data Acquisition

The data acquisition system comprised a Hewlett Packard model 9825A programmable calculator and a model 9871A printer-plotter. Load, deflection, and strain readings were recorded, then stored on magnetic tape and later tabulated and plotted.

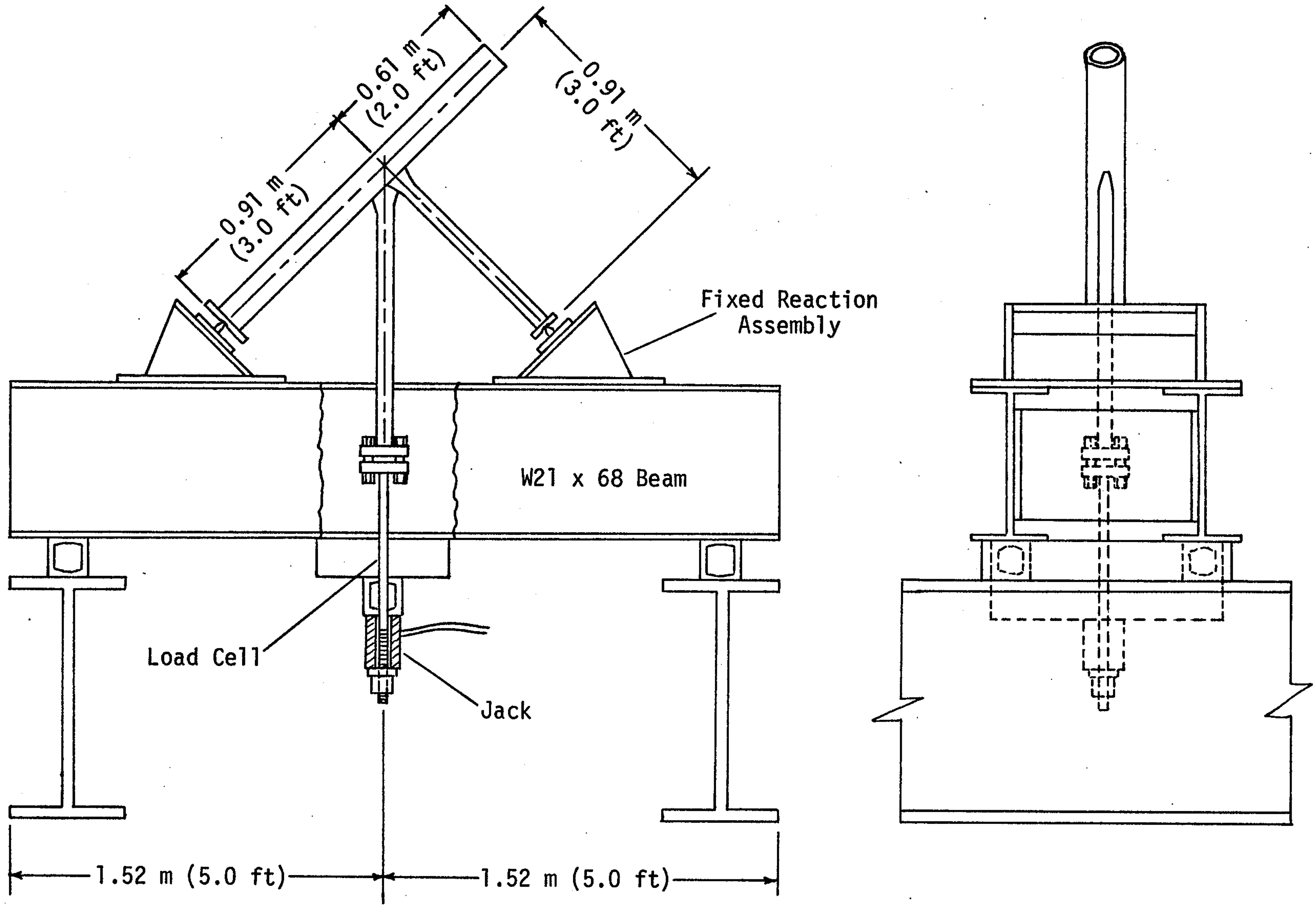

Fig. 2.11 - Loading frame.

CHAPTER 3

TEST RESULTS AND DISCUSSION

In this chapter, the modes of failure, joint strength, and joint flexibility of cropped-web joints involving round chords are discussed with reference to the joint parameters. In addition, the measured strains and deformations of several test specimens are compared and discussed.

3.1) Modes of Failure

The failure of a test specimen was assumed to coincide with attainment of its ultimate load. Specimen failure occurred in one or more of the following failure modes:

A) Large chord wall deformation.

B) Compression web buckling.

C) Tearing of the tension web near the crotch of the web members.

D) Shearing through the direct connection between the webs.

E) Tearing of the chord wall.

F) Weld fracture in the crotch of the web members.

G) Tension web failure.

H) Local buckling of the compression web wall near the joint.

A close examination of the specimens indicated, however, that the various failures can be classified into the following three general failure mode categories:

a) the joint failure, J

b) the joint--member failure, JM

c) the member failure, M.

The respective failure modes are indicated in table 3.1.

The specimen failures which were localized in the joint, with no evidence of web member failure, were considered joint failures. Shear failure through the direct connection between the web members as shown in Figure 3.1 or chord wall tearing as shown in Figure 3.2 were typical of the joint type failures. Joint failures usually occurred when the chord wall was extremely flexible compared to the web members.

Joint--member failures were those in which deformation of the chord face induced a web member failure. In these specimens, the chord face was somewhat less flexible. The failure mechanism for these specimens was consistent. As the chord wall deformed due to the web loading, end moments were applied to both the compression and tension webs at the joint. The moments continued to increase as load was applied. Eventually, this resulted in premature compression web buckling in a direction away from the tension web, as illustrated in Figure 3.3, or in a local crippling of the compression web wall near the interconnection of the webs, as shown in Figure 3.4. Furthermore, the development of high tensile stresses at the toe of the tension web usually led to tension web tearing in the heat affected zone, as illustrated in Figure 3.5, or a weld fracture at the crotch of the web members.

The third general failure mode, the member failure, encompassed specimen buckling failures, both local and overall, and tension web failures which were not induced by joint deformation. They occurred

TABLE 3.1

TEST RESULTS

Specimen	$N_{2u}=J_u/\cos 45^o$ KN	(Kips)	N_{2u}/N_{2e} (%)	J_u/N_{1b}	$J_u d_1/t_1 t_o d_o \sigma_{oe}$	Failure Type	General Failure Mode
1D00	108.7	24.43	52.5	0.84	8.67	A,E	J
1D50	143.2	32.19	69.1	1.12	11.48	A,C	JM
1D75	142.1	31.93	68.6	1.17	12.15	A,B,F	JM
2D00	205.2	46.12	100.5	1.60	11.69	A,E	J
2D50	170.3	38.28	81.2	1.41	9.83	A,B,C	JM
2D75	196.6	44.17	96.6	1.55	10.61	A,B,C	JM
3D00	231.8	52.10	112.7	1.86	7.77	A,B	JM
3D50	242.5	54.50	120.1	1.95	9.46	A,B	JM
3D75	244.8	55.00	121.2	1.96	8.56	B*	M
4D00	130.3	29.29	96.7	2.81	6.89	A,B	JM
4D50	140.2	31.50	104.0	3.01	6.71	B	M
4D75	148.0	33.25	110.6	3.18	7.72	B	M
5D00	158.3	35.57	117.4	3.37	6.85	B	M
5D50	153.9	34.59	112.5	3.31	6.65	B*	M
5D75	150.5	33.81	112.5	3.18	6.20	B	M
6D00	142.7	32.06	106.6	3.07	4.03	B	M
6D50	155.4	34.93	113.6	3.33	4.41	B	M
6D75	155.6	34.96	114.6	3.29	4.47	B*	M
1E00	119.1	26.77	33.8	0.43	7.99	A,E	J
1E50	198.9	44.69	55.6	0.71	14.46	A,D	J
1E75	249.6	56.09	69.7	0.89	16.60	A,D	J
2E00	190.4	42.78	54.0	0.67	8.99	A,E	J
2E50	261.0	58.65	72.4	0.93	12.24	A,C	JM
2E75	324.8	72.99	93.1	1.17	15.18	A,B,C	JM
3E00	366.0	82.25	104.1	1.36	12.40	A,E	J
3E50	357.0	80.23	102.9	1.29	10.50	A,B,C	JM
3E75	380.8	85.57	108.3	1.33	10.71	A,B,C	JM
4E00	160.5	36.07	106.9	2.29	9.38	A,B	JM
4E50	176.4	39.64	115.7	2.54	10.56	A,B	JM
4E75	176.3	39.61	115.6	2.55	10.85	B	M
5E00	212.2	47.69	134.9	2.96	9.70	B*	M
5E50	194.1	43.62	123.4	2.69	9.33	B	M
5E75	189.0	42.48	121.1	2.64	9.09	B	M

Note: B* indicates compression web buckling towards the tension web.

TABLE 3.1 (continued)

Specimen	$N_{2u}=J_u/\cos 45^o$ KN	(Kips)	N_{2u}/N_{2e} (%)	J_u/N_{1b}	$J_u d_1/t_1 t_o d_o \sigma_{oe}$	Failure Type	General Failure Mode
6E00	196.2	44.08	127.6	2.77	5.87	B	M
6E50	193.9	43.58	124.2	2.66	6.02	B	M
6E75	176.8	39.73	115.9	2.58	5.75	B	M
2F50	251.2	56.44	58.8	0.69	17.38	A,F,G	JM
2F75	282.0	63.37	65.5	0.77	19.46	A,F,G	JM
3F50	353.3	79.39	83.8	0.97	14.84	A,G,C	JM
3F75	395.0	88.77	95.2	1.09	16.65	A,G	JM
4F00	209.3	47.03	102.9	1.67	14.65	A,B	JM
4F50	227.6	51.14	113.2	1.68	14.79	A,B,F	JM
4F75	246.8	55.47	122.0	1.80	15.86	A,B,C	JM
5F50	284.0	63.83	141.1	2.11	13.92	B	M
5F75	291.0	65.40	144.5	2.15	14.27	B	M
6F50	290.9	65.36	143.0	2.17	10.58	B	M
6F75	274.3	61.64	136.2	2.05	10.20	B*	M
4G00	268.6	60.36	71.4	0.99	16.73	A,E,F	J
4G50	296.7	66.68	76.7	1.08	18.85	A,G,F	JM
4G75	318.7	71.62	84.2	1.15	19.82	A,B,F	JM
5G50	406.2	91.27	107.1	1.47	18.19	A,B,C	JM
5G75	430.6	96.77	108.7	1.55	19.55	A,B,C	JM
6G50	456.6	102.61	118.9	1.64	15.06	H	M
6G75	464.7	104.42	121.0	1.67	15.57	H	M
4H00	305.0	68.54	73.3	0.86	25.95	A,E,F	J
4H50	323.1	72.61	75.0	0.90	27.30	A,C,G	JM
4H75	353.7	79.49	82.7	0.99	29.39	A,C,G	JM
5H50	371.9	83.58	87.4	1.04	24.63	A,F,G	JM
5H75	411.2	92.41	94.7	1.15	27.59	A,F,G	JM
6H50	464.4	104.35	109.5	1.31	21.87	G	M
6H75	477.0	107.20	110.8	1.35	22.93	G	M

Definition of symbols.

N_{2u} = ultimate tension web load.

J_u = ultimate joint load.

N_{2e} = yield load of tension web.

N_{1b} = buckling load of compression web.

d_1 = compression web diameter.

t_1 = compression web thickness.

t_o = chord thickness.

d_o = chord diameter.

σ_{oe} = chord yield strength.

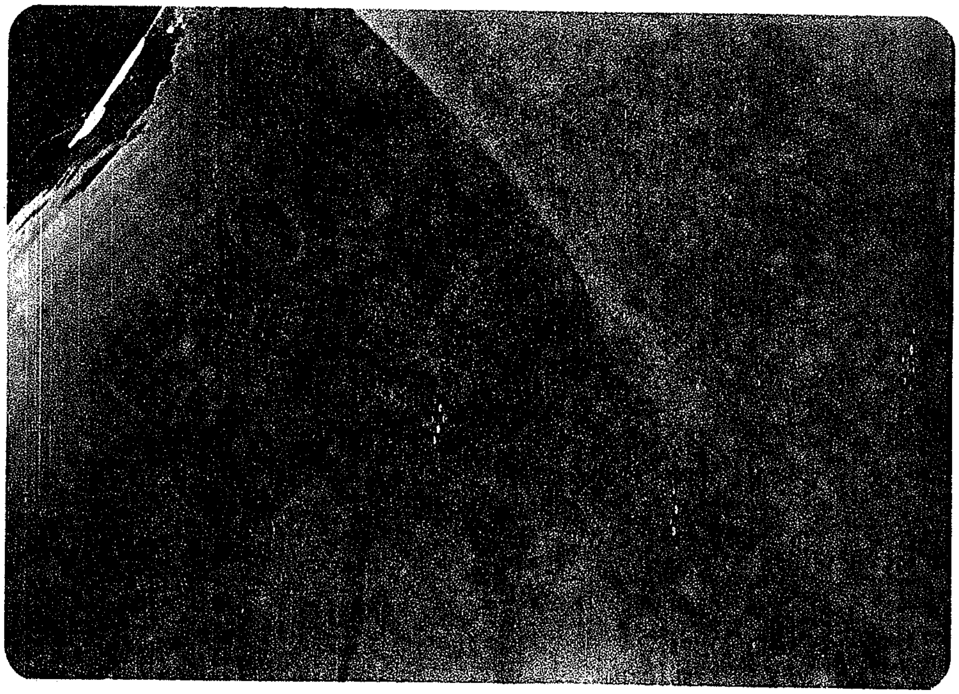

a) Shear through the web interconnection.

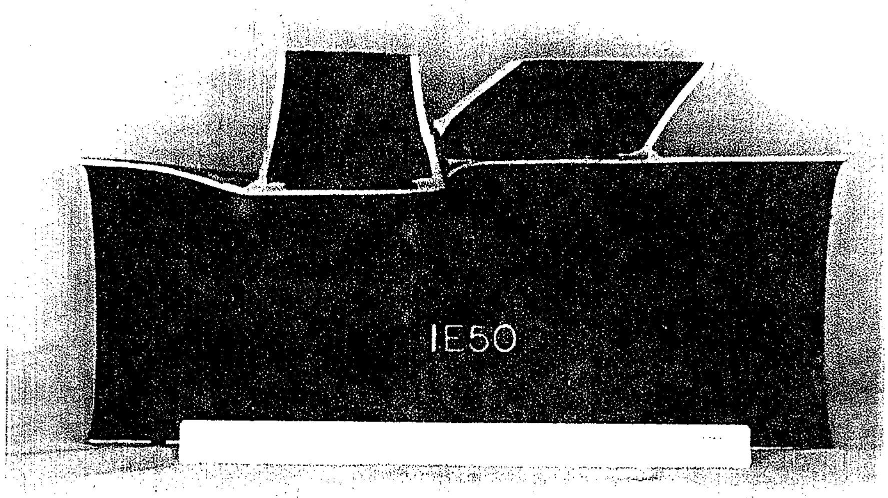

b) Joint cross-section.

Fig. 3.1 - Joint Failure - Specimen 1E50.

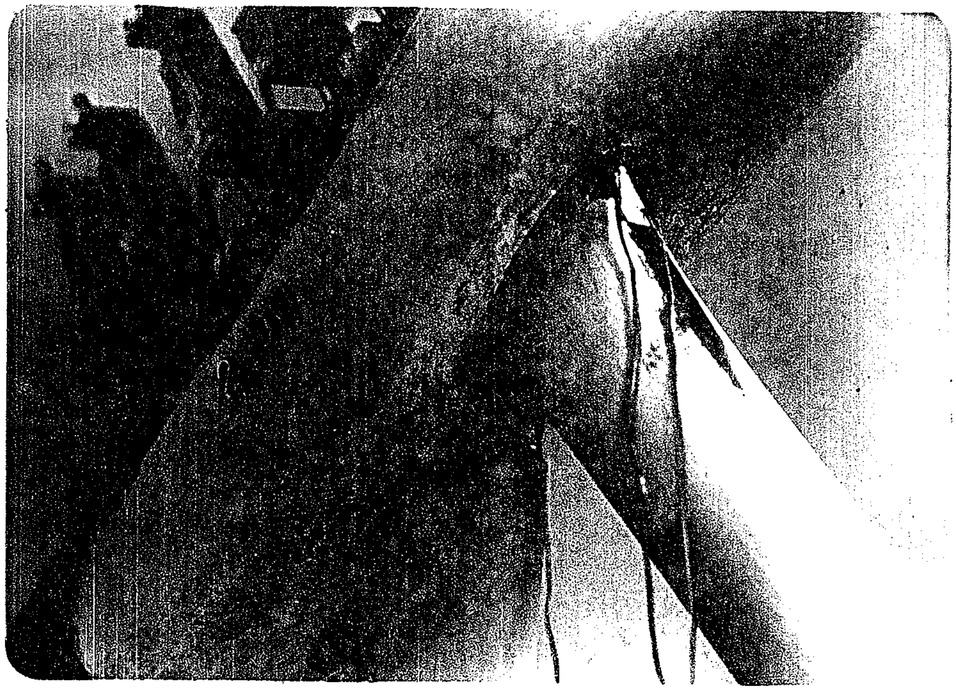

a) Chord face tearing.

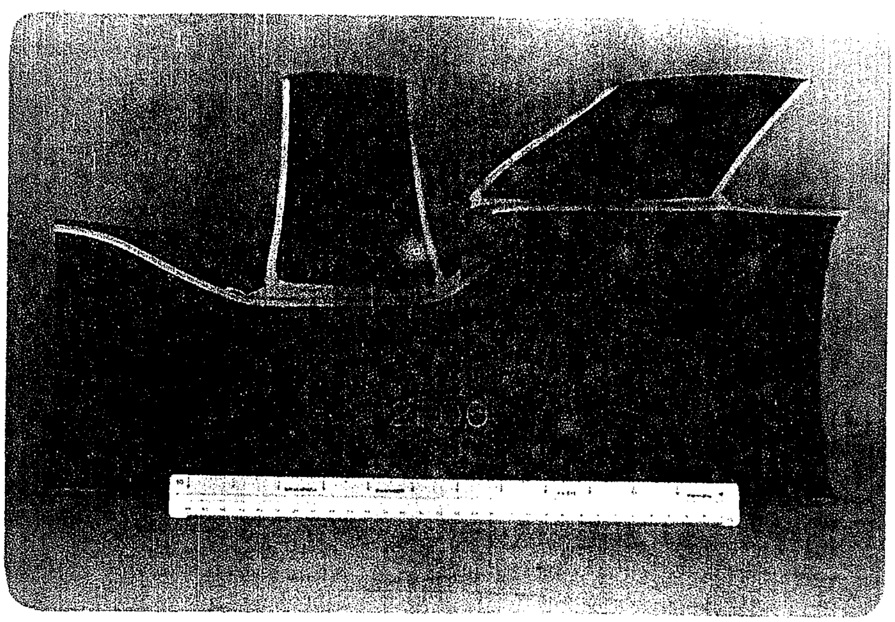

b) Joint cross-section.

Fig. 3.2 - Joint Failure - Specimen 2E00.

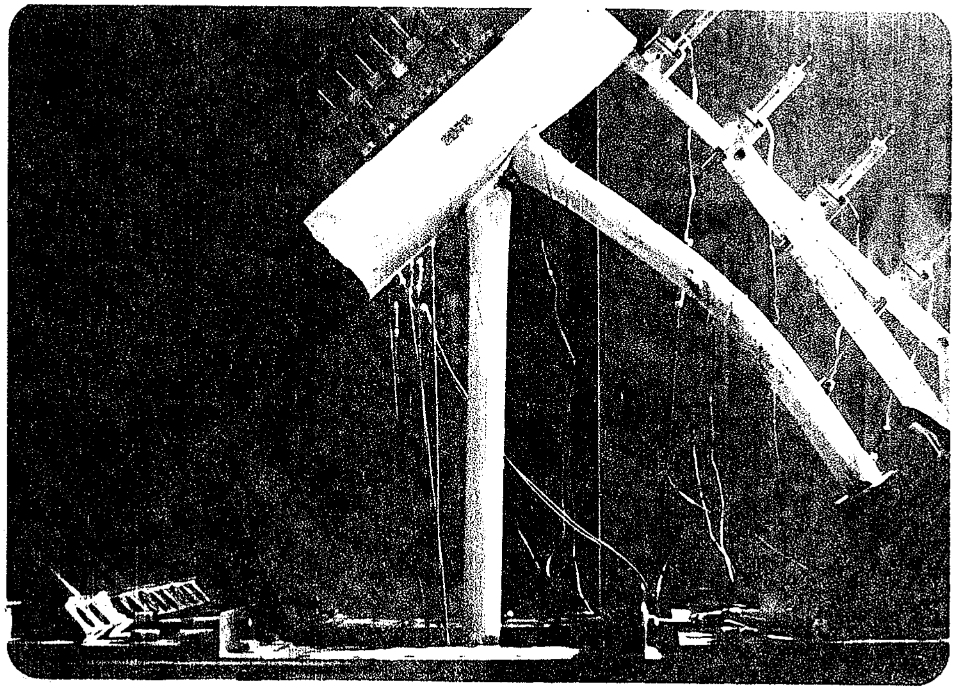

a) Pre-mature compression web buckling.

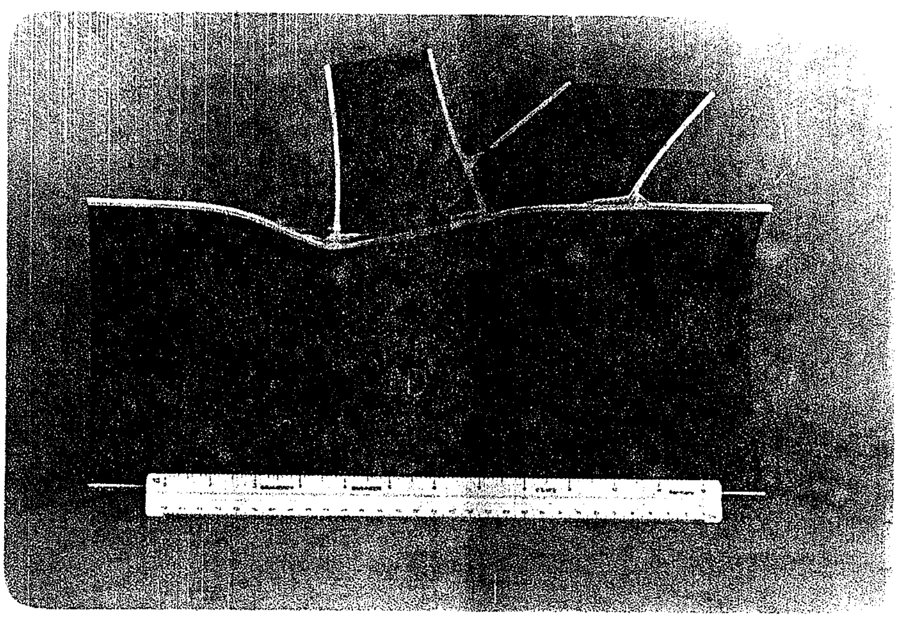

b) Joint cross-section.

Fig. 3.3 - Joint-member Failure - Specimen 2D75.

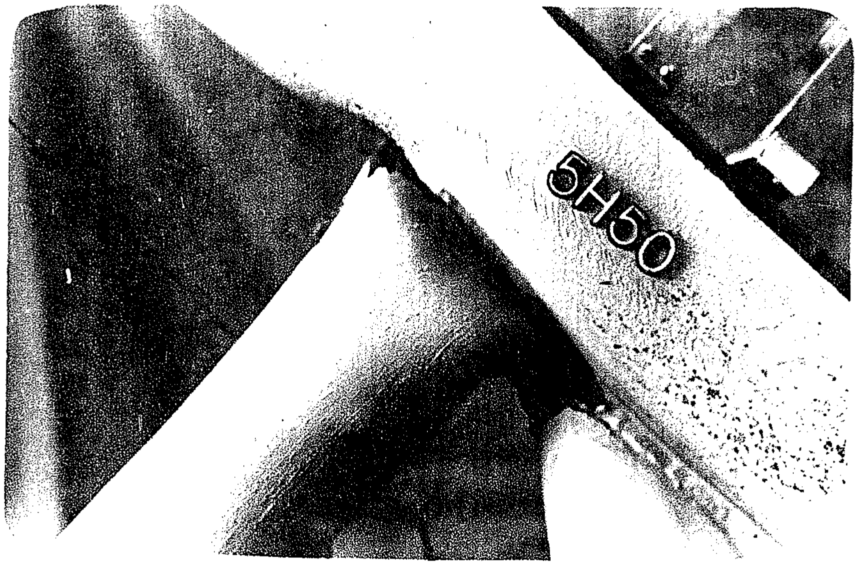

Fig. 3.4 - Crippling of compression web wall in a joint-member failure - Specimen 5H50.

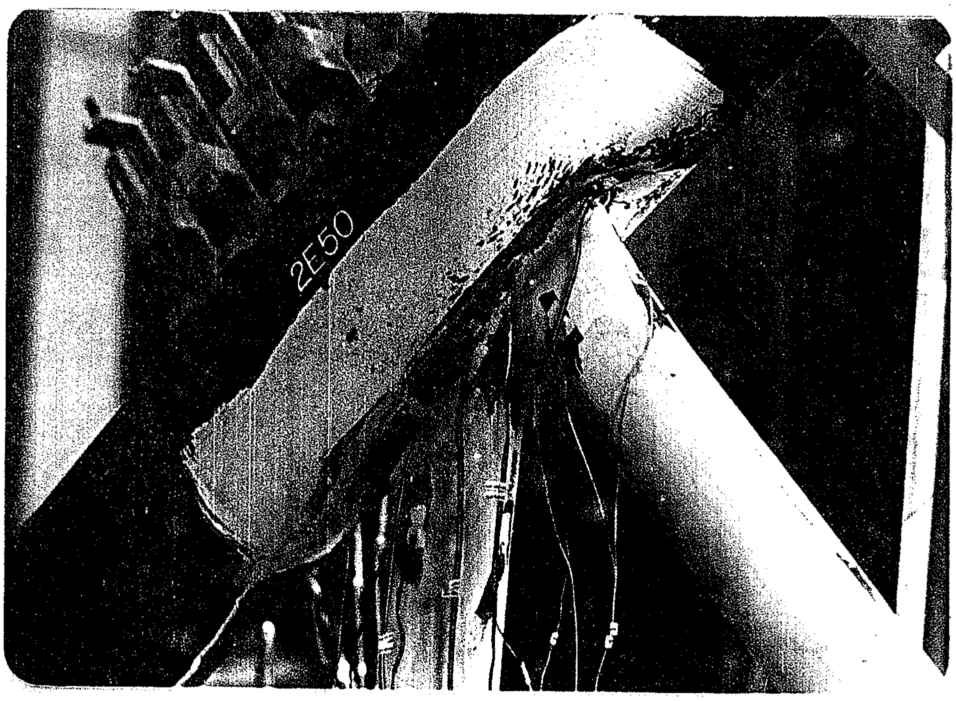

Fig. 3.5 - Tension web tearing in a joint-member failure - Specimen 2E50.

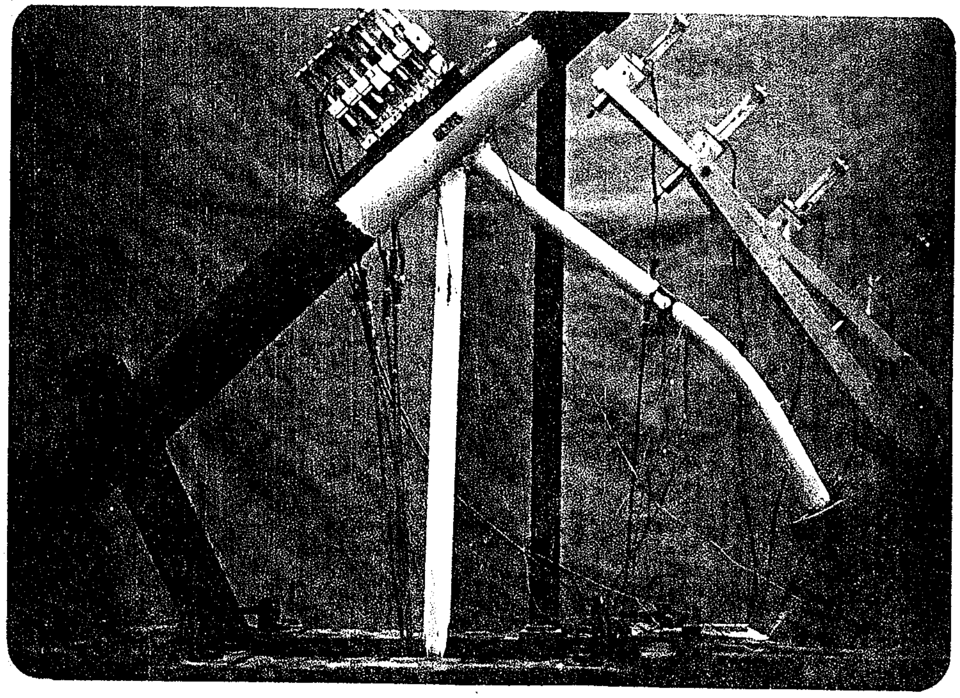

a) Compression web buckling.

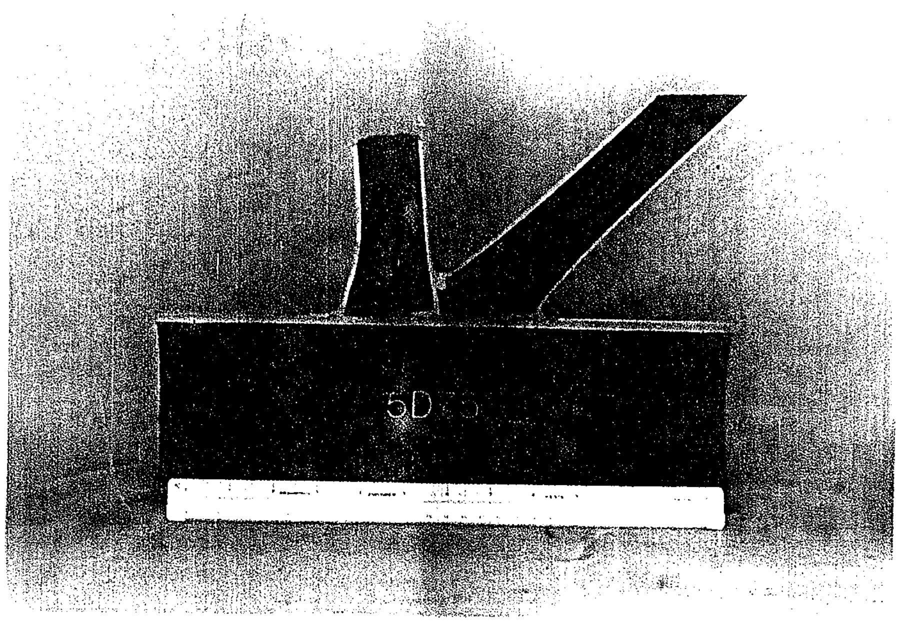

b) Joint cross-section.

Fig. 3.6 - Member Failure - Specimen 5D75.

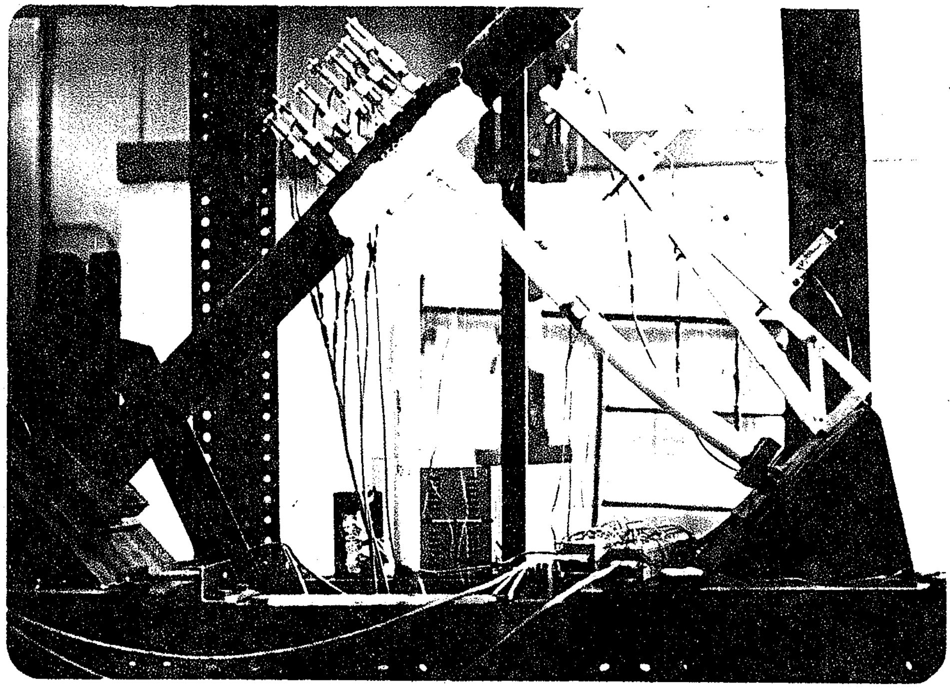

a) Compression web buckling towards the tension web - Specimen 5E00.

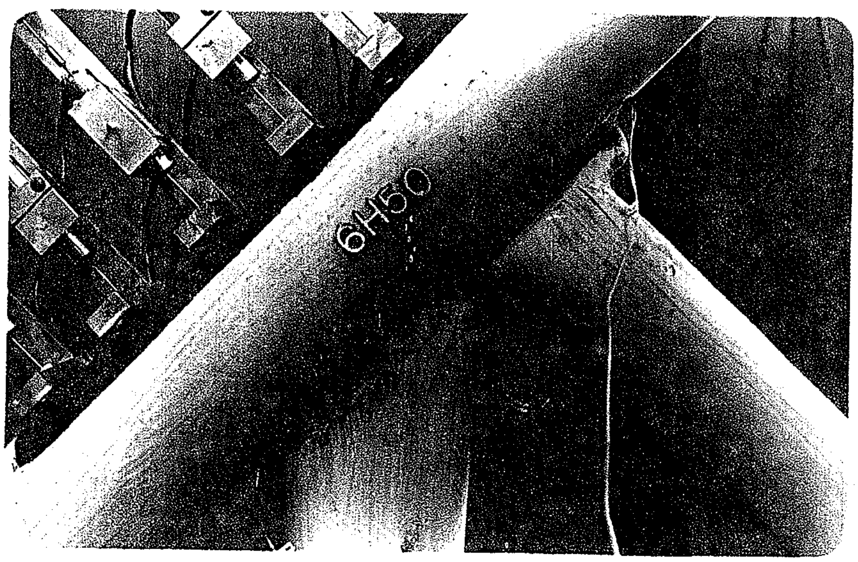

b) Compression web crippling - Specimen 6H50.

Fig. 3.7 - Typical Member Failures.

when the chord wall was extremely stiff, approximating a fixed-end condition. The compression web did not consistently buckle away from the tension web, as was observed for joint--member failures. This was evidenced in specimens 3D75, 5D50, 6D75, 6F75, and 5E00. Figures 3.6 and 3.7 show typical member failures.

Compression web buckling failures were characteristic of both joint--member and member failures. Hence, it was decided arbitrarily that a means of distinguishing buckling in member failures from that in joint--member failures was to compare the ultimate compression web load to its factored resistance. If the ultimate compression web load was larger than its factored resistance, a member failure was assumed. In computing the factored resistance of the compression web, the web was assumed to be a column fixed at one end and pin supported at the other.

3.2) Joint Strength

Ideally, for an accurate prediction of the strength of any tubular truss joint, there should be a strength formula for each of the failure modes, or in this case, each of the general failure modes. However, for design purposes, a single strength equation which is independent of the failure type is more desirable. With this in mind, various dimensionless strength parameters were investigated in an attempt to find a parameter which best relates the strengths of all of the joints tested to a few common geometric joint parameters.

In addition, the familiar strength parameters, joint efficiency and joint load factor, were investigated.

3.2.1) Joint Strength ($J_u d_1/t_1 t_o d_o \sigma_{oe}$)

The dimensionless strength parameter $J_u d_1/t_1 t_o d_o \sigma_{oe}$ was found to best fit the above-mentioned criteria. J_u is the load in the compression web at failure, d_1 is the diameter of the compression web, t_1 is the wall thickness of the compression web, t_o is the chord wall thickness, d_o is the chord diameter, and σ_{oe} is the yield strength of the chord material. A stepwise multiple linear regression analysis, described in Appendix A, was employed and the following empirical equation was generated.

$$J_u d_1/t_1 t_o d_o \sigma_{oe} = 8.96 + 40.2(d_1/d_o)^2 - 144(t_o/d_o) \qquad 3.1(a)$$

Rearranging equation 3.1(a), the following expression was obtained for estimating the ultimate load of a cropped-web tubular truss joint with no gap.

$$J_u = (t_1 t_o d_o \sigma_{oe}/d_1)\left[8.96 + 40.2(d_1/d_o)^2 - 144(t_o/d_o)\right] \qquad 3.2(b)$$

The variables $(d_1/d_o)^2$ and (t_o/d_o) in equation 3.1(a) accounted for 94 percent of the variation in $J_u d_1/t_1 t_o d_o \sigma_{oe}$. Web lap was included in several variables in the regression analysis. However, because its effect was inconsistent, it did not correlate well. Thus it was not incorporated into the regression equation. Statistically, the independent variables, $(d_1/d_o)^2$ and (t_o/d_o), were found to be significant at the 0.1 percent level as were their coefficients. The coefficient of variation of the test results relative to equation 3.1(a) was 11.5 percent. For comparison, the coefficient of variation for Theinsiripipat's (1979) strength equation for cropped-web joints with square chords was 12.6 percent.

The experimental and predicted values of $J_u d_1/t_1 t_o d_o \sigma_{oe}$ are illustrated in Figure 3.8. It can be seen that the test and predicted values are in good agreement. The largest deviations from the predicted results involved those zero lap joints with t_o/d_o ratios smaller than 0.045. Consequently, a second regression was performed on the parameter $J_u d_1/t_1 t_o d_o \sigma_{oe}$, employing the identical independent variables, with the previously mentioned joints excluded. This produced the following empirical equation.

$$J_u d_1/t_1 t_o d_o \sigma_{oe} = 10.5 + 40.6(d_1/d_o)^2 - 172(t_o/d_o) \qquad 3.2(a)$$

or

$$J_u = \left(t_1 t_o d_o \sigma_{oe}/d_1\right)\left[10.5 + 40.6(d_1/d_o)^2 - 172(t_o/d_o)\right] \qquad 3.2(b)$$

Again the independent variables and partial regression coefficients were significant at 0.1 percent level. However, the variables $(d_1/d_o)^2$ and (t_o/d_o) this time accounted for 98 percent of the variation in $J_u d_1/t_1 t_o d_o \sigma_{oe}$. Furthermore, the coefficient of variation for equation 3.2(a) was reduced to 7.9 percent. It can be seen in Figure 3.9 that the experimental and predicted results are in extremely good agreement.

Equations 3.1(a) and 3.2(a) are both valid over a range of d_1/d_o from 0.3 to 0.8, a range of t_o/d_o from approximately 0.02 to 0.07 and for t_1/d_1 or t_2/d_2 ratios ranging from about 0.04 to 0.08. Equation 3.1(a) is valid for web laps ranging from zero to 75 percent, while squation 3.2(a) does not account for zero lap joints with t_o/d_o ratios smaller than 0.045. The advantage of the latter is that for lap joints of 50 or 75 percent, the predicted ultimate lcad is higher than that given by equation 3.1(a) when t_o/d_o is smaller than 0.04.

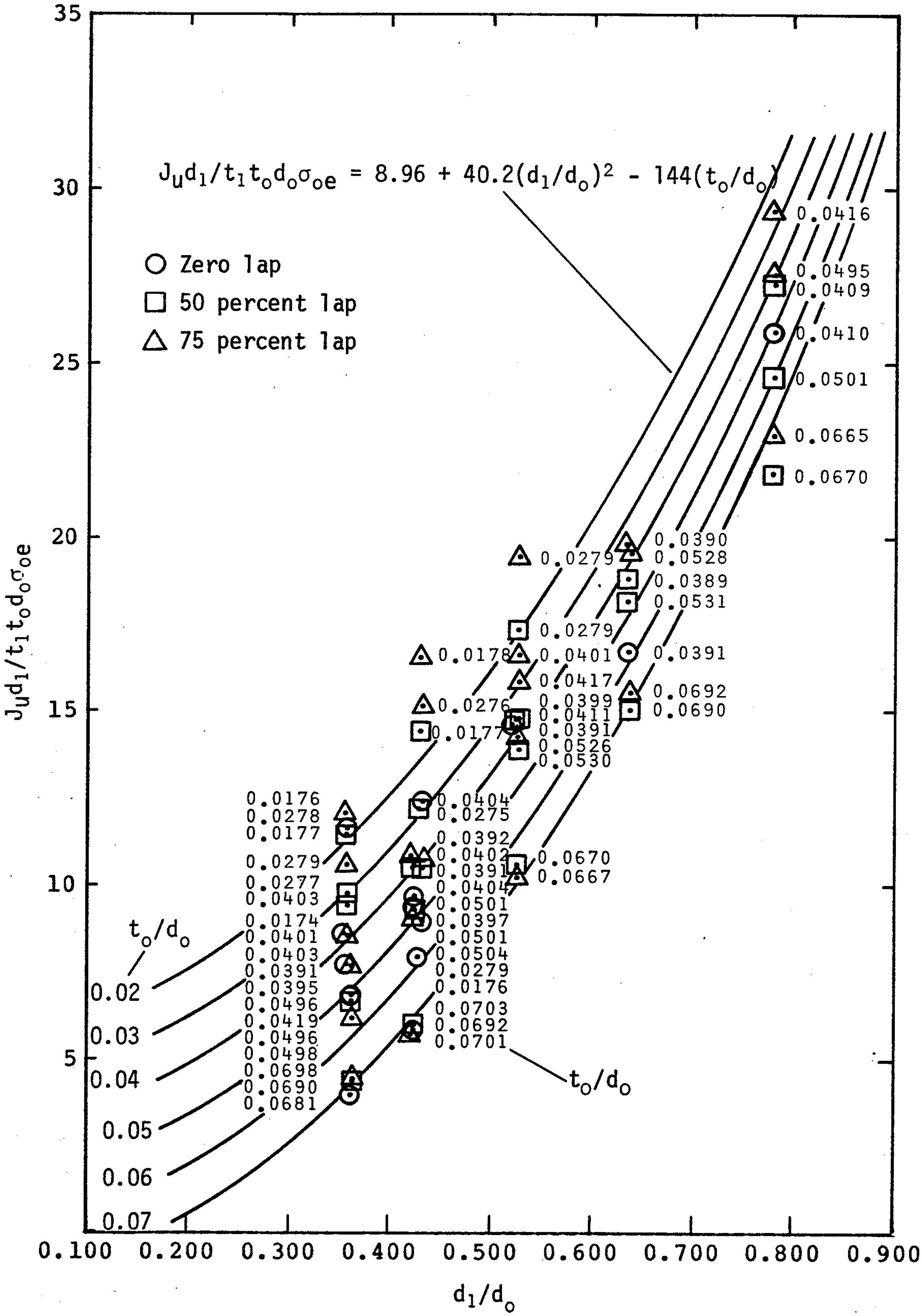

Fig. 3.8 - Influence of d_1/d_o on Joint Strength.

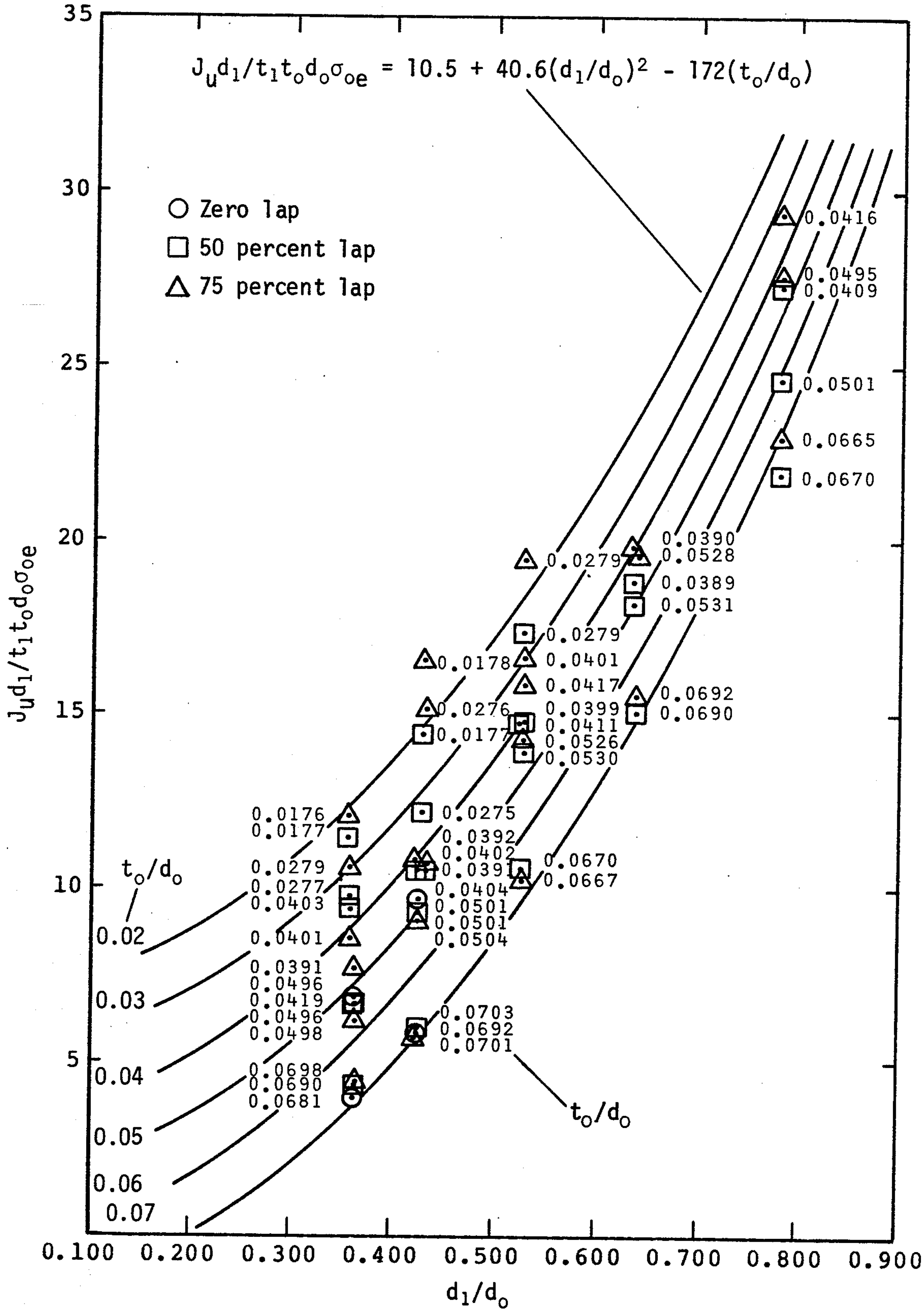

Fig. 3.9 - Influence of d_1/d_o on Joint Strength.

For use in limit states design (LSD), equations 3.1(b) and 3.2(b) would be reduced by a capacity reduction factor, ϕ. The appropriate value of ϕ, determined statistically in appendix B, was found to be 0.9. Thus, the joint resistance (J_r) is calculated as $J_r = \phi J_u$. For design purposes, this value would be compared to the factored resistances of the compression and tension members. The limiting resistance value would then govern the design.

3.2.2) Joint Efficiency

The joint efficiency, defined as the ratio of the ultimate tension web load (N_{2u}) sustained in the specimen to the yield load (N_{2e}) of that tension web, is an expression of the joint strength in terms of the tension web capacity.

The influence of the parameter t_o/d_o on joint efficiency is illustrated in Figure 3.10. It can be seen that the joint efficiency increased approximately linearly with t_o/d_o up to a t_o/d_o value of 0.05. For larger t_o/d_o values it was virtually constant. The joint efficiencies ranged from 33 percent to 145 percent, with 100 percent or larger values usually obtained when t_o/d_o was 0.05 or larger.

The effect of d_1/d_o on joint efficiency was somewhat inconsistent. However, an increase in web lap usually led to an increase in efficiency when t_o/d_o was 0.05 or smaller.

Bouwkamp (1968) tested profiled web joints of sizes similar to those tested in this study. The joint efficiencies for his joints are plotted in Figure 3.11. It can be seen that, as for the cropped-web joints, the efficiencies increased with an increase in t_o/d_o. The

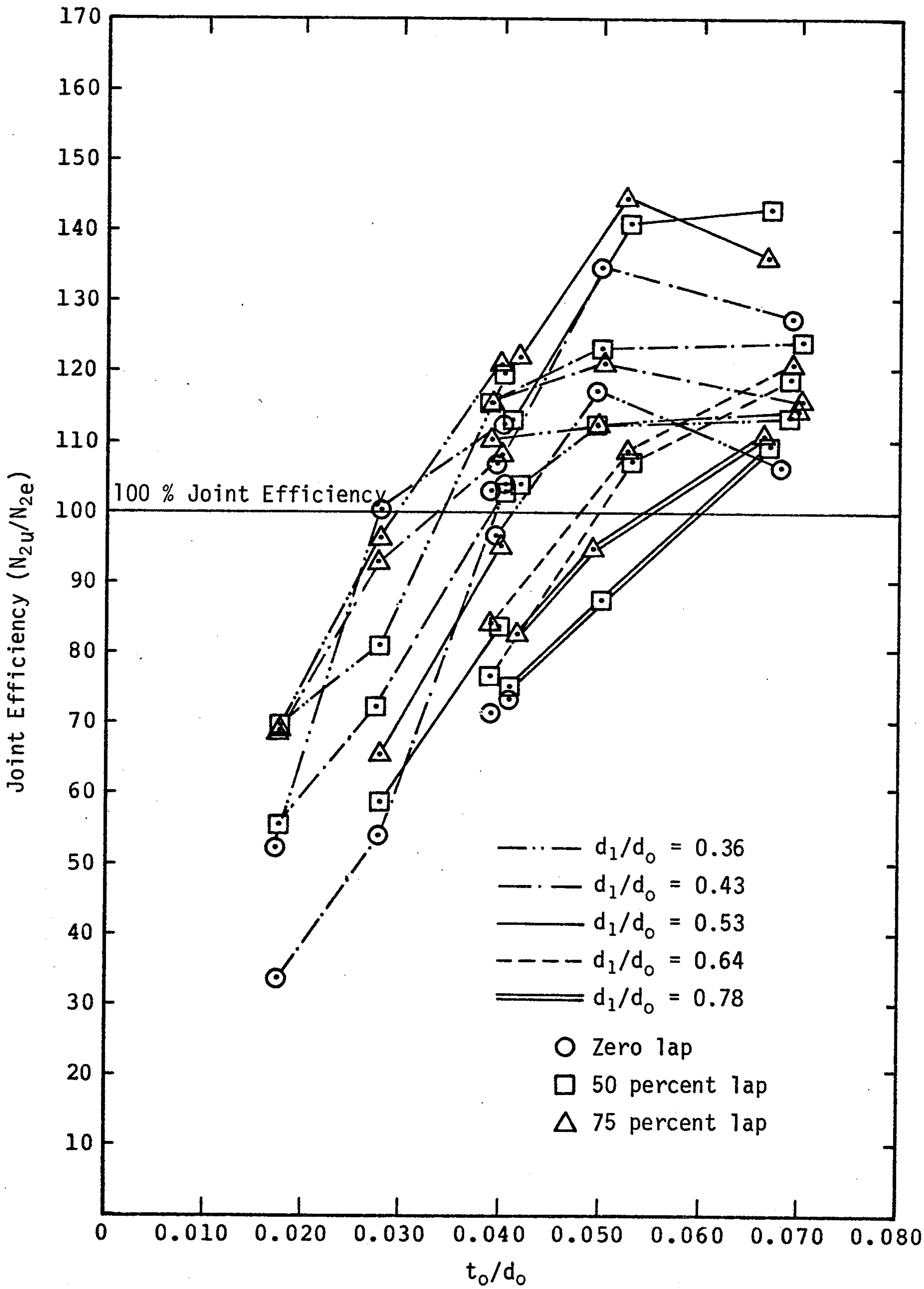

Fig. 3.10 - Influence of t_o/d_o on Joint Efficiency.

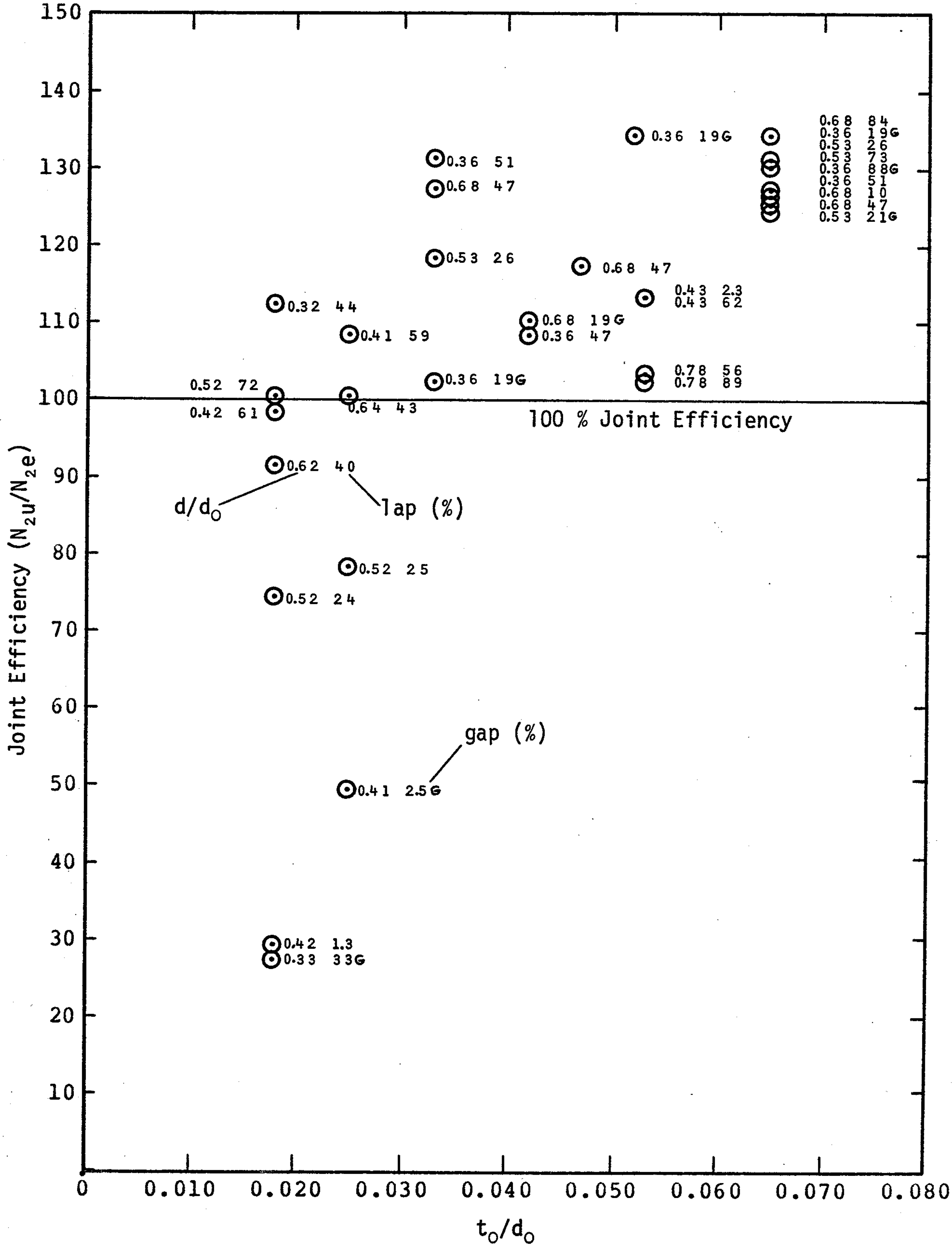

Fig. 3.11 - Influence of t_o/d_o on joint efficiency for profiled-web joints. (Bouwkamp 1968)

range of efficiencies, 28 to 135 percent, was also comparable to that of cropped web joints. However, an efficiency of 100 percent or more was achieved for profiled joints for a t_o/d_o ratio of 0.03 or larger. The influence of the d_1/d_o ratio and the web lap or gap on the efficiencies of the profiled-web joints was inconsistent.

In terms of joint efficiency, it appears that the strengths of cropped-web joints and profiled web joints are similarly influenced by variations in the t_o/d_o and d/d_o ratios. However, the strengths of the former joints tend to be slightly smaller than those of the latter, when t_o/d_o is smaller than 0.05.

3.2.3) Joint Ultimate Load Factor

The joint ultimate load factor is defined as the ratio of the ultimate joint force (J_u) normal to the chord to the computed factored resistance (N_{1_b}), or in this case, the buckling strength of the compression web.

As indicated in table 3.1, several of the test specimens exhibited unusually large ultimate load factors. This was because the computed buckling loads of the compression webs were based on an effective length, for out-of-plane buckling, equal to the depth of the modelled truss. However, in the test specimens, a buckling failure of this type was precluded and the resulting ultimate buckling loads were relatively large.

A plot of ultimate load factor versus the t_o/d_o ratio is presented in Figure 3.12. It can be seen that the influence of the t_o/d_o ratio on the ultimate load factor is similar to its influence on joint

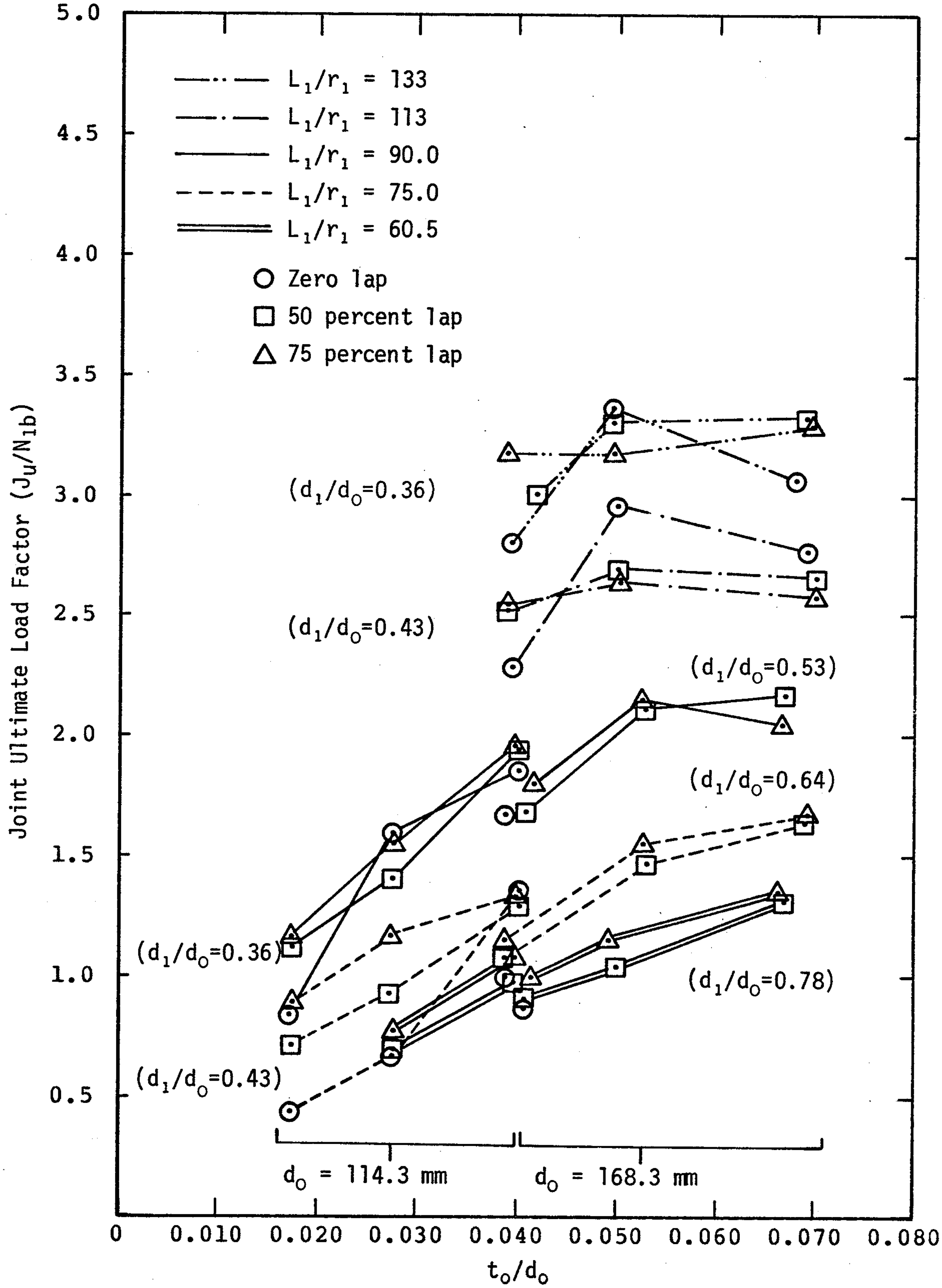

Fig. 3.12 - Influence of t_o/d_o on the Joint Ultimate Load Factor.

efficiency. It increased with an increase in t_o/d_o up to a t_o/d_o value of approximately 0.05. Then it remained virtually constant for larger t_o/d_o values and L_1/r_1 ratios larger than about 75. Futhermore, an increase in web lap usually improved the ultimate load factor when the t_o/d_o ratio was smaller than 0.05.

Because compression web buckling occurred in a larger number of the specimens, the d_1/d_o ratio and the compression web slenderness ratio significantly influenced the ultimate load factor. However, Figure 3.12 shows that a decrease in d_1/d_o increased the ultimate load factor, but only for specimens of the same chord diameter. An increase in the compression web slenderness ratio, on the other hand, consistently increased the ultimate load factor for constant t_o/d_o values, regardless of the chord diameter. Thus, for the joint ultimate load factor, the L_1/r_1 ratio is a more significant joint parameter than d_1/d_o.

It appears that for a given t_o/d_o ratio, a compression web slenderness exists such that when larger values are used, the ultimate joint capacity exceeds the buckling strength of the compression web. For example, for a t_o/d_o ratio of 0.04, the L_1/r_1ratio should be approximately 75 or larger. Furthermore, the minimum allowable L_1/r_1 ratio decreases for correspondingly larger t_o/d_o ratios.

3.2.4) Summary - Joint Strength

Equation 3.1(b) provides an accurate estimation of the ultimate joint load for cropped web joints involving round chords with zero to 75 percent web laps. Equation 3.2(b) is applicable, provided a 50 to

75 per cent lap is used, when the t_o/d_o ratio is smaller than 0.045. Equation 3.2(b) gives higher predicted loads than equation 3.1(b), when the t_o/d_o ratio is smaller than 0.045. Based on a statistical procedure, the capacity reduction factor for both equations was found to be 0.9.

Considering joint efficiency, the joint can sustain at least the yield strength of the tension web providing the t_o/d_o ratio is about 0.05 or larger. To ensure failure in the compression web rather than the joint, the L_1/r_1 ratio must be larger than a limiting L_1/r_1 value, which is dependent upon the t_o/d_o ratio for the joint as indicated in figure 3.12. Lastly, the joint strength usually increases with an increase in web lap. This effect is increasingly significant with a decrease in t_o/d_o and/or an increase in d_1/d_o.

3.3) Joint Flexibility

The lack of a central web support in an HSS section tends to result in a relatively flexible joint. To investigate this problem, joint flexibility coefficients were developed to provide a means of predicting additional truss deflections due to deformation and to evaluate the extent of this additional deflection.

3.3.1) Joint Flexibility Coefficients

In an earlier study (Theinsiripipat 1979), joint deformation was expressed in terms of joint stiffness coefficients. For several reasons, it was decided in this study, to employ flexibility coefficients rather than stiffness coefficients. They eliminate problems associated with negative or infinite values of stiffness. A negative or infinite stiffness may result if the joint undergoes a chord face translation, in addition to a rotation, as was observed in this study. Furthermore, flexibility coefficients tend to be less sensitive than stiffness coefficients to small or zero chord deformation readings.

The joint flexibility was computed in terms of the compression and tension web loads and the corresponding joint deformations along their axes. Thus, compression and tension flexibilities were determined.

Because the joint load--deformation behaviour was non-linear at early load stages in many cases, it was decided to compute the flexibilities at a load level equal to the estimated ultimate value, using equation 3.1, divided by 1.7. This approximated the working load of the joint. Furthermore, since translational deformations were found to neutralize each other when calculating overall truss deflections, only joint deformations due to joint rotation were considered.

As illustrated in figure 3.13, the joint compression flexibility was defined as $f_c = \delta_1/N_1$. N_1 is the predicted ultimate compression web load divided by 1.7 and δ_1 is the corresponding chord face deformation along the compression web axis. The joint tension flexibility is similarly defined as $f_t = \delta_2/N_2$, where N_2 and δ_2 are, respectively, the predicted ultimate tension web load divided by 1.7 and the corresponding chord face deformation along the axis of the tension web.

The joint flexibilities were expressed in terms of the dimensionless parameter $fEd_o^2/d = fEd(d_o/d)^2$, where E is the modulus of

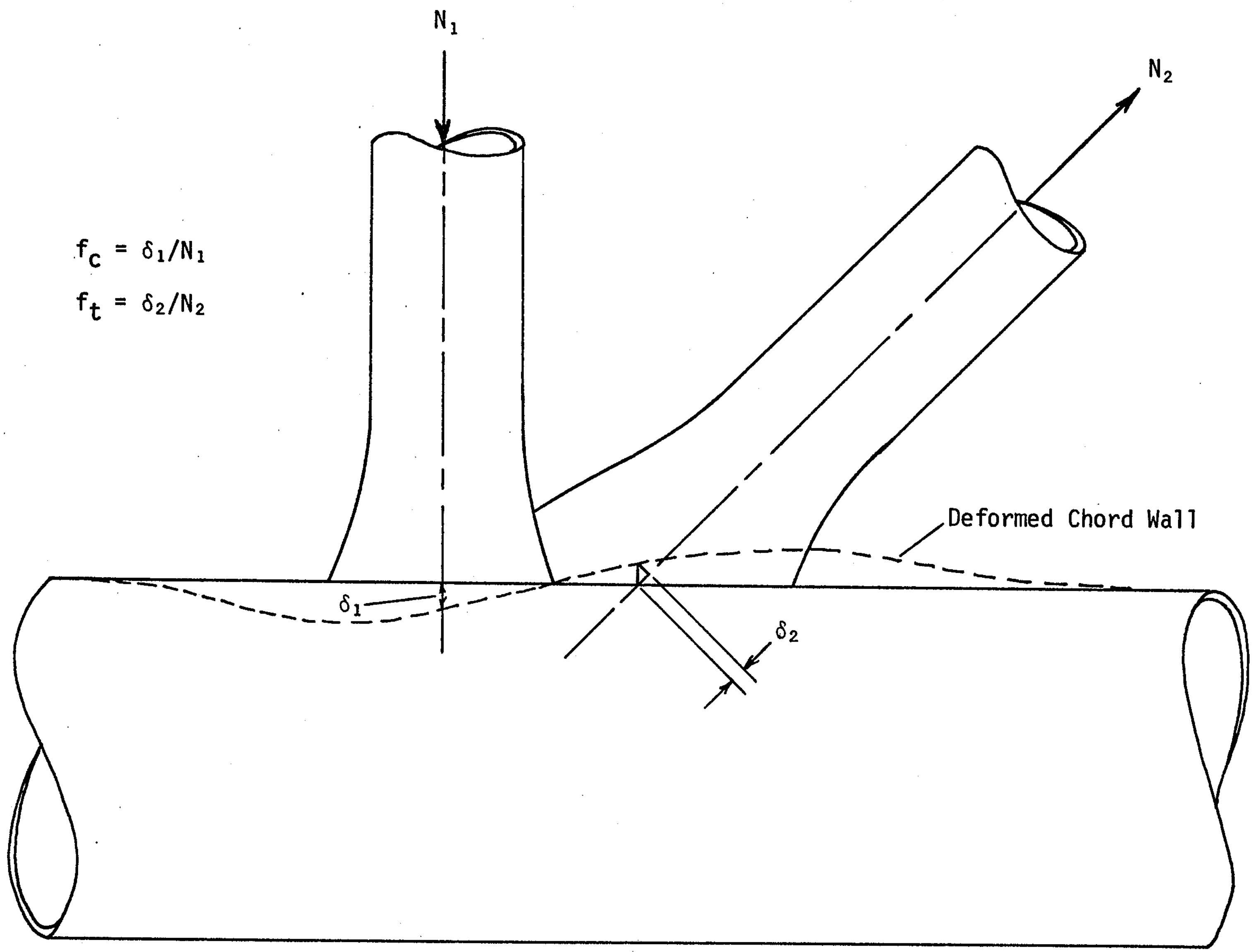

Fig. 3.13 - Joint Flexibility.

elasticity, d_o is the chord diameter, and d is the diameter of the web for which the flexibility is being determined. The specimen flexibilities and the parameters fEd_o^2/d are listed in table 3.2.

Plots of $f_cEd_o^2/d_1$ and $f_tEd_o^2/d_2$ versus the t_o/d_o ratio are given in Figures 3.14 and 3.15 respectively. A multiple regression analysis was again employed and the following empirical formulae were generated for estimating the joint compression and tension flexibilities.

$$f_cEd_o^2/d_1 = 34.2 + 0.278(d_o/t_o)^2 - 0.196(d_o/t_o)^2 0_v \qquad 3.3$$

$$f_tEd_o^2/d_2 = 10.3 + 0.219(d_o/t_o)^2 - 0.286(d_o/t_o)^2 0_v \qquad 3.4$$

where 0_v is the web lap.

Specimens 1D00 and 1E00 were excluded from the flexibility regression analysis because the joints became plastic at extremely low load levels.

The independent variables and their partial regression coefficients in equations 3.3 and 3.4 are significant at the 0.1 percent level. The independent variables $(d_o/t_o)^2$ and $(d_o/t_o)^2 0_v$ account for 89 and 85 percent of the variation in $f_cEd_o^2/d_1$ and $f_tEd_o^2/d_2$, respectively. The coefficient of variation for equation 3.3 was 20.3 percent. A somewhat high coefficient of variation, equal to 63.7 percent, resulted for equation 3.4. The latter value implies relatively large deviations of the test results from the estimated mean values. However, the actual deviations for tension flexibility were of the same order of magnitude as those which occurred for the compression flexibility.

The experimental results and predicted values using equations 3.3

TABLE 3.2

SPECIMEN FLEXIBILITIES

Specimen	$f_c \times 10^3$		$f_t \times 10^3$		$f_c E d_0^2/d_1$	$f_t E d_0^2/d_2$
	mm/kN	in/kip	mm/kN	in/kip		
1D00	-	-	-	-	-	-
1D50	7.13	1.248	2.55	0.446	638.7	234.9
1D75	5.77	1.010	0.76	0.134	536.0	69.3
2D00	4.62	0.809	3.75	0.657	413.4	314.8
2D50	3.87	0.678	1.25	0.219	351.6	114.7
2D75	3.53	0.617	0.61	0.107	340.4	58.1
3D00	2.49	0.436	1.95	0.342	228.6	164.0
3D50	1.95	0.341	0.66	0.115	181.5	59.5
3D75	1.77	0.310	0.30	0.052	160.7	27.7
4D00	3.70	0.647	1.99	0.349	225.4	134.0
4D50	2.62	0.459	0.54	0.094	155.7	27.5
4D75	2.36	0.413	0.39	0.069	140.9	22.1
5D00	2.19	0.384	1.68	0.294	135.8	100.8
5D50	1.84	0.322	0.60	0.105	113.2	36.4
5D75	1.45	0.255	0.29	0.050	86.6	16.4
6D00	1.33	0.232	0.78	0.136	83.8	51.0
6D50	1.06	0.185	0.31	0.054	72.9	19.2
6D75	0.84	0.148	0.14	0.024	55.0	8.6
1E00	-	-	-	-	-	-
1E50	6.08	1.066	1.66	0.290	450.1	124.8
1E75	4.48	0.785	0.6	0.111	351.7	41.9
2E00	10.87	1.903	9.34	1.634	519.1	446.1
2E50	3.48	0.610	1.19	0.208	261.4	89.1
2E75	3.09	0.541	0.45	0.079	225.9	33.5
3E00	2.55	0.447	1.79	0.313	190.3	131.9
3E50	2.09	0.366	0.68	0.119	158.6	51.7
3E75	2.09	0.366	0.27	0.046	151.1	18.7
4E00	3.45	0.604	2.43	0.426	178.6	142.3
4E50	2.87	0.502	0.98	0.171	149.9	51.5
4E75	2.38	0.417	0.48	0.084	128.8	26.1
5E00	2.56	0.448	1.75	0.306	132.8	88.8
5E50	2.13	0.374	0.67	0.118	112.6	34.0
5E75	1.58	0.277	0.36	0.063	87.5	18.8

TABLE 3.2 (continued)

Specimen	$f_c \times 10^3$		$f_t \times 10^3$		$f_c E d_o^2/d_1$	$f_t E d_o^2/d_2$
	mm/kN	in/kip	mm/kN	in/kip		
6E00	1.48	0.258	0.89	0.156	78.5	47.7
6E50	1.20	0.210	0.36	0.064	65.6	19.3
6E75	1.10	0.193	0.17	0.030	60.5	8.8
2F50	4.22	0.739	1.65	0.289	264.5	106.4
2F75	3.43	0.601	0.77	0.134	215.6	49.2
3F50	2.74	0.480	0.88	0.155	165.7	56.2
3F75	2.39	0.419	0.42	0.073	148.5	27.6
4F00	5.09	0.892	4.01	0.702	201.7	158.0
4F50	2.81	0.492	1.18	0.207	121.0	49.7
4F75	2.30	0.404	0.43	0.075	103.8	19.3
5F50	2.06	0.361	0.67	0.117	88.0	28.1
5F75	1.88	0.328	0.32	0.057	79.7	13.5
6F50	1.44	0.252	0.46	0.081	62.3	19.6
6F75	1.05	0.184	0.21	0.036	45.4	8.8
4G00	6.11	1.069	5.36	0.939	174.5	147.2
4G50	3.06	0.537	1.19	0.208	107.7	41.8
4G75	2.90	0.508	0.52	0.091	101.6	19.1
5G50	2.17	0.380	0.75	0.131	75.6	26.4
5G75	2.02	0.353	0.31	0.054	70.1	11.1
6G50	1.34	0.234	0.47	0.083	45.6	16.4
6G75	1.35	0.236	0.17	0.030	45.7	6.5
4H00	6.58	1.153	4.07	0.712	170.4	108.1
4H50	3.47	0.607	1.24	0.217	94.5	35.6
4H75	3.14	0.550	0.62	0.109	90.9	18.1
5H50	3.00	0.526	1.03	0.181	79.6	29.4
5H75	2.52	0.441	0.46	0.080	71.1	13.5
6H50	1.91	0.335	0.50	0.088	51.9	14.8
6H75	1.67	0.292	0.26	0.046	46.7	7.2

Definition of symbols.

f_c = joint compression flexibility.

f_t = joint tension flexibility.

E = Young's modulus of elasticity.

d_o = chord diameter.

d_1 = compression web diameter.

d_2 = tension web diameter.

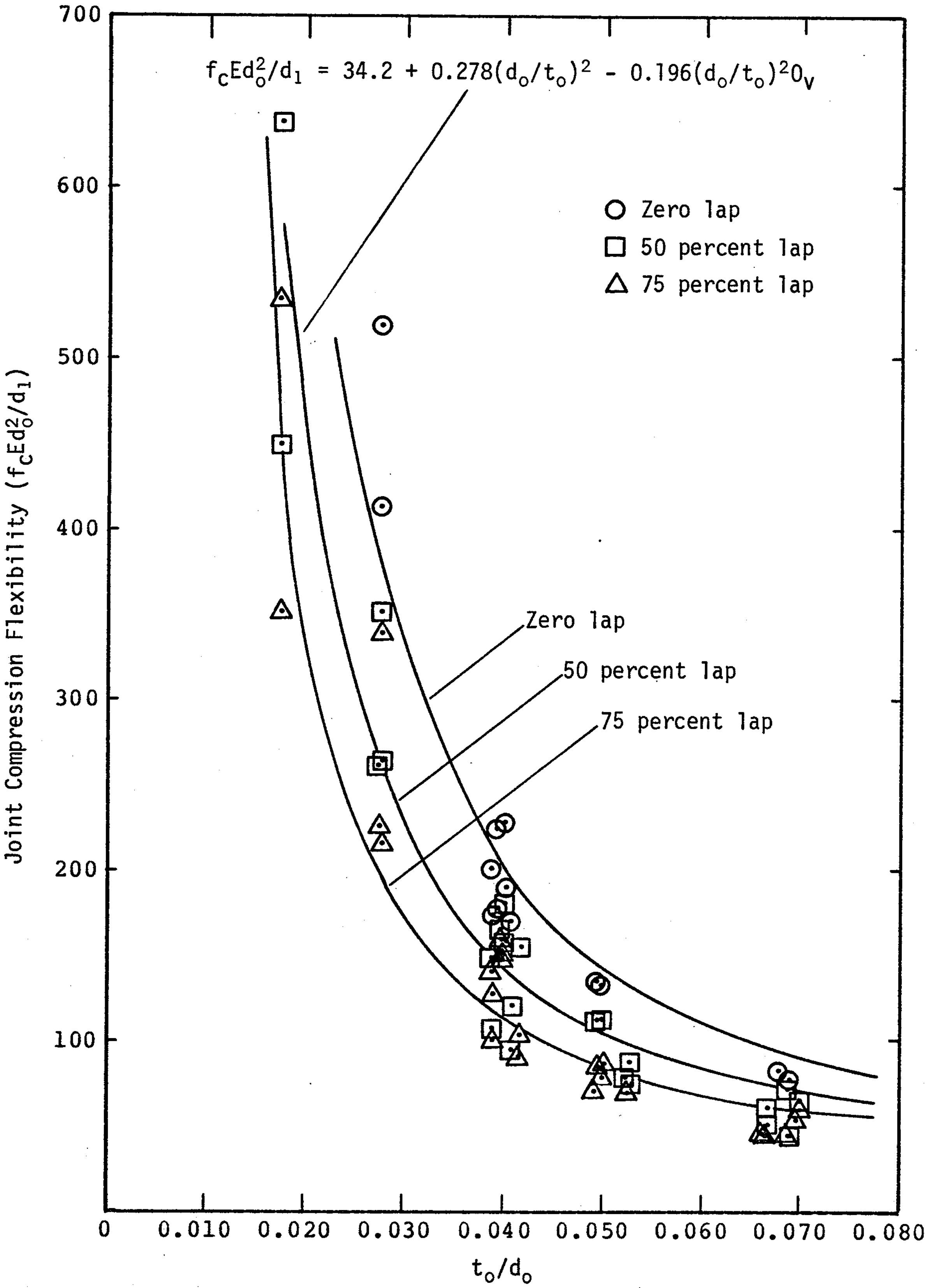

Fig. 3.14 - Influence of t_o/d_o on the Joint Compression Flexibility.

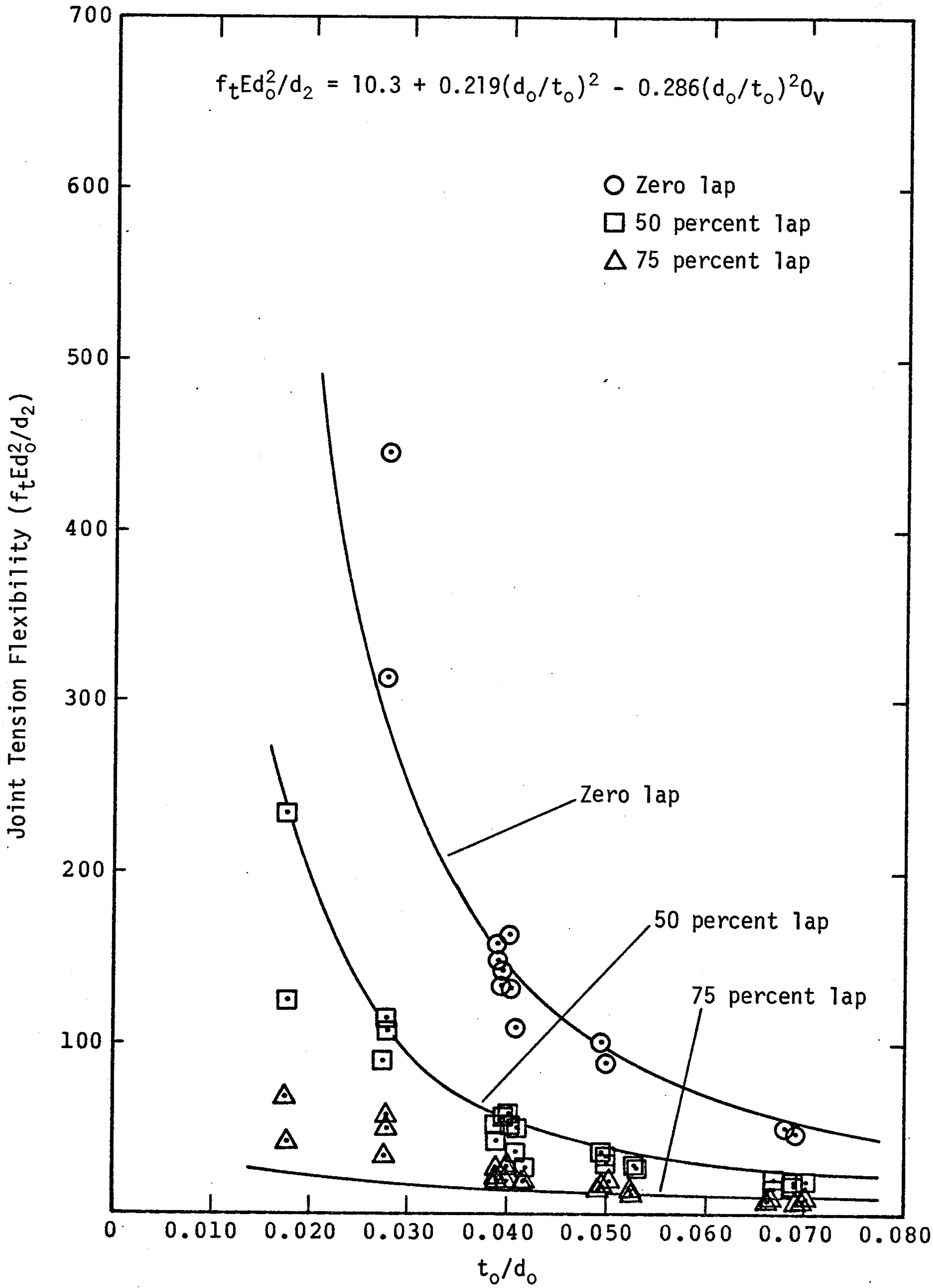

Fig. 3.15 - Influence of t_o/d_o on the Joint Tension Flexibility.

and 3.4 are illustrated in Figures 3.14 and 3.15. It can be seen that, as with the strength formula, the largest deviation occurs when t_o/d_o is small.

3.3.2) Truss Deflections

To investigate the effect of joint deformation on overall truss deflection, twelve Pratt trusses were analyzed in order to determine mid-span deflections. A common 14.6 m (48 ft.) span, a 1.83 m (6 ft.) depth, and a common load pattern (see Chapter 2, Figure 2.1) were chosen so as to accommodate all test joints and to facilitate comparison of results with those for similar cropped-web joints with square chords.

Using the method of virtual work, the mid-span deflection due to member deformation (Δ_m) was computed. Then the experimentally measured joint deformations were employed to determine the increment of deflection due to joint deformation (Δ_j). The values of Δ_m and Δ_j as well as the ratio Δ_j/Δ_m are presented in table 3.3.

To illustrate the effect of t_o/d_o on the increase in truss deflection due to joint deformation, Δ_j/Δ_m was plotted against t_o/d_o as shown in Figure 3.16. It can be seen that Δ_j/Δ_m is usually less than 20 percent but that it can become large for small t_o/d_o ratios or for zero lap joints.

Similar results for cropped-web joints involving square chords based on trusses of identical geometry, span, and load pattern presented by Theinsiripipat (1979) are shown in Figure 3.17. Clearly, cropped-web joints with square chords contribute two to three times as

TABLE 3.3

TRUSS DEFLECTIONS

Joint Type	Δ_m mm	Δ_m in.	Δ_j mm	Δ_j in.	Δ_j/Δ_m %
1D00	24.8	0.975	-	-	-
1D50	24.8	0.975	4.0	0.157	16.1
1D75	24.8	0.975	2.5	0.098	10.1
2D00	20.2	0.795	3.8	0.150	18.9
2D50	20.2	0.795	2.1	0.083	10.4
2D75	20.2	0.795	1.6	0.063	7.9
3D00	17.7	0.695	2.0	0.079	11.4
3D50	17.7	0.695	1.1	0.042	6.0
3D75	17.7	0.695	0.8	0.032	4.6
4D00	31.5	1.24	2.5	0.097	7.8
4D50	31.5	1.24	1.2	0.049	4.0
4D75	31.5	1.24	1.1	0.042	3.4
5D00	29.0	1.14	1.8	0.069	6.1
5D50	29.0	1.14	1.0	0.039	3.4
5D75	29.0	1.14	0.7	0.027	2.4
6D00	26.2	1.03	0.9	0.036	3.5
6D50	26.2	1.03	0.6	0.022	2.1
6D75	26.2	1.03	0.4	0.015	1.5
1E00	20.0	0.789	-	-	-
1E50	20.0	0.789	3.1	0.123	15.6
1E75	20.0	0.789	2.0	0.077	9.8
2E00	15.4	0.608	9.3	0.365	60.0
2E50	15.4	0.608	1.9	0.076	12.5
2E75	15.4	0.608	1.4	0.054	8.9
3E00	12.9	0.508	1.9	0.076	15.0
3E50	12.9	0.508	1.1	0.045	8.9
3E75	12.9	0.508	0.9	0.035	6.9
4E00	28.4	1.12	2.6	0.104	9.3
4E50	28.4	1.12	1.6	0.062	5.5
4E75	28.4	1.12	1.1	0.044	3.9
5E00	25.9	1.02	1.9	0.076	7.5
5E50	25.9	1.02	1.1	0.045	4.4
5E75	25.9	1.02	0.8	0.030	2.9

TABLE 3.3 (continued)

Joint Type	Δ_m mm	Δ_m in.	Δ_j mm	Δ_j in.	Δ_j/Δ_m %
6E00	23.1	0.911	1.0	0.041	4.5
6E50	23.1	0.911	0.6	0.025	2.7
6E75	23.1	0.911	0.5	0.019	2.1
2F50	15.1	0.594	2.5	0.065	10.9
2F75	15.1	0.594	1.7	0.065	10.9
3F50	12.6	0.496	1.5	0.058	11.7
3F75	12.6	0.496	1.1	0.043	8.7
4F00	25.7	1.01	4.1	0.163	16.1
4F50	25.7	1.01	1.7	0.066	6.5
4F75	25.7	1.01	1.1	0.042	4.2
5F50	21.7	0.853	1.1	0.044	5.2
5F75	21.7	0.853	0.9	0.034	4.0
6F50	19.7	0.774	0.8	0.031	4.0
6F75	19.7	0.774	0.5	0.019	2.5
4G00	20.4	0.804	5.3	0.208	25.9
4G50	20.4	0.804	1.8	0.070	8.7
4G75	20.4	0.804	1.3	0.052	6.5
5G50	17.0	0.669	1.2	0.047	7.0
5G75	17.0	0.669	0.9	0.035	5.2
6G50	15.0	0.590	0.8	0.030	5.1
6G75	15.0	0.590	0.6	0.023	3.9
4H00	19.1	0.753	4.7	0.185	24.6
4H50	19.1	0.753	2.0	0.077	10.2
4H75	19.1	0.753	1.5	0.058	7.7
5H50	17.1	0.672	1.7	0.066	9.8
5H75	17.1	0.672	1.2	0.046	6.8
6H50	13.0	0.511	1.0	0.038	7.4
6H75	13.0	0.511	0.7	0.029	5.7

Definition of symbols.

Δ_m = truss deflection due to member deformation.

Δ_j = truss deflection due to joint deformation.

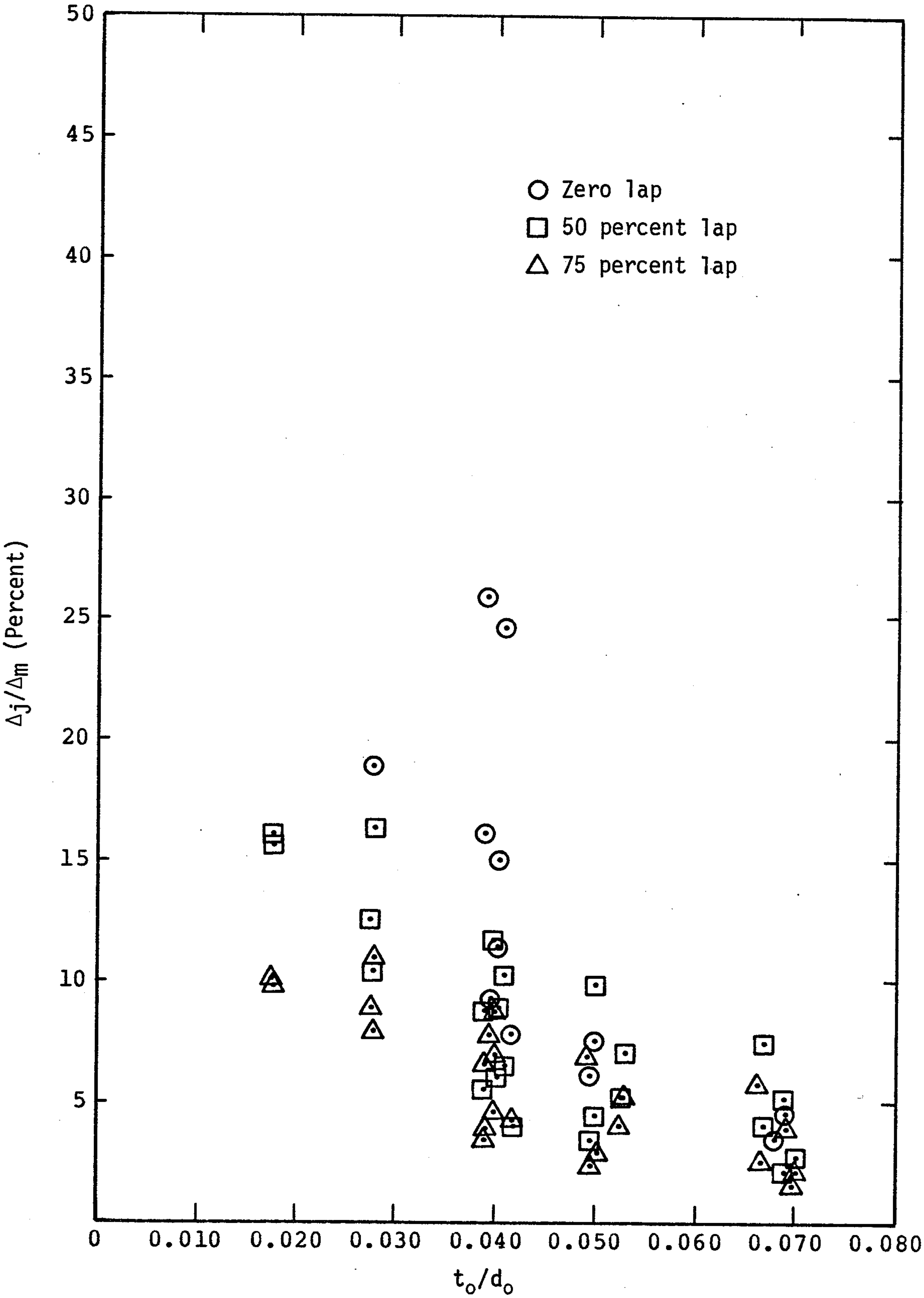

Fig. 3.16 - Percent increase in truss deflection due to joint deformation.

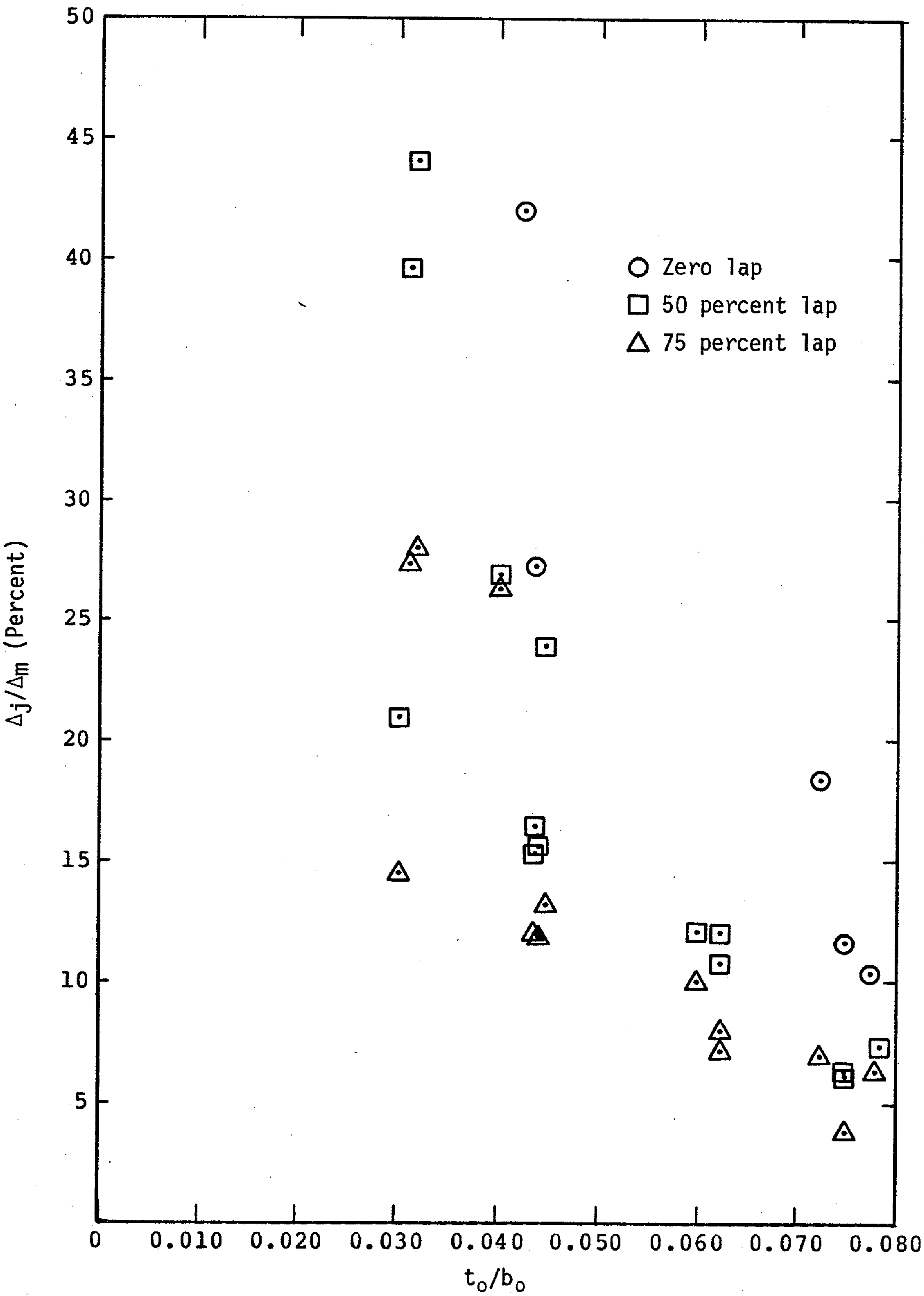

Fig. 3.17 - Percent increase in truss deflection due to joint deformation. (Square Chords, Thiensiripipat 1979)

much to truss deflection as do cropped-web joints with round chords.

The values of Δ_j/Δ_m shown in Figure 3.16 represent an extreme case because of the relatively large depth-to-span ratio chosen for the truss. If the span were increased without a change in the load pattern, the increase in Δ_m would be greater than the increase in Δ_j. As a result, for smaller depth-to-span ratios, the effect of joint deformation on overall truss deflection would be even less significant.

3.4) Joint Deformation

3.4.1) General Behaviour

The load-deformation behaviour for specimen 4E50, shown in Figure 3.18, was typical of the majority of specimens that experienced joint-member failures. The onset of local chord wall yielding in the vicinity of the joint resulted in the increasingly non-linear load-deformation behaviour indicated. Specimens which experienced joint failures generally displayed similar load-deformation behaviour to that shown in Figure 3.18, up to the ultimate load. However, at the ultimate load sudden fracture and loss of capacity occurred. Member failures displayed only the linear portion of the load-deformation plot shown in Figure 3.18.

Figure 3.19 illustrates the in-plane joint deformations for specimen 4E50 for various load levels. In conjunction with Figure 3.18, it can be seen that, in the linear range, the chord wall deformations beneath the compression and tension webs were approximately equal in magnitude and opposite in direction. In addition, the chord face exhibited a characteristic inflection point about which the joint rotated at the base

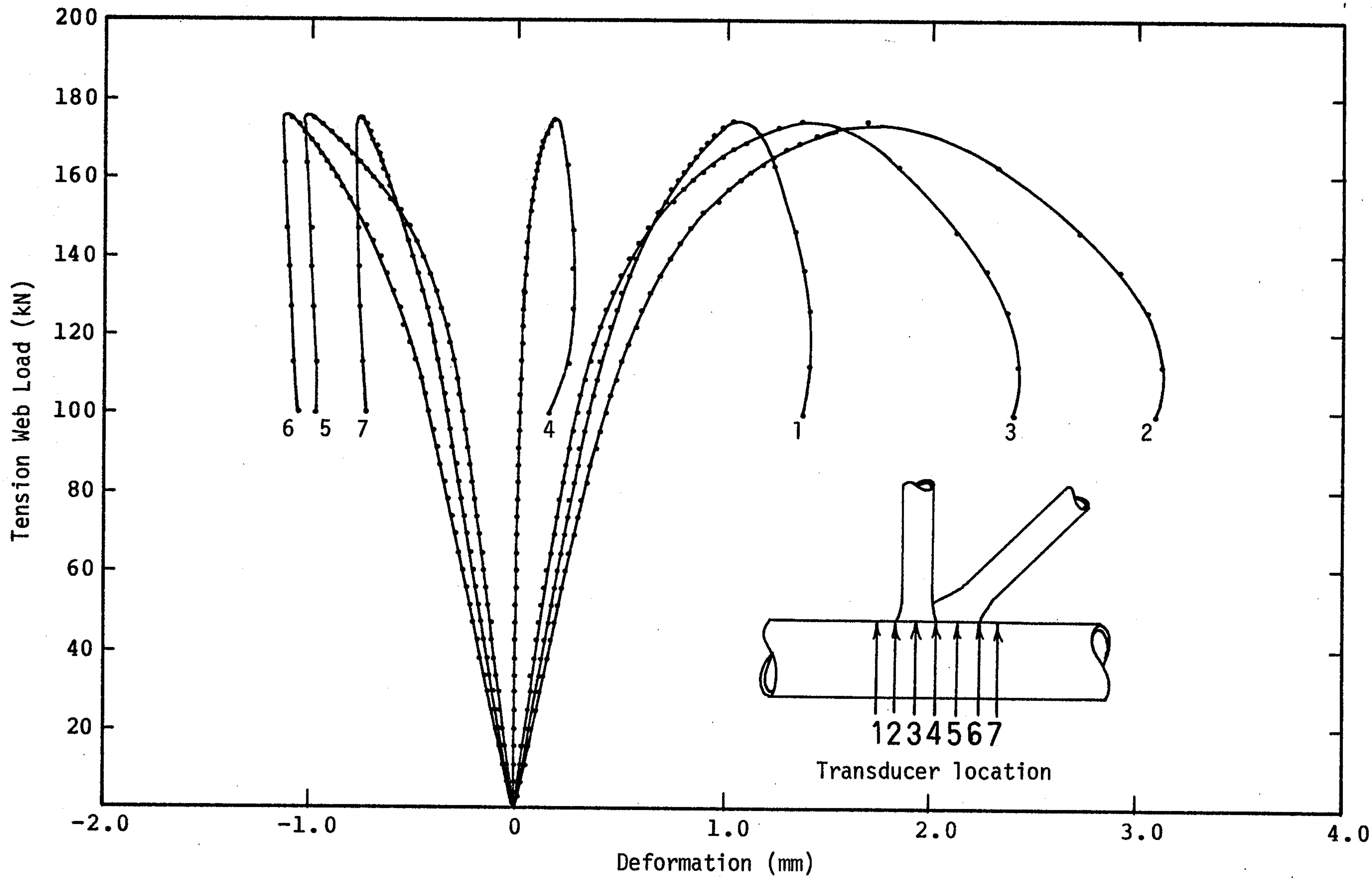

Fig. 3.18 - Typical load-deformation behaviour of chord wall - Specimen 4E50.

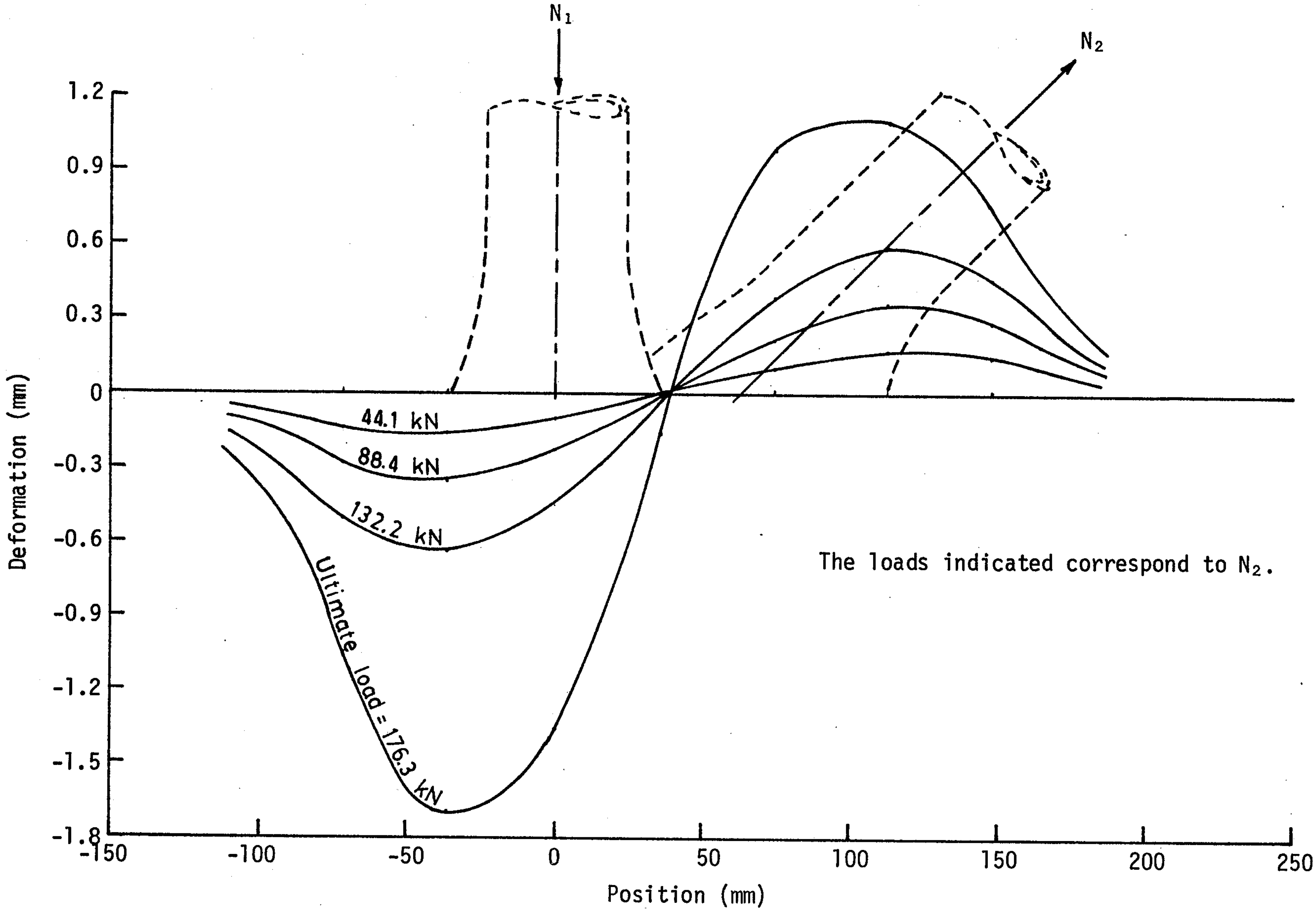

Fig. 3.19 - Deformation of chord wall - Specimen 4E50.

of the web interconnection. This was observed for all specimens.

In the non-linear range, the chord wall deformations became excessive at the base of the compression web, while beneath the tension web they were relatively small. The inflection point tended to translate toward the axis of the chord. However, the deformations beneath the compression and tension webs relative to this point generally continued to be approximately equal in magnitude and opposite in direction. Joint deformations in specimens that involved extremely thin walled chords behaved non-linearly at early load stages. In these cases, particularly for specimens 1D50, 1D75, 1E50, and 1E75, the chord wall deformations were dominated by joint translation.

As illustrated in Figure 3.20, specimens 1D00, 1E00, 2D00, 2E00, 3E00, 4G00, and 4H00, displayed a load-deformation behaviour which was somewhat different to that normally observed. The flat segments of the load-deformation curves corresponded to longitudinal yielding of the chord wall and toe of the tension web at the crotch between the web members. As this area strain-hardened, the load continued to increase until a sudden fracture occurred. This behaviour occurred in zero lap joints when the flexibility of the webs was relatively small compared to that of the chord wall. As a result, these joints tended to behave less as a unit than did the others.

3.4.2) Influence of t_o/d_o

The effect of the t_o/d_o ratio on joint deformation is illustrated in Figure 3.21, which shows chord face deformation for specimens 4E50, 5E50, and 6E50. These specimens were similar except for their t_o/d_o

ratios. Because the joint deformation is dependent upon the local bending resistance of the chord wall, an increase in its thickness or a decrease in the chord diameter would be expected to reduce the deformation. It can be seen that the joint deformation did in fact decrease as t_o/d_o increased.

3.4.3) Influence of d_1/d_o

An increase in d_1/d_o, resulting from an increase in the web diameter, improved the load distribution on the chord face. It also resulted in an increase in the moment arm between the axes of the webs at the chord wall. This produced an increase in the joint moment. These two factors tended to nullify one another and to lead to small, inconsistent variations in the maximum chord wall deformations in the linear range, as illustrated in Figure 3.22. This behaviour was not consistent with that of profiled-web joints. For them, an increase in d_1/d_o allowed more load to be transferred directly to the side walls of the chord and thus reduce the chord wall deformations.

Furthermore, an increase in d_1/d_o generally extended the linear range of the joint. This was due mainly to the fact that an increase in web diameter, and thus in the bending capacity of the webs, resulted in a rotationally less flexible joint. An increase in web diameter also resulted in a longer direct connection between the webs, for the same percentage of web lap. This permitted more transfer of load directly through the web interconnection. Unlike conventional profiled-web joints, the web load in a cropped-web joint is concentrated longitudinally along the chord, equidistant from the chord side walls.

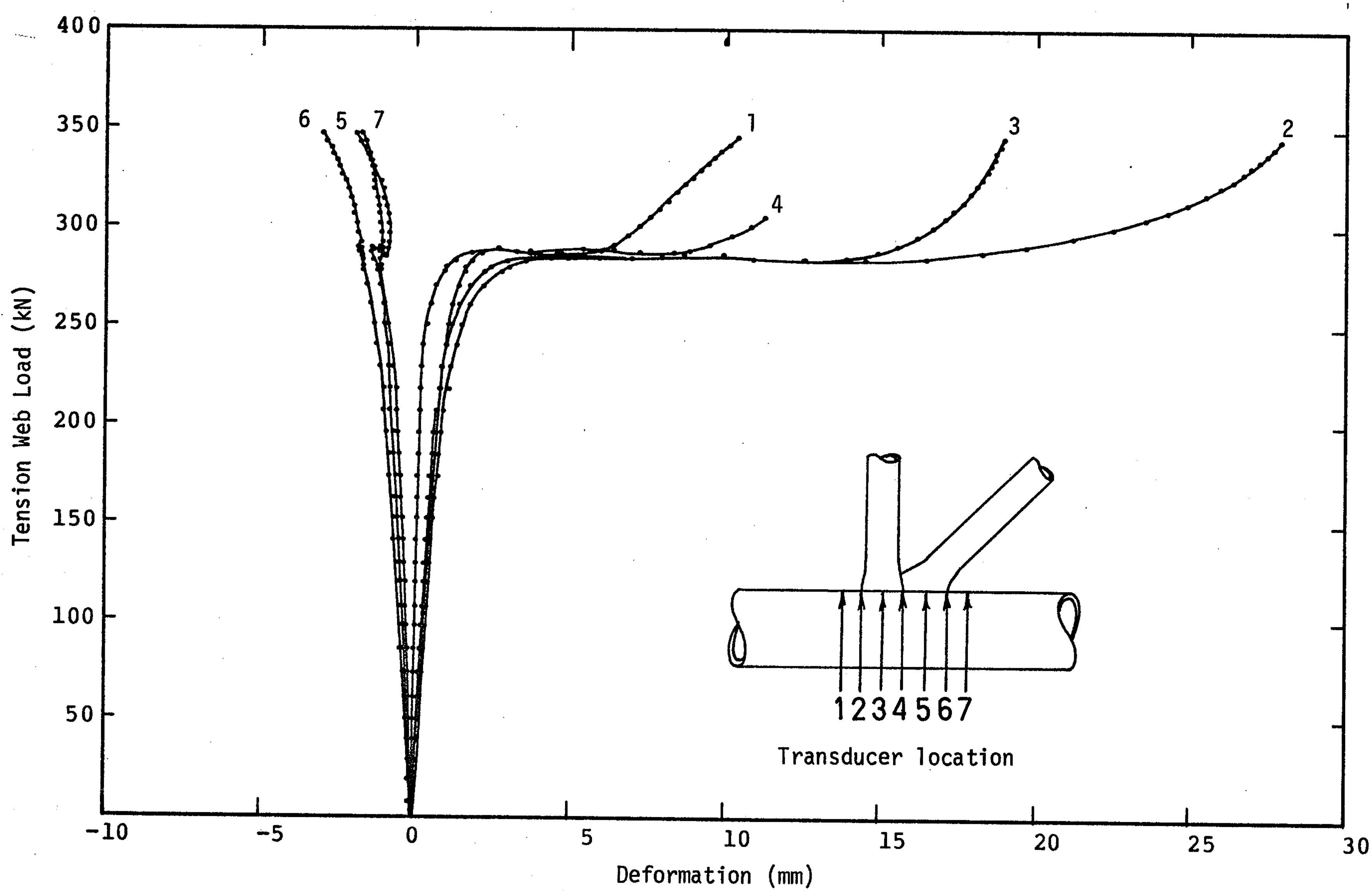

Fig. 3.20 - Load-deformation behaviour of specimen 3E00.

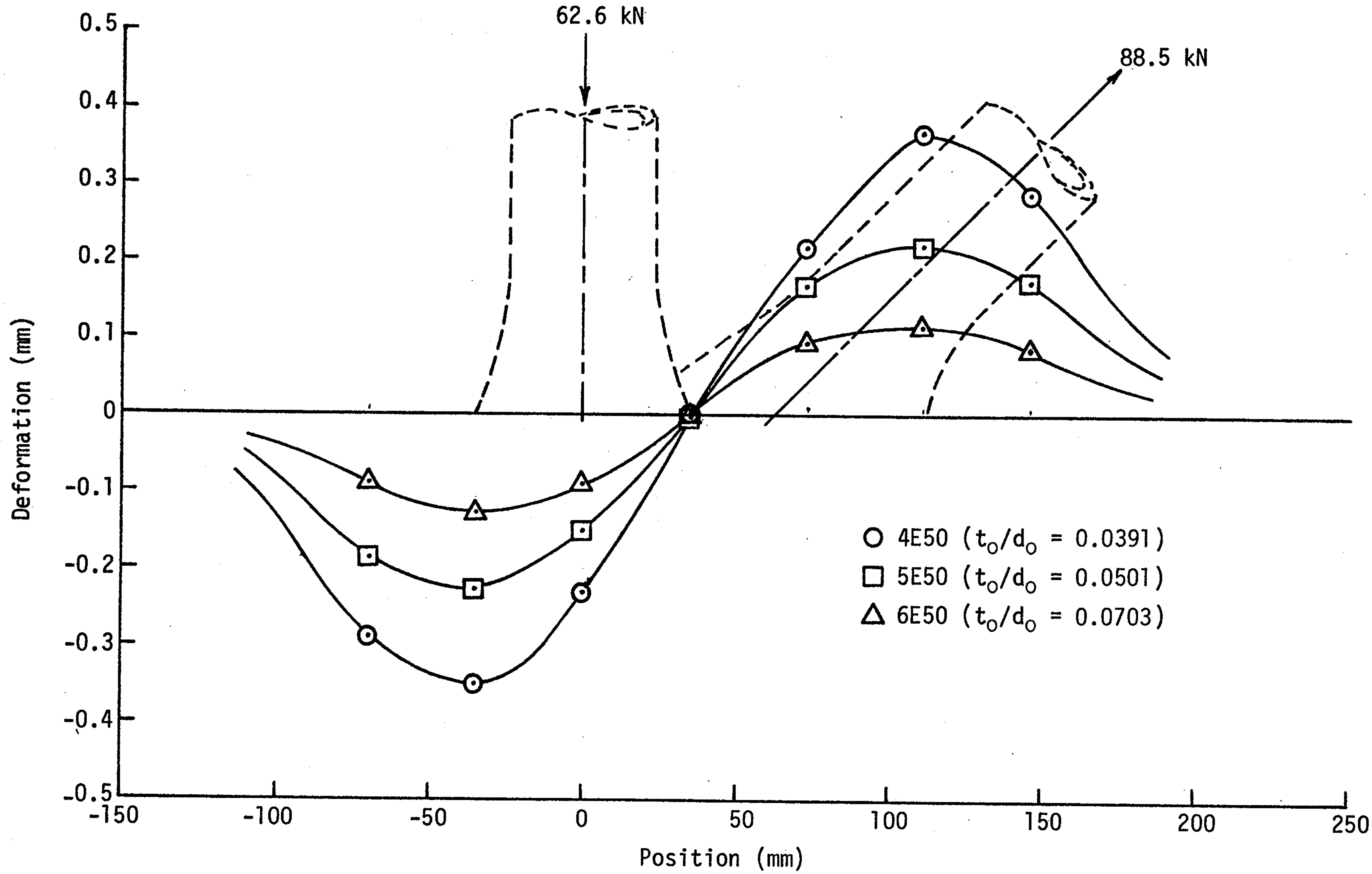

Fig. 3.21 - Influence of t_o/d_o on chord wall deformation.

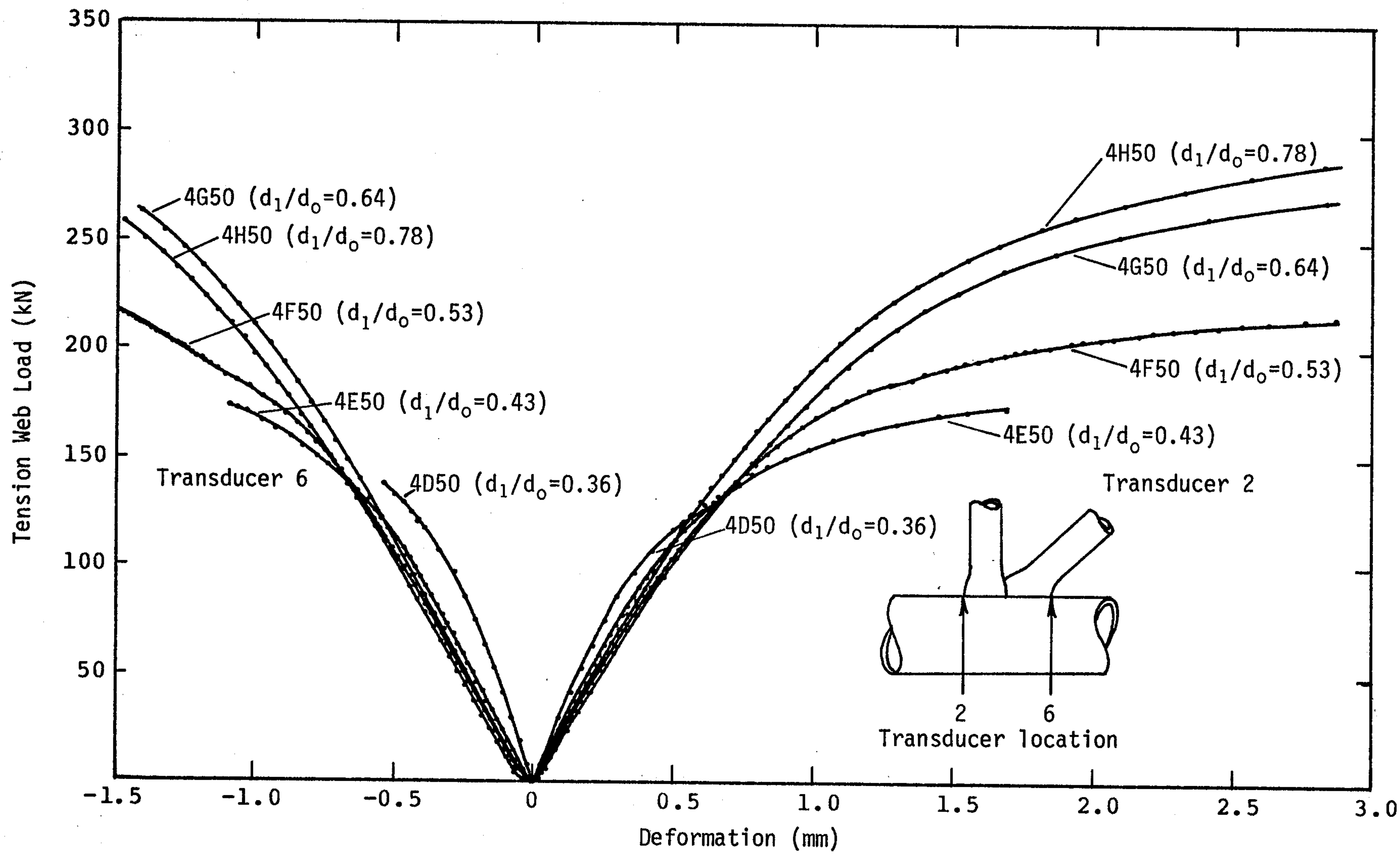

Fig. 3.22 - Influence of d_1/d_o on chord wall deformation.

This resulted in the preservation of the joint ductility as d_1/d_0 was increased.

3.4.4) Influence of Compression Web Slenderness

A parameter which was found to affect joint performance, but which was not examined explicitly in previous investigations, is the bending resistance of the compression web. The chord wall deformation was associated with rotation of the chord face at the joint, which was influenced by the flexibility of the web members. The less flexible the web members, the smaller the chord face deformations.

The slenderness ratio of the compression web provides a reasonable measure of the web member flexibility. A comparison of joint deformations for specimens 3E50 and 4E50, which were similar except for the L_1/r_1 ratios of their webs, is presented in Figure 3.23. The joint deformations can be seen to decrease with a decrease in L_1/r_1. Again, an increase in the web diameter to produce a decrease in L_1/r_1 resulted in an increase in the length of the direct connection between the webs.

3.4.5) Influence of Web Lap

Figure 3.24 illustrates the typical influence of web lap on the joint deformations, using specimens 4G00, 4G50, and 4G75, as examples. The larger direct connection between the webs (for the 50 percent and 75 percent lap specimens) extended the linear load-deformation range of the joint. Furthermore, an increase in web lap reduced the distance between the axes of the incident web members at the chord

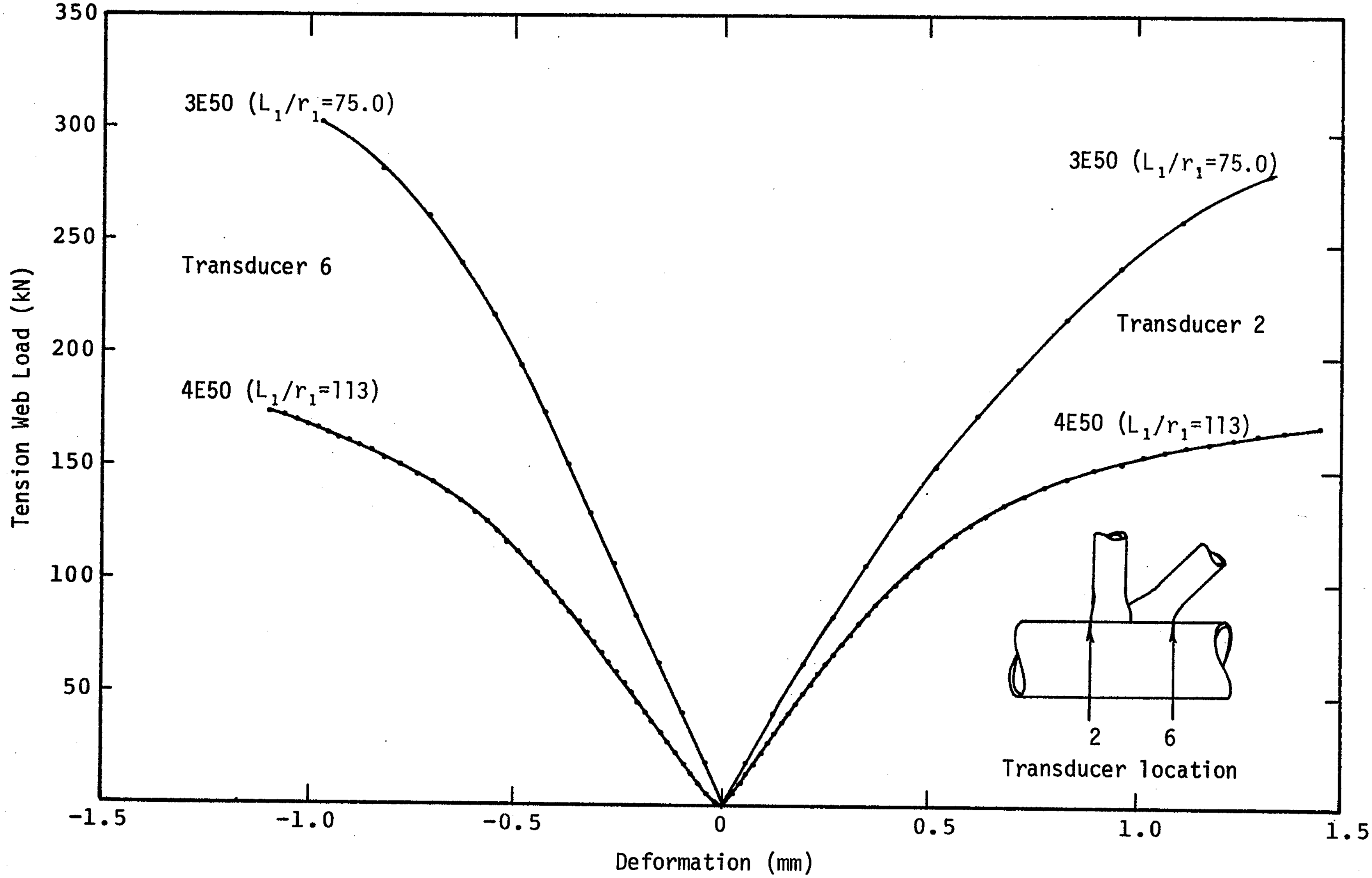

Fig. 3.23 - Influence of L_1/r_1 on chord wall deformation.

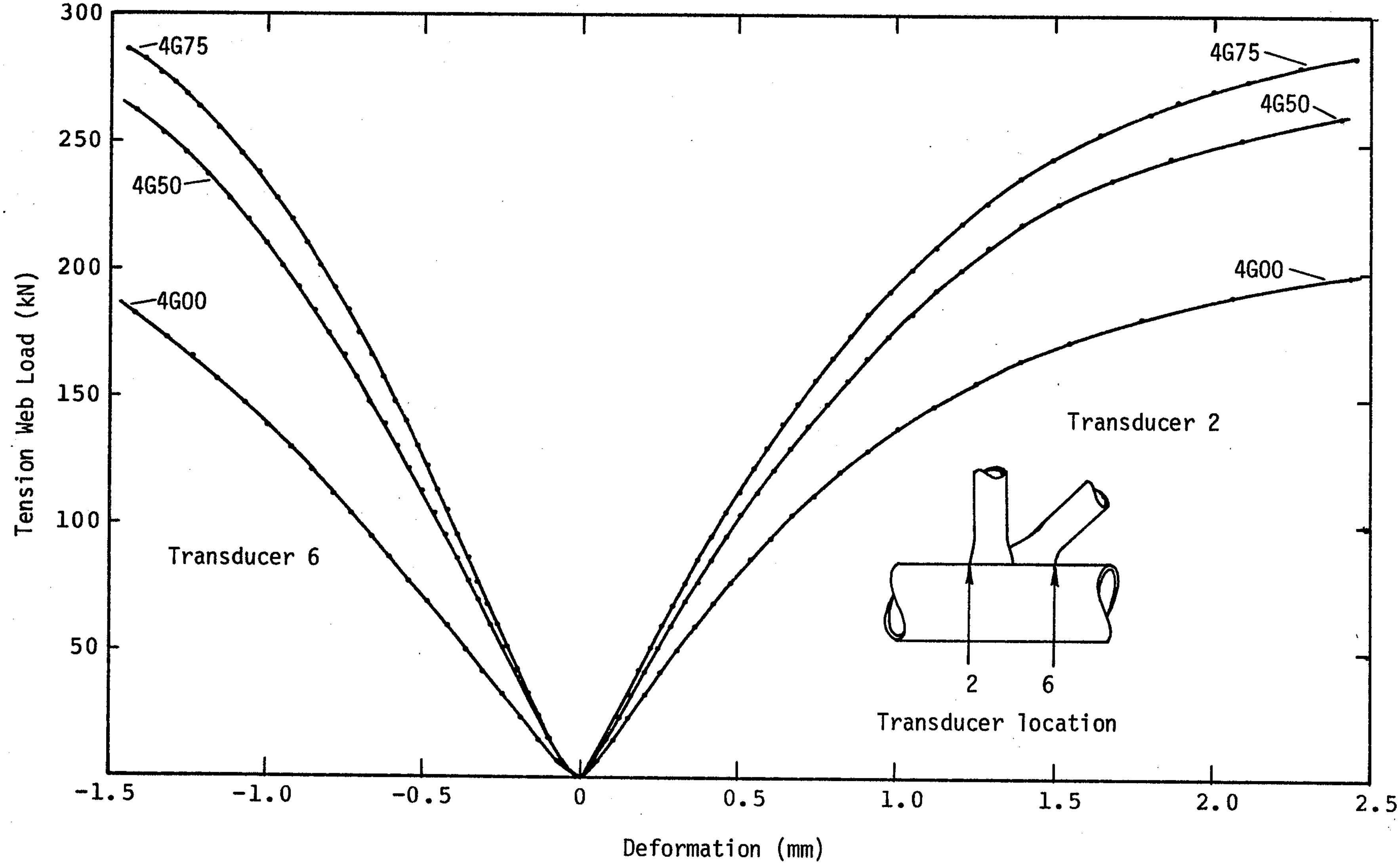

Fig. 3.24 - Influence of web lap on chord wall deformation.

wall. This reduced the applied joint moment and usually resulted in a decrease in joint deformations in the linear load-deformation range.

3.5) Buckling of the Compression Web

Compression web buckling failures were observed in 37 of the 61 test specimens. Because of the large in-plane joint moments, the buckling consistently occurred in the plane of the specimen. In addition, the specimen support conditions accommodated in-plane buckling while they hindered out-of-plane buckling.

The compression web buckling was inelastic in nature, as the L_1/r_1 ratios for the compression webs in the specimens ranged from 30-67.

Buckling failure was characteristic of both joint--member and member type failure modes. In joint--member failures, however, it occurred prematurely because of large end-moments created by excessive chord wall deformation. Consequently, the compression web typically bent slowly away from the tension web as the ultimate load was approached and buckling usually followed. Figure 3.25 illustrates a buckling failure of this type.

In a member failure in which the compression web buckled, it behaved as a column with a pinned support at one end and fixed support at the other, as shown in Figure 3.26(a). When the buckling load was reached, the maximum chord face deformation at the base of the compression web was usually smaller than one percent of the chord diameter. As a result, the end-moment applied to the compression web was small. Thus, buckling could occur in either direction in the plane of the specimen, as was evidenced in specimens 3D75, 5D50, 6D75,

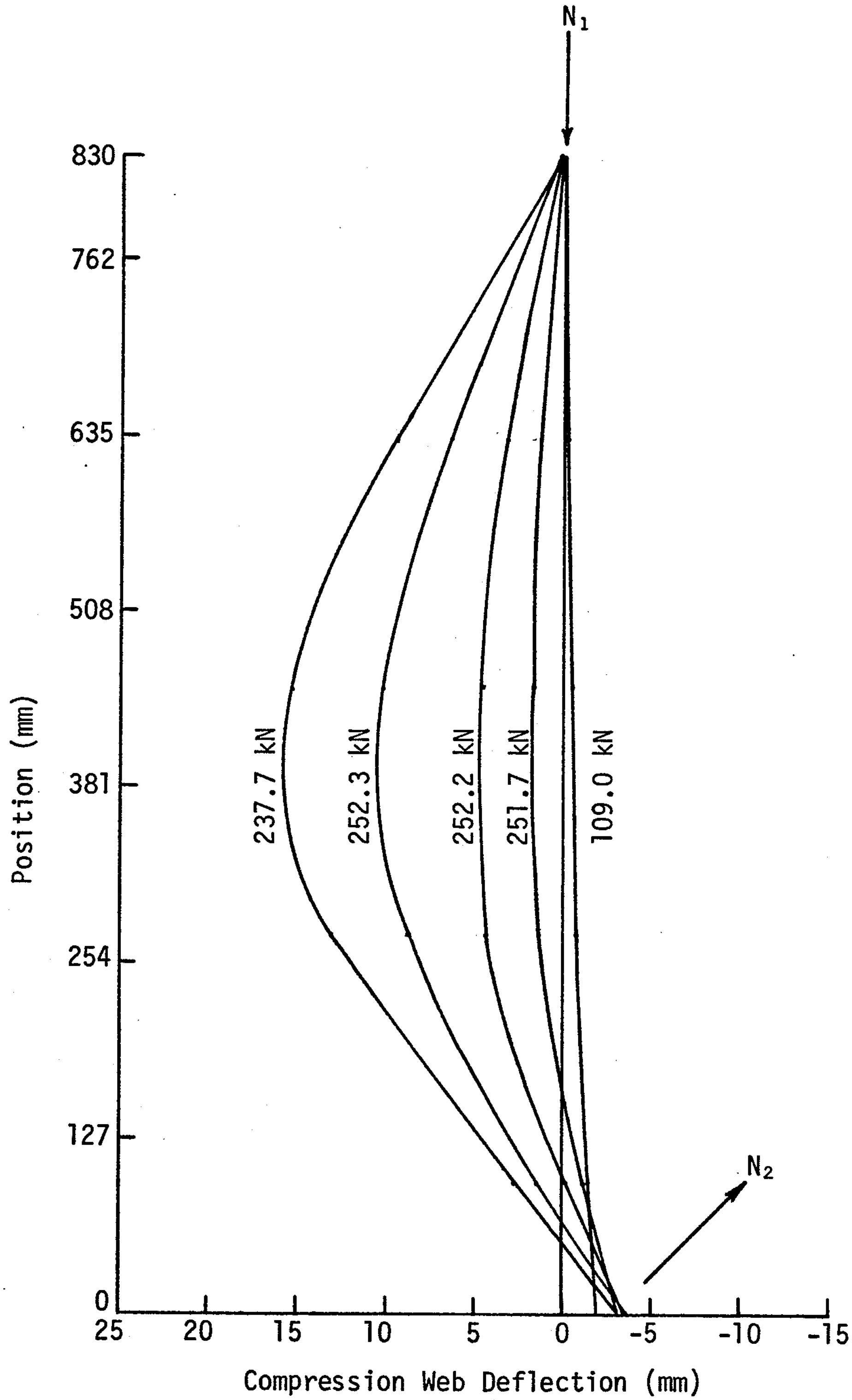

Fig. 3.25 - Compression web buckling for specimen 3E50.

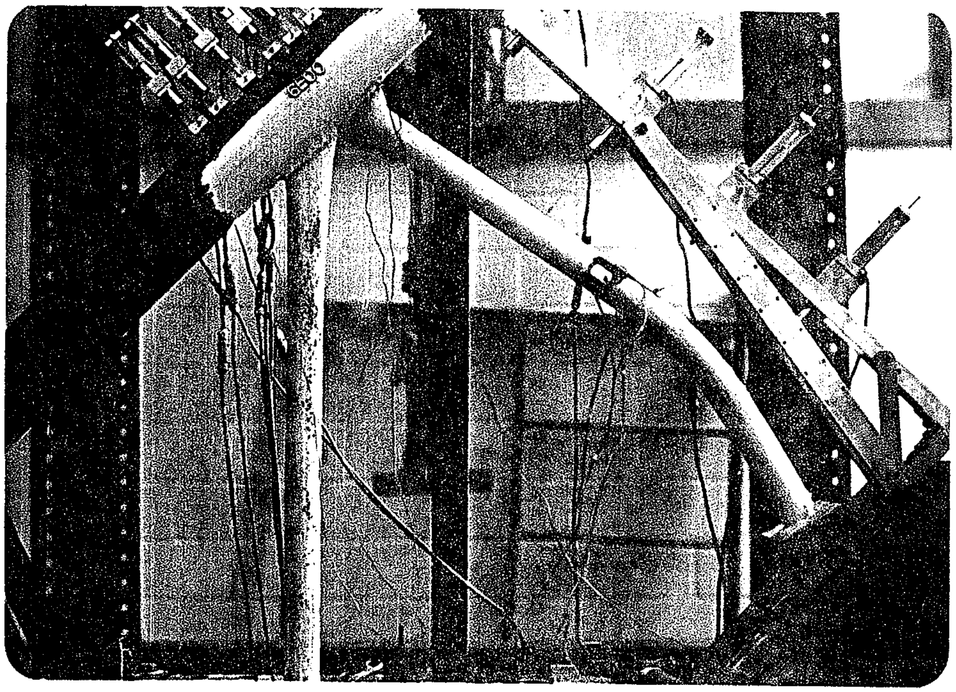

a) Buckling of compression member - Specimen 6E00.

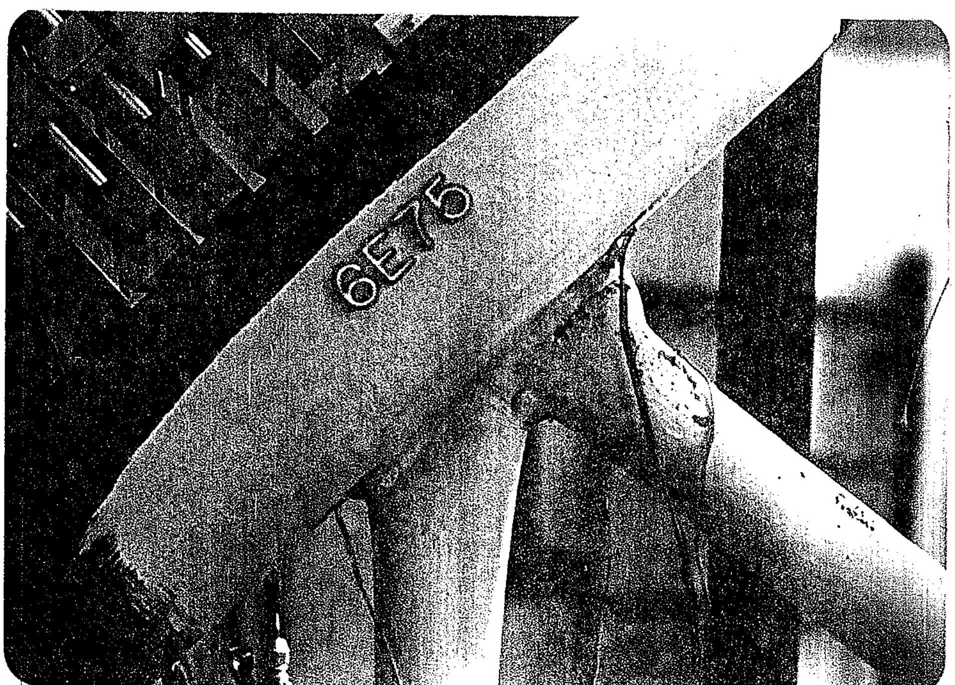

b) Web crippling - Specimen 6E75.

Fig. 3.26 - Compression web buckling failures.

6F75 and 5E00.

Several of the 3.50-inch diameter compression webs experienced a local wall crippling at the cropped-end due to stress concentrations caused by the geometry of the cropped-end. CSA Standard S16.1 states that for circular hollow sections, local buckling should not be a problem providing d_1/t_1 is less than or equal to $2600/F_y$, where d_1 and t_1 are the compression web diameter and thickness, respectively, and F_y is the material yield strength. The tests suggest, however, that for cropped-web members, the d_1/t_1 ratio should be smaller than $1000/F_y$ to ensure that a local buckling failure does not occur at the cropped end.

Post-buckling behaviour in member failures was also characterized by compression web crippling near the joint opposite the web interconnection, as shown in Figure 3.26(b).

3.6) Circumferential Chord Strains

As illustrated for specimen 4E75 in Figures 3.27 and 3.28, the circumferential strain was approximately zero adjacent to the interconnection of the webs and it gradually increased along the base of the joint, to a maximum at the joint extremities. Figure 3.27 shows that the chord strains were proportional to the applied load, up to the approximate yield strain of the chord material.

In the elastic range of the chord material, the joint tended to rotate as a unit, with approximately equal maximum circumferential chord strains at the joint extremities. However, as these strains approached yield magnitude, the chord wall became unstable beneath the compression web and large deformations resulted. Beneath the tension web, chord wall stability was not a problem, and the deformations remained small. Furthermore, as the webs rotated at the joint, the web loading enhanced further rotation in the compression web but it hindered the rotation of the tension web. This behaviour caused the circumferential chord strains to be largest adjacent to the compression web. This is illustrated in Figures 3.27 and 3.28.

The circumferential chord strain distributions at cross-sections corresponding to the joint extremities are indicated in Figures 3.29(a) and 3.29(b). It can be seen that the maximum circumferential strains occurred at the loaded chord face. The strains decreased substantially within an inch of the joint, changing from compression to tension. Figures 3.29(a) and 3.29(b) illustrate that inflection points occurred at 25 to 30 degrees from the vertical. These inflection points remained virtually stationary in the linear range.

The influence of the various joint parameters on circumferential chord strain was similar to their effect on chord deformation, since both were related to local chord wall bending. Figures 3.30, 3.31, 3.32 and 3.33 show the typical variation in circumferential chord strain as it was influenced by the joint parameters, t_o/d_o, d_1/d_o, L_1/r_1, and web lap, respectively.

In general, an increase in t_o/d_o produced the most significant reduction in chord strains. An increase in web lap usually resulted in a small decrease in chord strain.

The effect of d_1/d_o on the maximum circumferential strain was generally small and inconsistent. However, a decrease in L_1/r_1 usually decreased the circumferential chord strains.

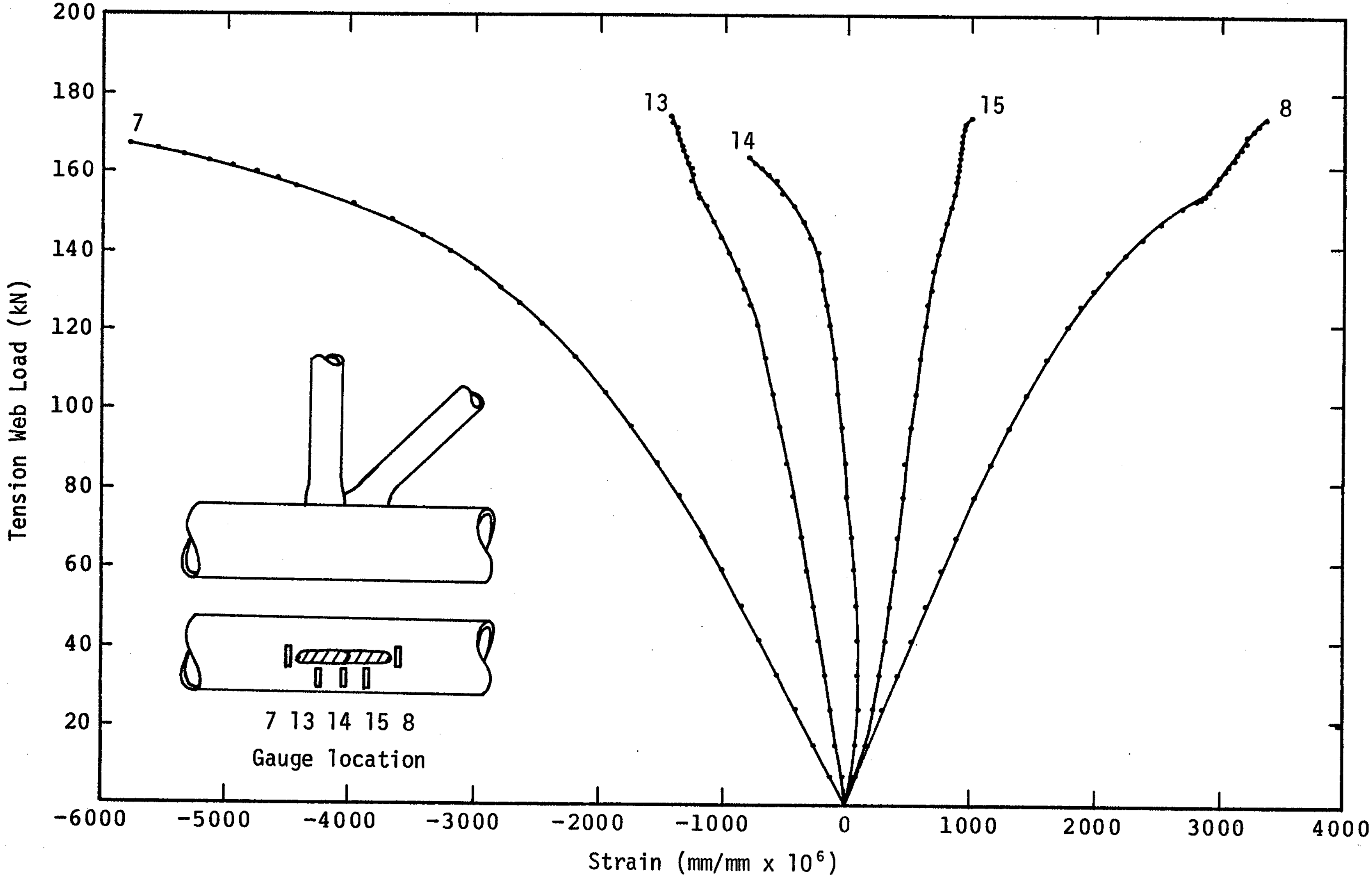

Fig. 3.27 - Circumferential chord strains - Specimen 4E75.

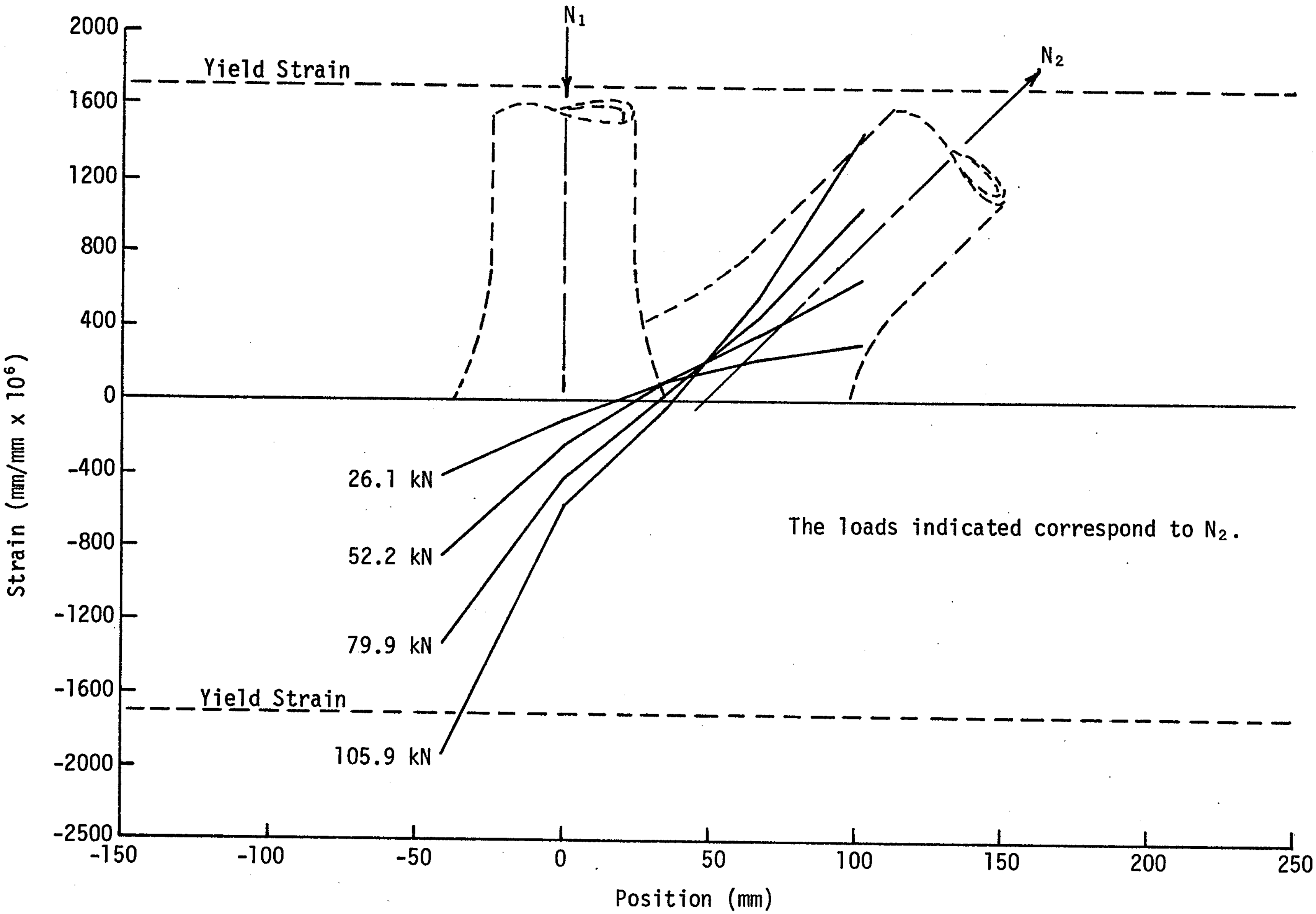

Fig. 3.28 - Circumferential chord wall strains - Specimen 4E75.

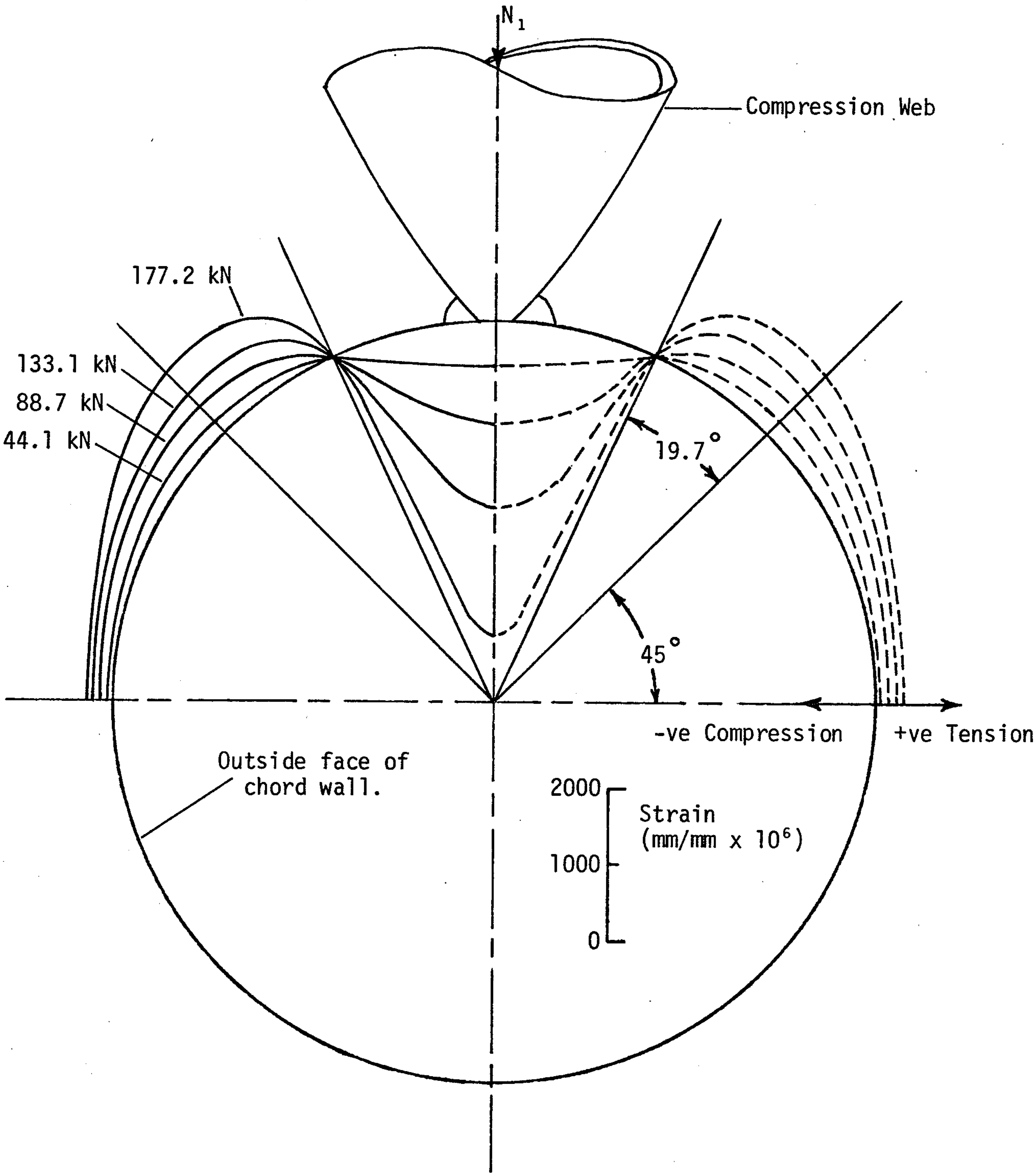

——— Measured strains on outside face of chord wall.

- - - - Assumed symmetrical compliment.

Fig. 3.29(a) - Circumferential chord strain distribution for a chord section next to the compression web - Specimen 4G50.

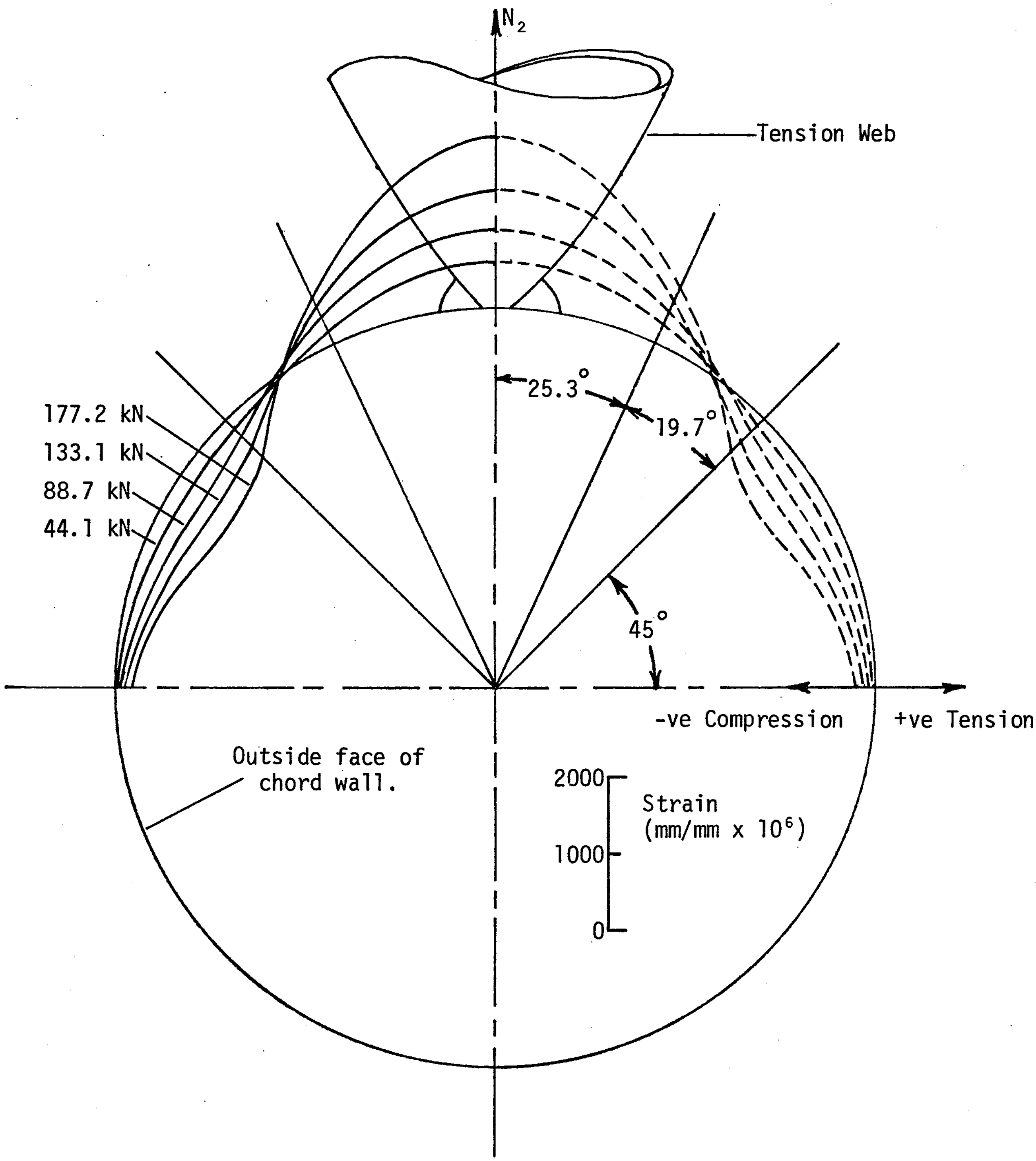

——— Measured strains on outside face of chord wall.

- - - - Assumed symmetrical compliment.

Fig. 3.29(b) - Circumferential chord strain distribution for a chord section next to the tension web - Specimen 4G50.

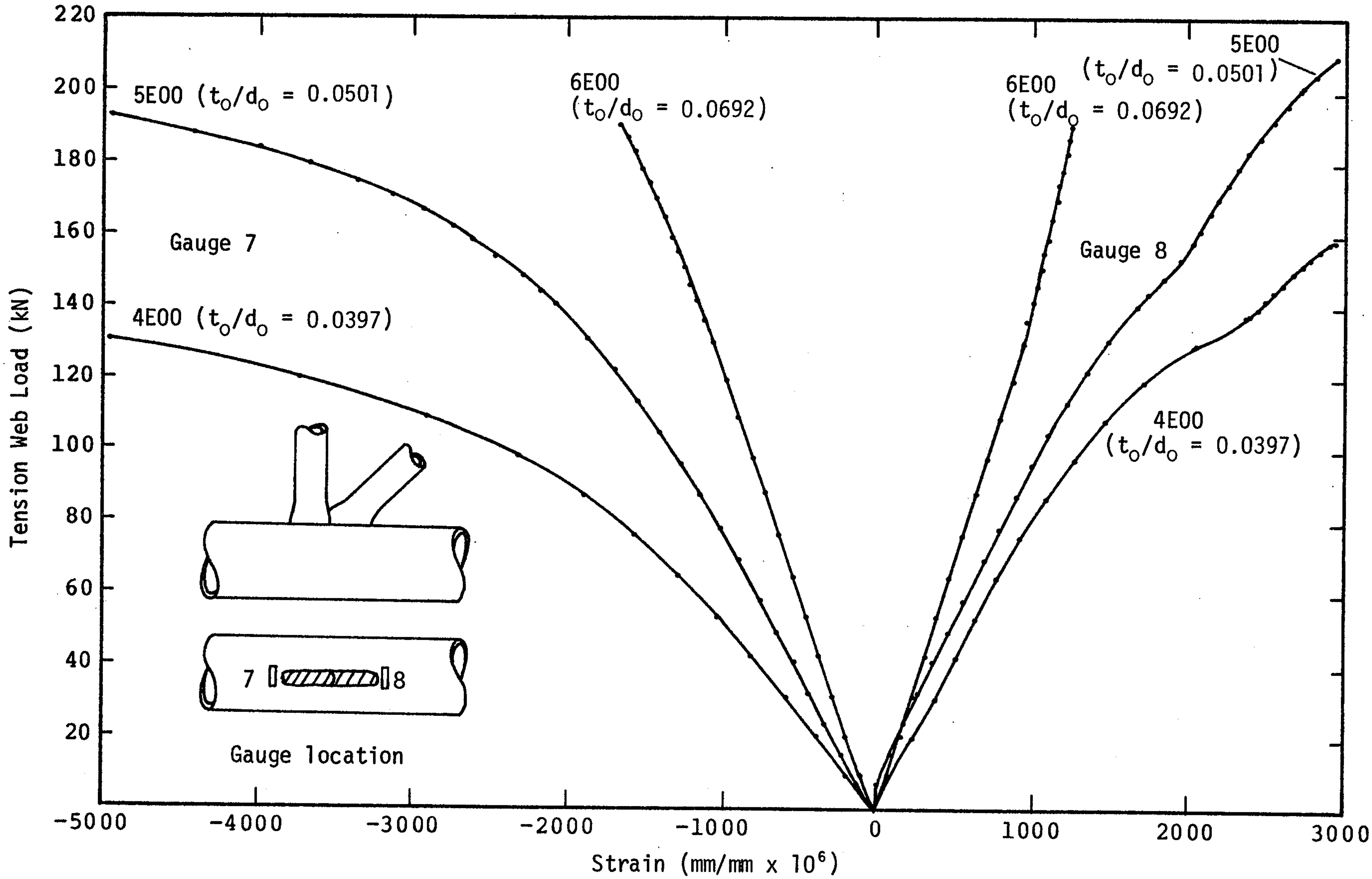

Fig. 3.30 - Influence of t_o/d_o on circumferential chord strain.

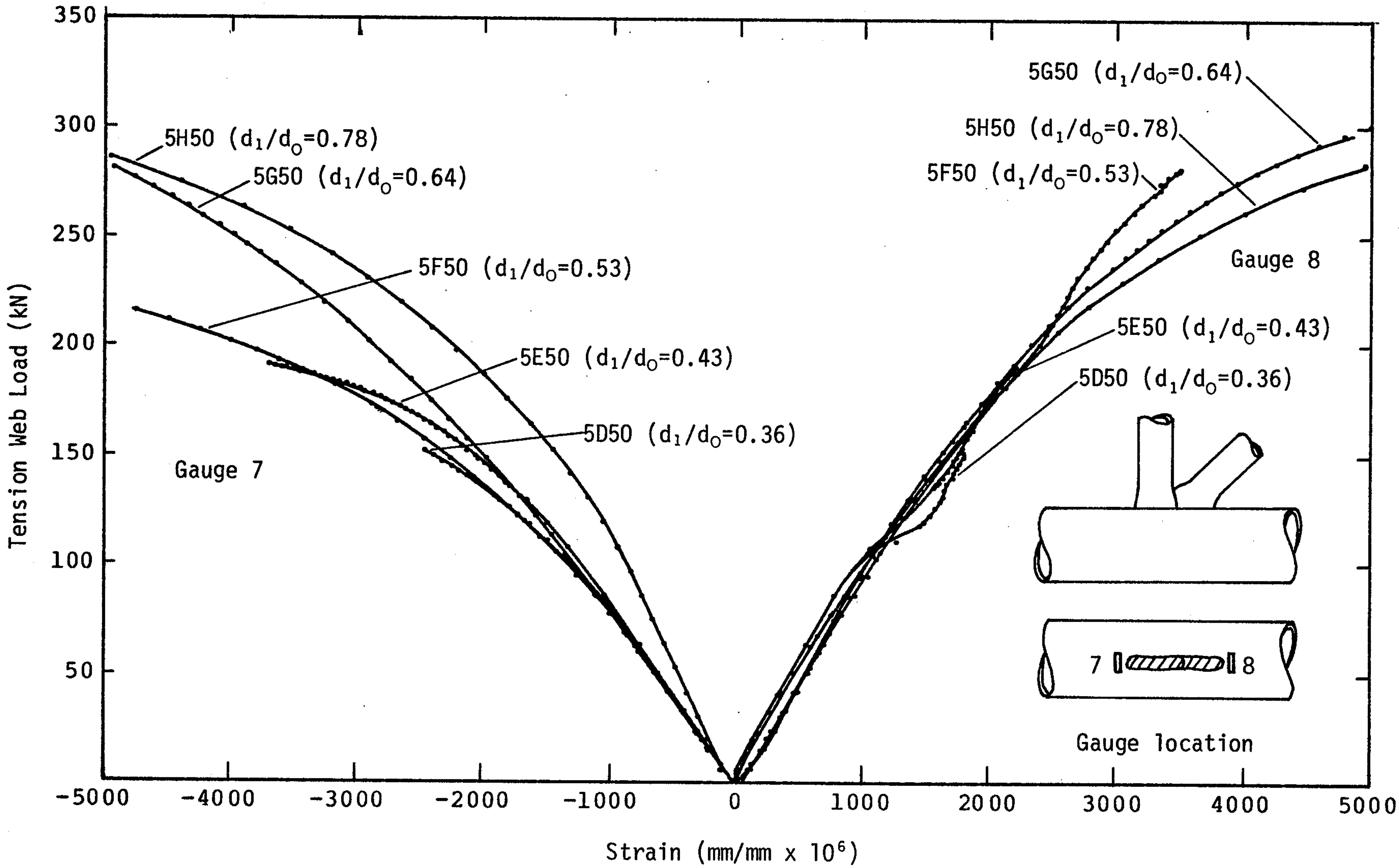

Fig. 3.31 - Influence of d_1/d_o on circumferential chord strain.

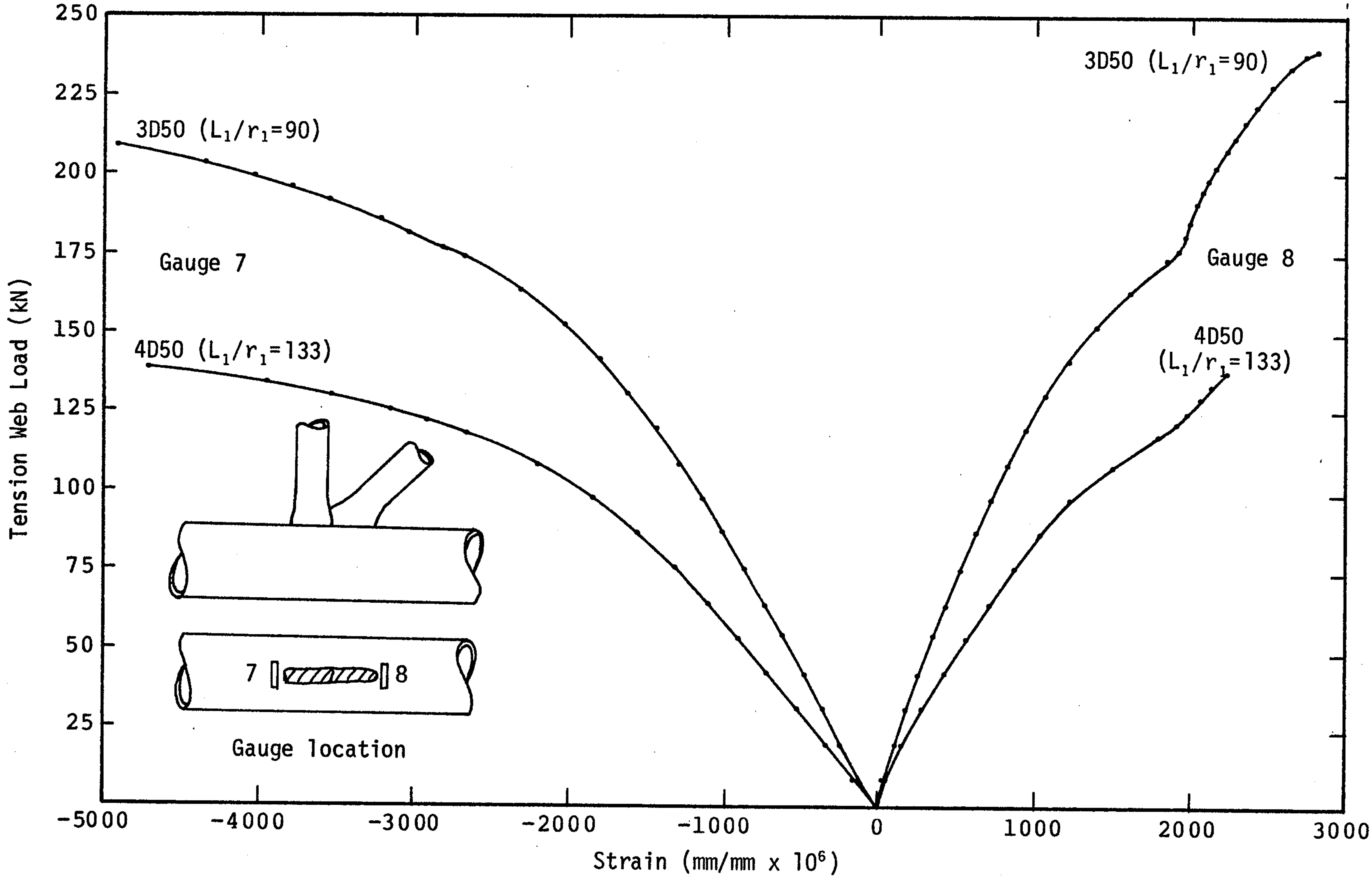

Fig. 3.32 - Influence of L_1/r_1 on circumferential chord strain.

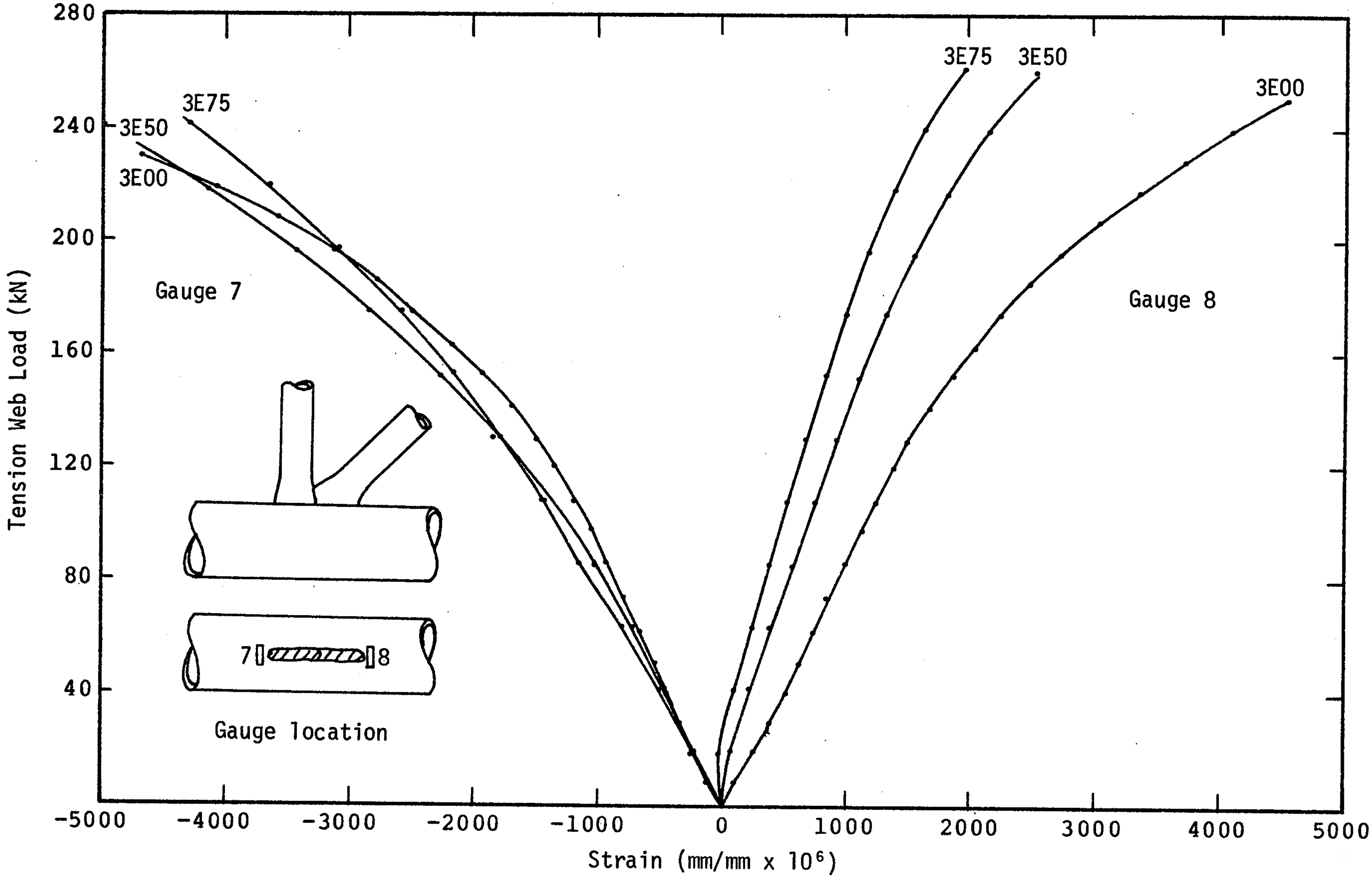

Fig. 3.33 - Influence of web lap on circumferential chord strain.

Although the circumferential chord strains were generally more severe than the longitudinal ones, evidence of chord wall yielding adjacent to the crotch in specimen 3E00, shown in Figure 3.34, suggests the presence of large longitudinal stresses in this area. This behaviour occurred when the chord wall was relatively flexible in comparison to the webs.

3.7) Compression Member Strain Measurements

The longitudinal strains measured at the mid-lengths of the compression webs were usually non-uniform, indicating both in- and out-of-plane bending. The compression web mid-length load-strain behaviour shown in Figure 3.35 for specimen 4G50, was typical for specimens with t_o/d_o ratios larger than 0.03. It was often observed that for these specimens, as for specimen 4G50, the out-of-plane bending was larger than the in-plane bending. However, as the mid-length longitudinal strains approached yield magnitude, in-plane bending began to dominate and buckling followed immediately. In specimens with t_o/d_o ratios smaller than 0.03, in-plane compression web bending generally dominated over the entire load range.

Figure 3.36 indicates the load-strain behaviour at a compression web section near the joint for specimen 4G50. The longitudinal strain distribution was highly non-uniform. The strains were large in the plane of the specimen, indicating a stress concentration. Perpendicular to this plane, the longitudinal strain was comparatively small. This was typical behaviour near the cropped-end of the compression web.

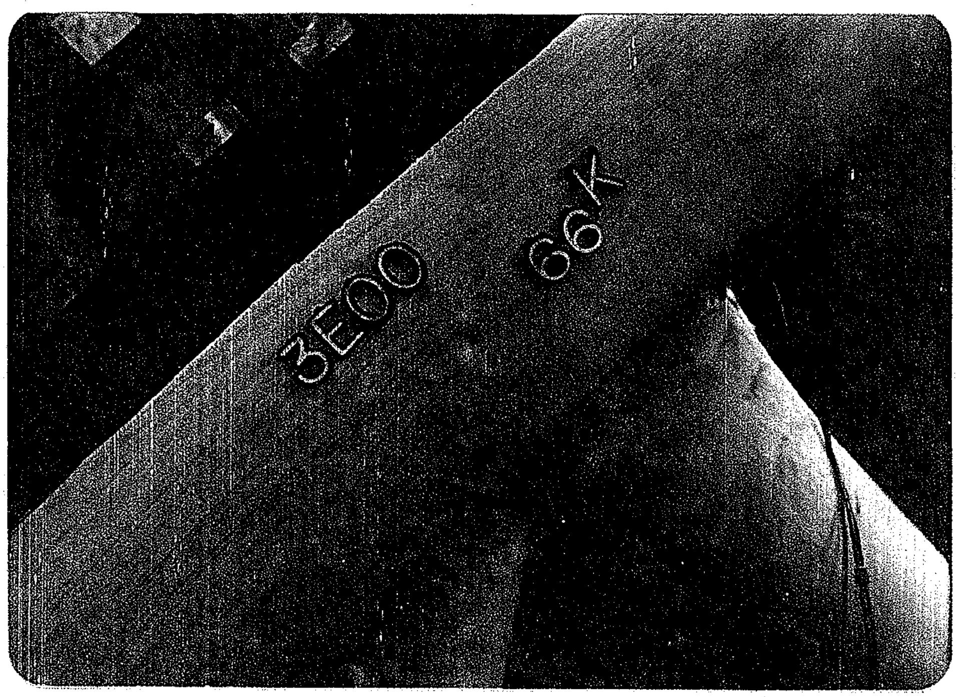

Fig. 3.34 - Chord wall yielding adjacent the crotch of the web members - Specimen 3E00.

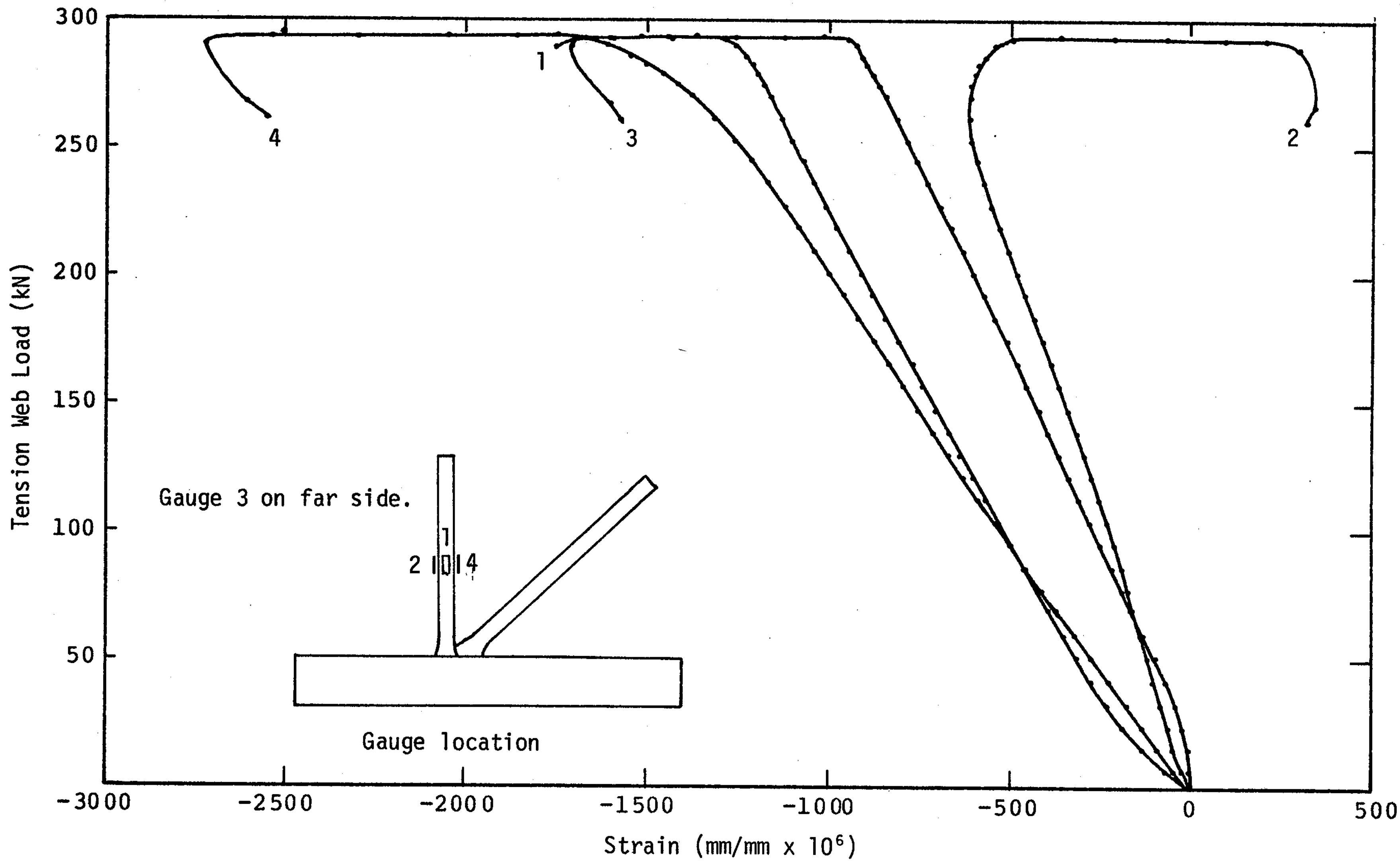

Fig. 3.35 - Longitudinal compression web strains at the mid-length of the compression web - Specimen 4G50.

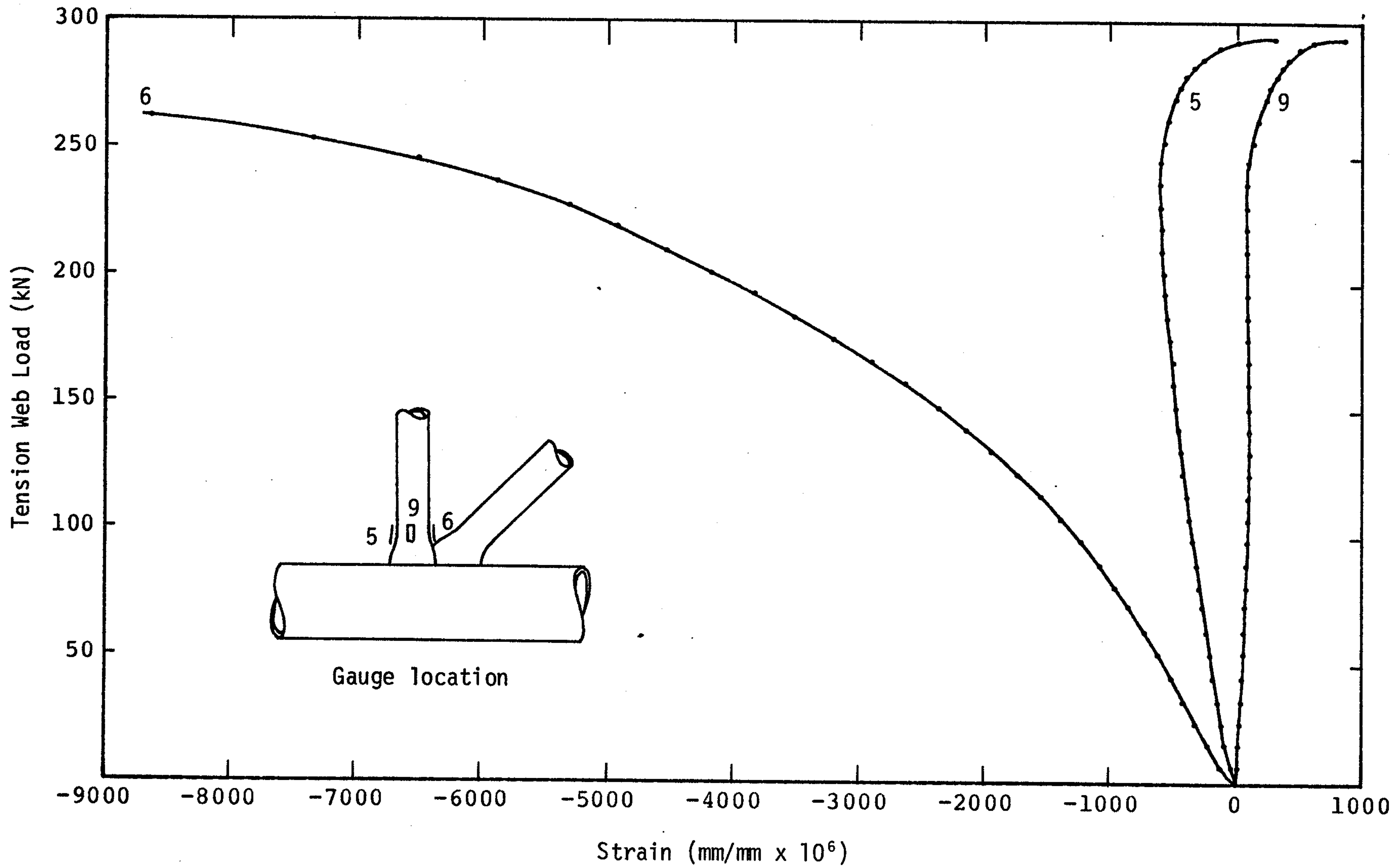

Fig. 3.36 - Longitudinal compression web strains near the joint - Specimen 4G50.

In addition, large in-plane end-moments tending to bend the compression web away from the tension web were indicated by the strain measurements near the joint. However, the magnitude of these end-moments was heavily influenced by the t_o/d_o ratio, as illustrated in Figure 3.37. It can be seen that as the t_o/d_o ratio increased, the difference in the in-plane longitudinal strains near the joint decreased. In specimens 3D75, 5D50, 6D75, and 5E00, in which the compression web buckled toward the tension web, the in-plane strains near the joint were approximately equal, indicating pure axial load.

It was observed, usually in specimens with t_o/d_o ratios larger than 0.03, that a moment reversal such as indicated in Figure 3.38, occurred in the compression web near the joint as buckling progressed. The deformation of the chord face initially produced a compression web end-moment. However, as buckling proceeded it was evident that the chord wall resisted further deformation and the moment reversed. The compression web typically buckled in double curvature with an inflection point near the joint as shown in Figure 3.39.

The distribution of longitudinal compression web strain is illustrated in Figure 3.40 for specimen 4G50, at a tension web load of 133 kN (29.9 kips). The non-uniform strain distribution is clearly illustrated. Nevertheless, the average compressive mid-length strain (-0.0491 percent) was found to agree very well with the computed strain (-0.0487 percent) assuming an E value of 200,000 MPa (30,000 ksi).

3.8) Tension Web Strain Measurements

Strain measurement on the tension web was limited to locations

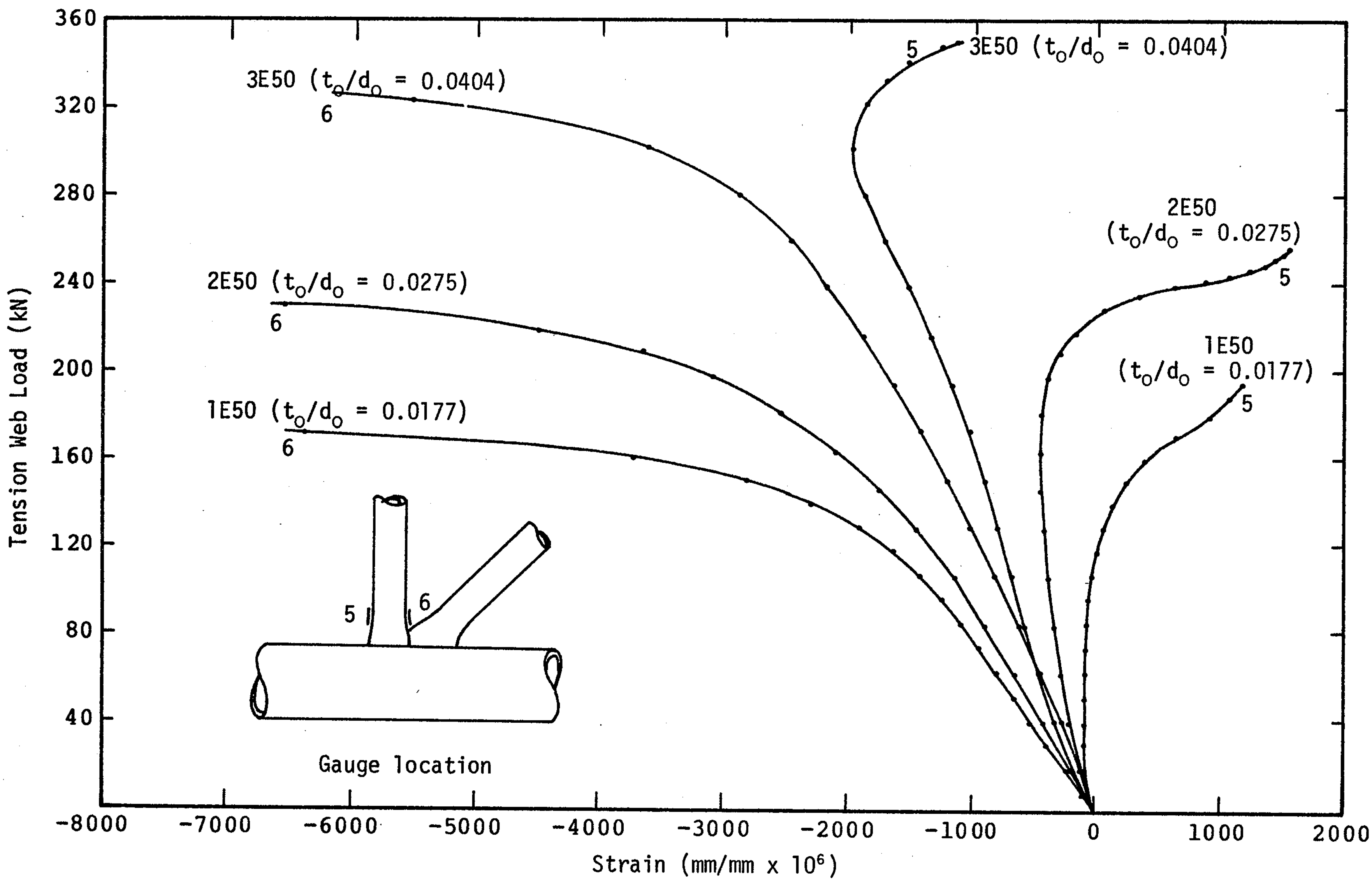

Fig. 3.37 - Influence of t_o/d_o on longitudinal compression web strains near the joint.

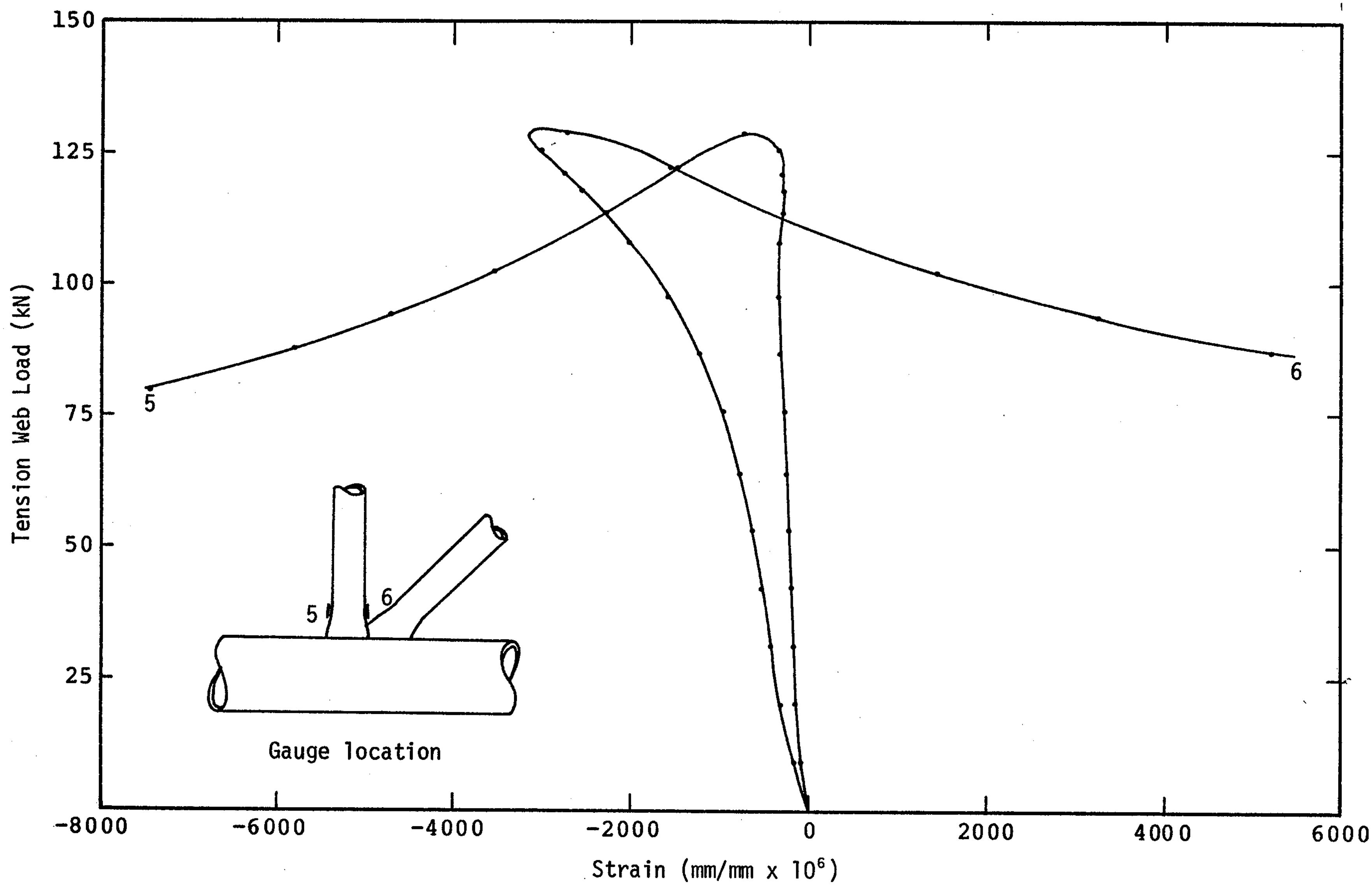

Fig. 3.38 - Illustration of the bending moment reversal at the base of the compression web of specimen 4D00.

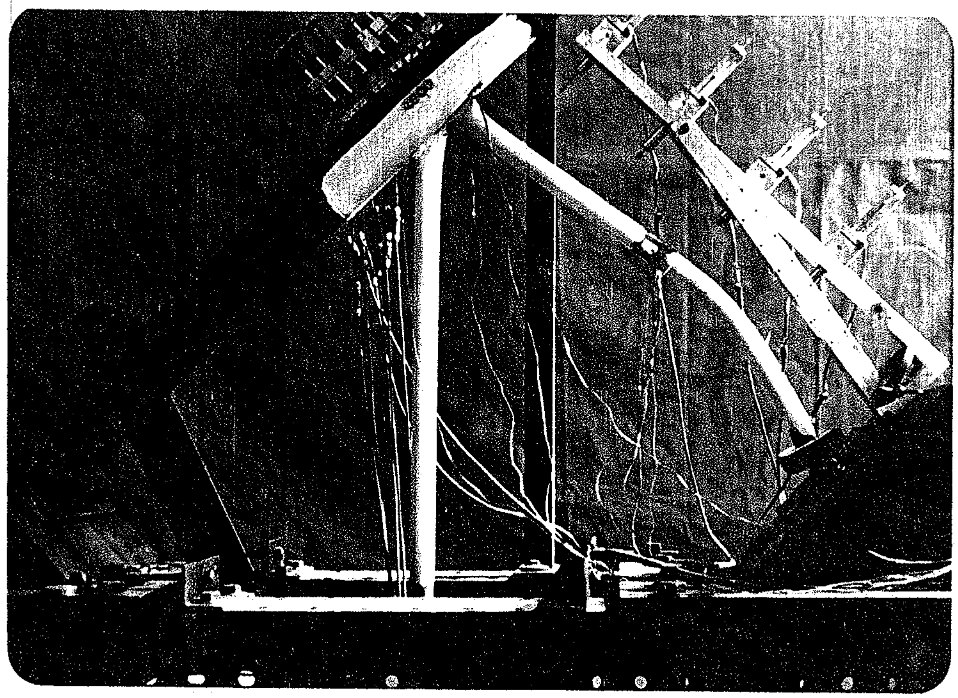

a) Compression web buckling - Specimen 4D00.

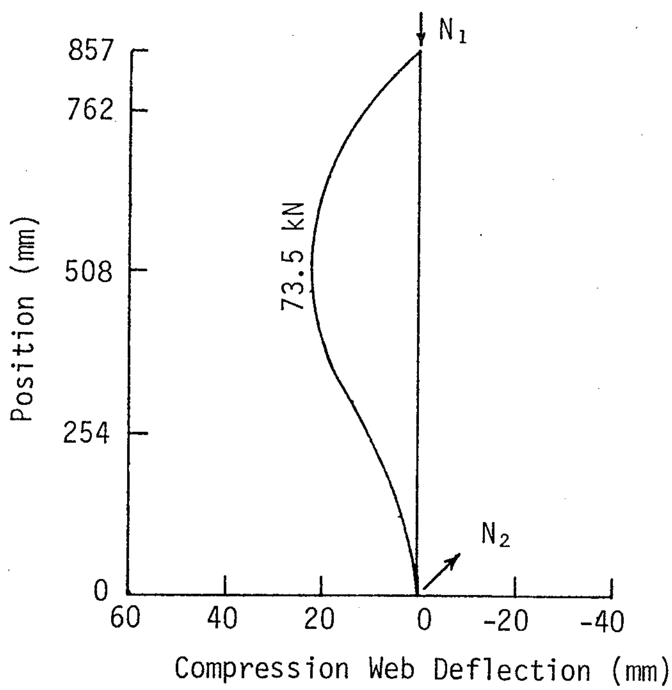

b) Compression web deflection - Specimen 4D00.

Fig. 3.39 - Illustration of compression web buckling in double curvature.

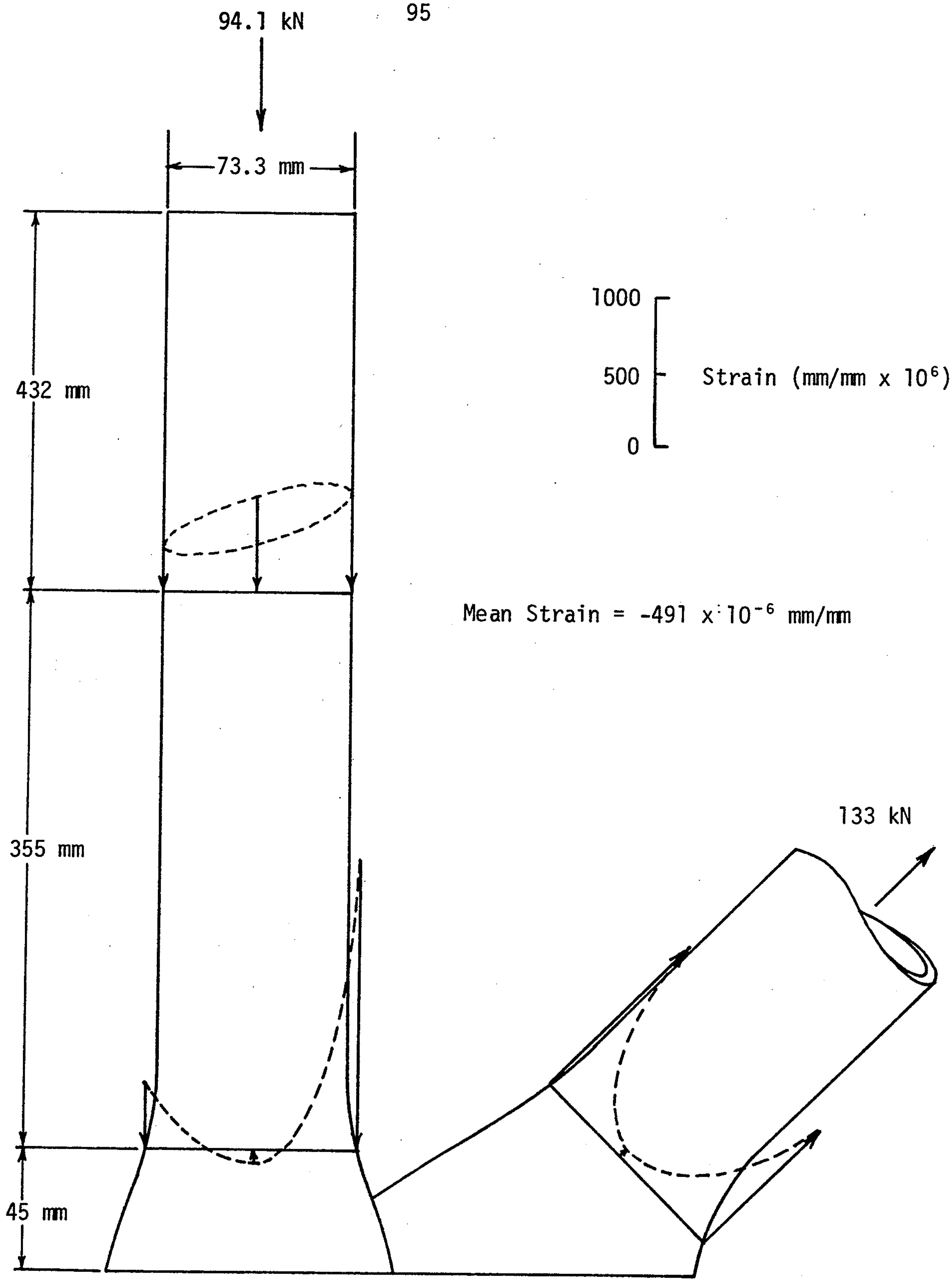

Fig. 3.40 - Longitudinal strains in webs of specimen 4G50.

near the joint. Figure 3.41 shows the longitudinal tension web load-strain behaviour near the cropped-end for specimens 4G50. As for the compression web, the strains in the plane of the specimen were large relative to those in the perpendicular one. Furthermore, because of joint rotation, the in-plane longitudinal strains were generally larger on the side facing the compression web than on the side opposite it.

The longitudinal strain was also measured at the toe of the tension web. The strain measurements indicated that the strains in this area were approximately equal to those circumferential chord strains measured next to the compression web.

The longitudinal strain distribution in the tension web near the joint is illustrated in Figure 3.40 for specimen 4G50.

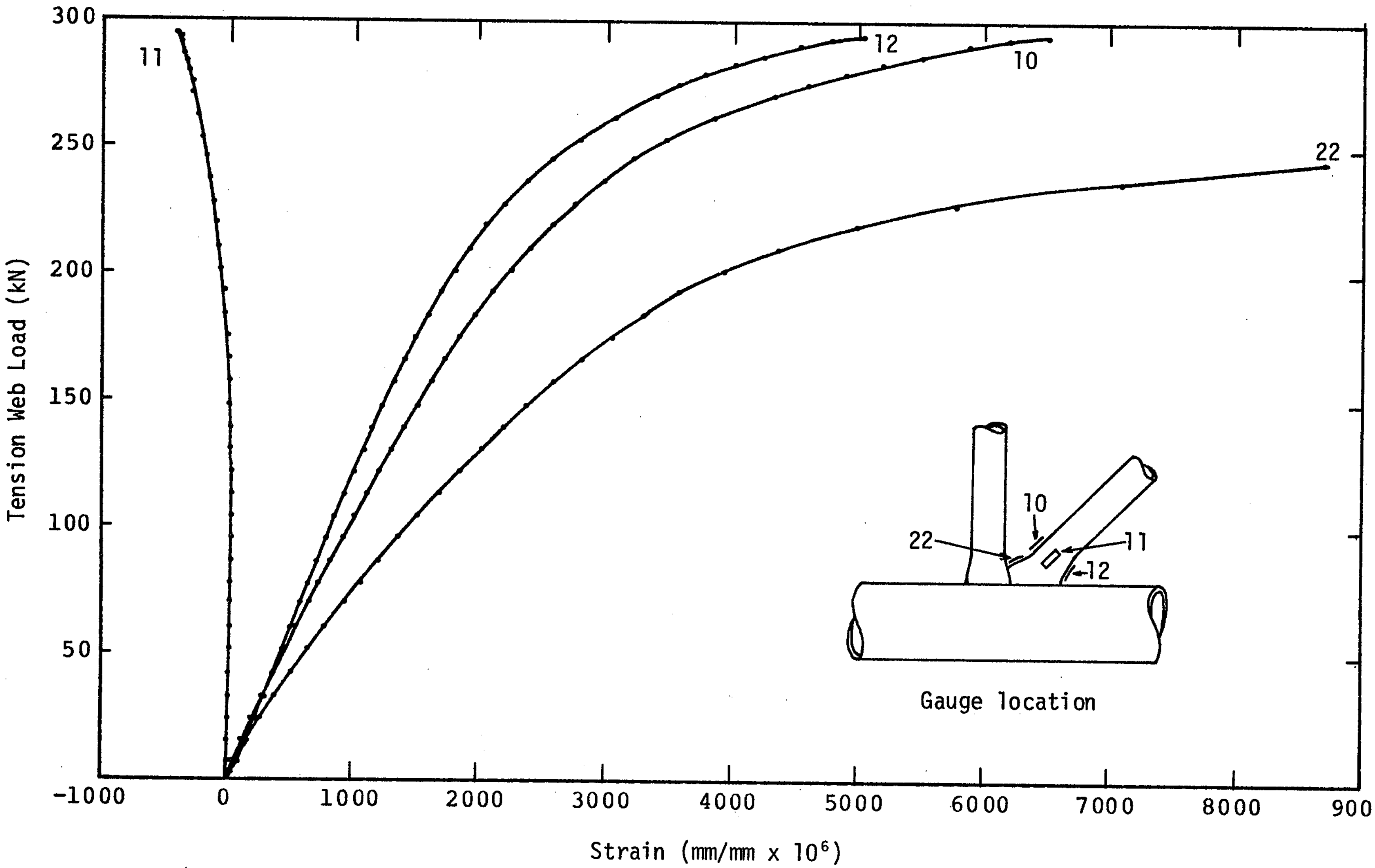

Fig. 3.41 - Longitudinal tension web strains near the joint - Specimen 4G50.

CHAPTER 4

CONCLUSIONS AND RECOMMENDATIONS

4.1) Conclusions

Based on the testing of 61 isolated Pratt-type cropped-web joints involving circular hollow sections in which the influence of three joint parameters, the chord thickness/width ratio, the web diameter/chord diameter ratio, and the web lap, was investigated, the following conclusions have been reached.

1) The ultimate strength of a cropped-web joint involving a round chord can be estimated with the following equations:

$$J_u = \left(t_1 t_o d_o \sigma_{oe}/d_1\right)\left[8.96 + 40.2(d_1/d_o)^2 - 144(t_o/d_o)\right] \qquad 4.1$$

$$J_u = \left(t_1 t_o d_o \sigma_{oe}/d_1\right)\left[10.5 + 40.6(d_1/d_o)^2 - 172(t_o/d_o)\right] \qquad 4.2$$

Equation 4.1 is valid over a t_o/d_o range of 0.02 to 0.07, a d_1/d_o range of 0.3 to 0.8, and a range of web lap from zero to 75 percent. The same applies for the second equation with the exception that for t_o/d_o ratios smaller than 0.045, the valid range of web lap is restricted to 50 to 75 percent.

2) The strengths of cropped-web joints are slightly smaller than those of profiled-web joints when t_o/d_o is smaller than 0.05.

3) The respective joint flexibilities along the compression and tension web axes can be estimated using the following equations:

$$f_c = \left(d_1/Ed_o^2\right)\left[34.2 + 0.278(d_o/t_o)^2 - 0.196(d_o/t_o)^2 O_v\right] \qquad 4.3$$

$$f_t = \left(d_2/Ed_o^2\right)\left[10.3 + 0.219(d_o/t_o)^2 - 0.286(d_o/t_o)^2 O_v\right] \qquad 4.4$$

The flexibility equations are valid over a t_o/d_o range of 0.02 to 0.07, a d_1/d_o range of 0.3 to 0.8, and web laps of zero to 75 percent.

4) Cropped-web joints generally display more ductile behaviour than do profiled-web joints, especially when d_1/d_o is large.

5) The contribution of joint deformation to truss deflection is usually less than 20 percent. However, it may become excessive for zero lap joints with t_o/d_o ratios smaller than 0.04.

6) Cropped-web joints involving round chords are only one-third to one-half as flexible as similar square chord cropped-web joints.

7) The L_1/r_1 ratio was found to have a significant influence on the behaviour of a cropped-web joint.

8) In general, the performance of a cropped-web joint may be improved by increasing the t_o/d_o ratio, the d_1/d_o ratio, and the web lap, and by decreasing the L_1/r_1 ratio of the compression web.

4.2) Design Recommendations

The use of cropped-web joints for statically loaded trusses consisting of circular hollow sections should conform to the following recommendations.

In general, it would be good practice to design truss chord members with t_o/d_o ratios of about 0.04 or larger. Joint performance could be improved further by overlapping the web members, and it is strongly suggested t_o/d_o be larger than 0.045. A compression web slenderness ratio of about 75 or larger (assuming K equals 1.0) would insure that the ultimate load capacity of the joint exceeds that of the compression web, thus allowing the design to be based on the capacity of the web member.

If t_o/d_o ratios smaller than 0.045 are unavoidable, joints with at least 50 percent lap and compression webs with slenderness ratios smaller than 90 should be employed to provide adequate strength and stiffness. In these cases, the joint strength usually governs the design.

In any case, within the specified parameter limitations, the ultimate joint load should be estimated using equations 3.1(b) or 3.2(b) and then compared to the ultimate capacity of the incident web members.

4.3) Recommendations for Future Research

Further research should be directed towards investigating the influence of the compression web slenderness ratio on the performance of cropped-web joints between circular hollow members. The ultimate loads of several of the isolated joint specimens were determined by compression web buckling. Had the compression web lengths been varied, significant differences in the ultimate loads would have resulted.

Web laps larger than 75 percent, and in particular, the lap that corresponds to the specific case where the axes of the incident web members intersect at the chord face, should be investigated. This geometry would eliminate the moment produced at the chord face by the webs which, in many cases, induced premature web member failure.

The effect of compression and tension web members of unequal diameter and the influence of the web thickness to web diameter ratio on the joint performance require further study.

Finally, joint geometries other than a Pratt N-configuration should be investigated.

REFERENCES

Anderson, C. W. 1961. "Circumferential Stresses in a Joint Between Structural Tubes", Special Report No. 22 of Commonwealth Experimental Building Station, Sydney, Australia.

Bouwkamp, J. G. 1964. "Concept of Tubular-Joint Design", Journal of the Structural Division, ASCE Proceedings, Vol. 92, ST2, April.

Bouwkamp, J. G. 1968. "Behaviour of Tubular Truss Joints under Static Loads, Phase 2", College of Engineering, University of California, Berkeley.

Canadian Institute of Steel Construction (CISC). 1975. "Handbook of Steel Construction", Fifth edition, Universal Offset Limited, Don Mills, Ontario.

Canadian Institute of Steel Construction (CISC). 1978. "Limit States Design Steel Manual", Second edition, Universal Offset Limited, Don Mills, Ontario.

Chebib, F., K. Carpenter and D. Reimer. 1976. "Manitoba Statistical Package", Computer Center, University of Manitoba.

Cran, J. A., E. B. Gibson, and S. Stadnyckyj. 1971. "Hollow Structural Sections - Design Manual for Connections", The Steel Company of Canada Limited, First edition.

Dasgupta, A. 1970. "The behaviour of Joints of Tubular Trusses", Ph.D. Thesis, Department of Civil Engineering, University of Nottingham.

Davie, J. and T. W. Giddings. 1971. "Research into the Strength of Welded Lattice Girder Joints in Structural Hollow Sections", CE 70/3, CIDECT Programme 5EC, University of Sheffield.

Dunn, O. J. and V. A. Clark. 1974. "Applied Statistics: Analysis of Variance and Regression", Wiley Series in Probability and Mathematical Statistics, John Wiley and Sons.

Eastwood, W., C. Osgerby, A. A. Wood, and D. I. Blockley. 1967. "An Experimental Investigation into the Behaviour of Joints between Structural Hollow Sections", Department of Civil and Structural Engineering, University of Sheffield.

Eastwood, W., C. Osgerby, A. A. Wood, and D. I. Blockley. 1967. "A Theoretical Investigation into the Elastic Behaviour of Joints between Structural Hollow Sections", University of Sheffield.

Eastwood, W., C. Osgerby, A. A. Wood, and B. L. Mee. 1970. "An Experimental Investigation of Joints in Rectangular Hollow Sections", Department of Civil and Structural Engineering, University of Sheffield.

Frovich, L. E. 1973. "A Preliminary Investigation into the Behaviour of Various Flattened-End Truss Connection Configurations", M.Sc. Thesis, Department of Civil Engineering, University of Manitoba.

Ghosh, A. 1979. "Statical Behaviour of Tubular Trusses with Cropped-End Connections", M.Sc. Thesis, Department of Civil Engineering, University of Manitoba.

Natarajan, M. and A. A. Toprac. 1969. "Studies on Tubular Joints in U.S.A. - Review of Research Reports", Structures Fatigue Research Laboratory, University of Texas, Austin, Texas.

Hlavacek, V. 1973. "Strength of Welded Tubular Joints in Lattice Girders", Building Research Institute, Technical University, Prague.

Jamm, W. 1951. "Form Strength of Welded Tubular Connections and Tubular Structures under Static Loading", (Translation from German), Schweissen Und Schneiden, Vol. 3.

Jamm, W., G. Zimmerman, and G. Lewton. 1952. "Welded Connections of Pipe Structures - Node Points", Patent Right No. 831 598, Class 37, Group 5, Republic of Germany Patent Office.

Mee, B. L. 1969. "The Structural Behaviour of Joints in Rectangular Hollow Sections", Ph.D. Thesis, Department of Civil and Structural Engineering, University of Sheffield.

Morris, G. A., L. E. Frovich, and N. Thiensiripipat. 1974. "An Experimental Investigation of Flattened-End Tubular Truss Joints", Department of Civil Engineering, University of Manitoba.

Morris, G. A. and N. Thiensiripipat. 1977. "Behaviour of Tubular Truss Joints with End-Cropped Webs", Proceedings of International Symposium on Hollow Structural Sections, CIDECT, Toronto, Canada.

Robinson, H. C. 1969. "Literature Survey on Tubular Steel Joints", Part Thesis for Ph.D. Degree, Department of Civil and Structural Engineering, University of Sheffield.

Steel, Robert G. D. and James H. Torrie. 1960. "Principles and Procedures of Statistics", McGraw-Hill Book Company, Inc.

Stelco. 1973. "Structural Steels - Selection and Uses", The Steel Company of Canada, Limited.

Thiensiripipat, N. 1974. "Statical Behaviour of Cropped-End Connections in Tubular Trusses", M.Sc. Thesis, University of Manitoba.

Thiensiripipat, N. 1979. "Statical Behaviour of Cropped-Web Joints in Tubular Trusses", Ph.D. Thesis, University of Manitoba.

Tubemakers of Australia Limited. 1960. "Report on Behaviour of Welded Joints in Tubular Structures", Stewarts and Lloyds Division, Technical Office.

Wardenier, J. 1977. "Testing and Analysis of Truss Joints made from Rectangular HSS", Proceedings of International Symposium on Hollow Structural Sections, CIDECT, Toronto, Canada.

Washio, K., T. Togo, and Y. Mitsui. 1968. "Experimental Study on Local Failure of Chords in Tubular Truss Joints (II)", Paper No. 874.

White, R. N., P. Gergely, and R. G. Sexsmith. 1972. "Structural Engineering", Vol. 2, John Wiley and Sons, Inc.

APPENDIX A

STEPWISE MULTIPLE LINEAR REGRESSION ANALYSIS

Equations 3.1(a), 3.2(a), 3.3, and 3.4 were generated by means of a stepwise multiple linear regression analysis (Chebib et al. 1976) briefly described herein. The development of equation 3.1(a) is described. A similar procedure was used for the other equations.

Before the actual regression procedure was employed, the ultimate joint loads were expressed in terms of various dimensionless strength parameters such as $J_u/t_o^2\sigma_{oe}$, $J_u/t_od_o\sigma_{oe}$, $J_ud_1/t_1t_od_o\sigma_{oe}$ and so on. These were then plotted against the joint parameters (t_o/d_o) and (d_1/d_o). From inspection of the various plots, it could be seen which strength parameters and joint parameters correlated best. The best correlation was found between $J_ud_1/t_1t_od_o\sigma_{oe}$ and the d_1/d_o ratio. Thus, $J_ud_1/t_1t_od_o\sigma_{oe}$ was chosen as the dependent variable in the regression analysis.

All 61 of the test results were used in the analysis. A total of 23 independent variables, consisting of the three joint parameters, t_o/d_o, d_1/d_o, and 0_V, including various multiples and cross-multiples of these, were investigated. In step one of the regression program, the dependent variable was chosen for the equation. In this case, d_1/d_o was chosen. Table A-1 shows the typical output of the regression program, indicating the equation and pertinent information for the analysis of variance. With one independent variable entered the regression equation took the form

$$J_u d_1/t_1 t_o d_o \sigma_{oe} = 3.60 + 36.4(d_1/d_o)^2 \qquad \text{A-1}$$

The variable $(d_1/d_o)^2$ accounts for 81.7 percent of the variation in $J_u d_1/t_1 t_o d_o \sigma_{oe}$.

In step two of the regression program, a second independent variable which had the highest correlation with $J_u d_1/t_1 t_o d_o \sigma_{oe}$, with the condition that $(d_1/d_o)^2$ had already been entered, was chosen. Thus, the variable (t_o/d_o) was entered next. Table A-2 indicates the results of this step. The regression equation with two variables now took the form

$$J_u d_1/t_1 t_o d_o \sigma_{oe} = 8.96 + 40.2(d_1/d_o)^2 - 144(t_o/d_o) \qquad \text{A-2}$$

With the two independent variables entered, 94 percent of the variation in $J_u d_1/t_1 t_o d_o \sigma_{oe}$ was accounted for.

This process continued until all of the variables were eventually entered. However, because it is desirable to use as few variables as possible the regression equation at the end of step two was chosen. The analysis of variance proceeded as follows.

First, the F-test was performed to test the null hypothesis that the coefficients of the independent variables were zero, or in other words, that the independent variables did not significantly influence the dependent variable. As shown in table A-2 the calculated F-value was 451. This was compared to $F(\lambda, \nu_1, \nu_2)$ obtained from statistical tables, where $\lambda = 1-\alpha/2$ is the confidence level and α is the significance level, ν_1 is equal to the number of independent variables, and ν_2 is the degrees of freedom equal to $61-1-\nu_1$. Thus, for a significance

Table A-1 - Results of Step-wise Multiple Regression Analyses.

STEP 1

VARIABLE ENTERED.....19

SUM OF SQUARES REDUCED IN THIS STEP..........1874.297
PROPORTION REDUCED IN THIS STEP.............. 0.817

CUMULATIVE SUM OF SQUARES REDUCED............1874.297
CUMULATIVE PROPORTION REDUCED................ 0.817 OF 2293.516

FOF 1 VARIABLES ENTERED
MULTIPLE CORRELATION COEFFICIENT..... 0.904
(ADJUSTED FOR D.F.)............. 0.904
F-VALUE FOR ANALYSIS OF VARIANCE.....263.784
STANDARD ERROR OF ESTIMATE........... 2.666
(ADJUSTED FOR D.F.)............. 2.666

VARIABLE NUMBER	REGRESSION COEFFICIENT	STD. ERROR OF REG. COEFF.	COMPUTED T-VALUE
19	36.38042	2.23997	16.241

INTERCEPT......3.60066

Table A-2 - Results of Step-wise Multiple Regression Analysis.

STEP 2

VARIABLE ENTERED......9

SUM OF SQUARES REDUCED IN THIS STEP...........280.616
PROPORTION REDUCED IN THIS STEP............... 0.122

CUMULATIVE SUM OF SQUARES REDUCED............2154.912
CUMULATIVE PROPORTION REDUCED................ 0.940 OF 2293.516

FOF 2 VARIABLES ENTERED
MULTIPLE CORRELATION COEFFICIENT..... 0.969
(ADJUSTED FOR D.F.)............. 0.969
F-VALUE FOR ANALYSIS OF VARIANCE.....450.872
STANDARD ERROR OF ESTIMATE........... 1.546
(ADJUSTED FOR D.F.)............. 1.559

VARIABLE NUMBER	REGRESSION COEFFICIENT	STD. ERROR OF REG. COEFF.	COMPUTED T-VALUE
19	40.15448	1.34491	29.857
9	-144.21159	13.30814	-10.836

INTERCEPT......8.96263

level of 0.1 percent, λ=99.95 percent and F(99.95; 2, 58)=7.78 (Dunn and Clark 1974). Since this value was much less than 451, the null hypothesis was rejected and therefore the independent variables are significant at the 0.1 percent level.

The statistical significance of the coefficients can also be determined by comparing the T-values calculated in table A-2 with the tabulated t-value, $t(\lambda;\nu_2)$. From statistical tables (Dunn and Clark 1974), t(99.95%; 58) was found to be equal to 3.47, which is less than both of the calculated T-values, which were 30 and 11. Therefore, the coefficients are also significant at the 0.1 percent level.

To demonstrate the confidence with which equation 3.1(a) predicts the ultimate loads, a 99.9 percent confidence belt was determined for a constant t_o/d_o ratio of 0.04. In other words, there is 99.9 percent confidence that the actual result will fall within the range of this belt. The confidence belt was calculated as follows:

$$CB(J_u d_1/t_1 t_o d_o \sigma_{oe}) = (J_u d_1/t_1 t_o d_o \sigma_{oe}) \text{ predicted}$$
$$\pm\ t_{1-\alpha} s\sqrt{(1/n + C_{11}x_1^2 + 2C_{12}x_1x_2 + C_{22}x_2^2)}$$

where $S = 1.56$ (the standard deviation)

$n = 61$ (number of observations)

$x_1 = ((d_1/d_o)^2 - 0.2596)$

$x_2 = ((t_o/d_o) - 0.04398)$

$1 - \alpha = 1 - 0.999 = 0.1$ percent (confidence level)

and $C = \begin{bmatrix} 0.7570 & -1.940 \\ -1.940 & 74.13 \end{bmatrix}$ (covariance values)

$t_{0.001} = 3.45$ (from statistical tables)

Figure A-1 illustrates the confidence belt for a constant t_o/d_o ratio. It can be seen that even with a 0.1 percent confidence level the confidence belt is narrow. This indicates that equation 3.1(a) gives an excellent prediction of joint strength. Similarly, confidence belts can be determined for other values of t_o/d_o.

Lastly, table A-3 lists the actual test results, the predicted results using the regression equation, and the residuals.

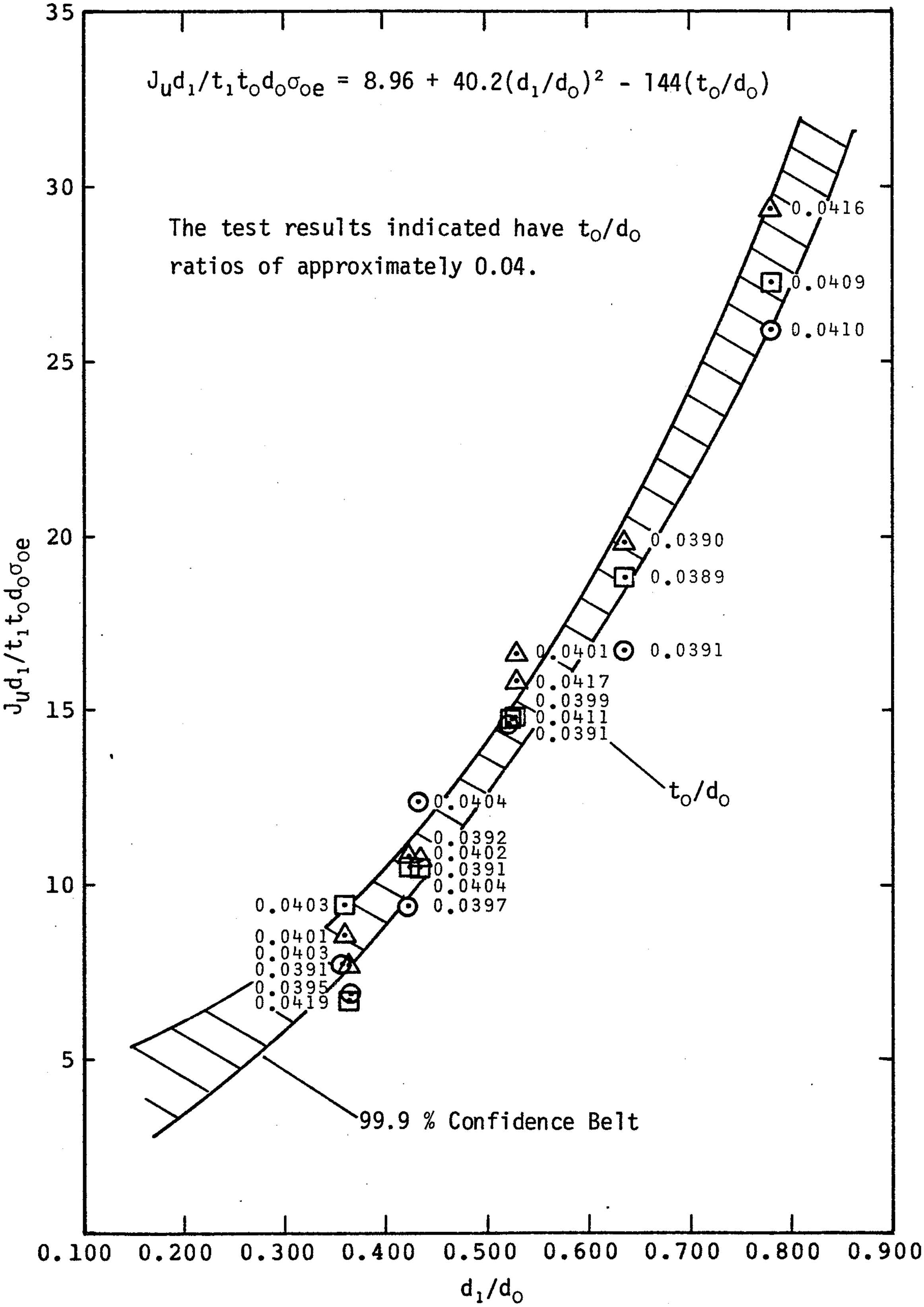

Fig. A-1 - Strength prediction confidence belt for t_o/d_o = 0.04.

Table A-3 - Values of Independent Variables Using Equation A-2.

CASE NO.	TEST VALUE	ESTIMATE	RESIDUAL
1	8.67000	11.50735	-2.83735
2	11.48000	11.53091	-0.05091
3	12.15000	11.51383	0.63617
4	11.69000	10.15098	1.53902
5	9.82600	10.16025	-0.33425
6	10.61000	10.11277	0.49723
7	7.77100	8.31878	-0.54778
8	9.46500	8.35122	1.11378
9	8.56300	8.37347	0.18953
10	6.88900	8.55317	-1.66417
11	6.71000	8.19471	-1.48471
12	7.71800	8.60859	-0.89059
13	6.85000	7.12794	-0.27794
14	6.64700	7.11991	-0.47291
15	6.20100	7.12031	-0.91931
16	4.02600	4.46054	-0.43454
17	4.40600	4.37842	0.02757
18	4.46600	4.26418	0.20182
19	7.98600	13.83444	-5.84844
20	14.46000	13.90835	0.55164
21	16.60000	13.88271	2.71728
22	8.99100	12.51802	-3.52702
23	12.24000	12.42713	-0.18713
24	15.18000	12.55325	2.62675
25	12.40000	10.72340	1.67660
26	10.50000	10.69128	-0.19128
27	10.71000	10.74906	-0.03906
28	9.37700	10.45142	-1.07442
29	10.56000	10.53600	0.02400
30	10.85000	10.49573	0.35427
31	9.69900	9.02823	0.67077
32	9.33400	9.01217	0.32183
33	9.08600	8.94049	0.14551
34	5.87300	6.25001	-0.37701
35	6.01800	6.12607	-0.10807
36	5.75000	6.08089	-0.33089
37	17.38000	16.23857	1.14142
38	19.46000	16.18411	3.27588
39	14.84000	14.44637	0.39363
40	16.65000	14.43277	2.21723
41	14.65000	14.41091	0.23909
42	14.79000	14.14401	0.64599
43	15.86000	14.19770	1.66230
44	13.92000	12.54001	1.37999
45	14.27000	12.58741	1.68259

Table A-3 - Con't.

CASE NO.	TEST VALUE	ESTIMATE	RESIDUAL
46	10.58000	10.44105	0.13895
47	10.20000	10.54907	-0.34907
48	16.73000	19.54665	-2.81665
49	18.85000	19.65868	-0.80869
50	19.82000	19.52205	0.29794
51	18.19000	17.59564	0.59435
52	19.55000	17.80786	1.74213
53	15.06000	15.41687	-0.35687
54	15.57000	15.39317	0.17683
55	25.95000	27.54930	-1.59930
56	27.30000	27.52213	-0.22214
57	29.39000	27.39883	1.99117
58	24.63000	26.22636	-1.59637
59	27.59000	26.32155	1.26845
60	21.87000	23.71661	-1.84662
61	22.93000	23.87192	-0.94193

APPENDIX B

CAPACITY REDUCTION FACTOR ϕ

As stated in the LSD handbook, the capacity reduction factor is a factor applied to a specific material property or the resistance of a member, connection or structure. For the limit state under consideration, it takes into account the variability of material properties, dimensions, workmanship, type of failure, and uncertainty in prediction of member resistance. The LSD handbook suggests a ϕ factor of 0.9 for connections. However, it has been suggested by L. Kennedy of the University of Windsor that the ϕ factor should be developed on a statistical basis from the test results using the following formulations:

$$\phi = (R_m/R_n)e^{(-\gamma\beta V_R)}$$

where $V_R = \sqrt{V_m^2 + V_P^2 + V_F^2}$

R_m = mean resistance from tests

R_n = nominal resistance as expressed by the design criteria

γ = a numerical factor equal to 0.55

β = a safety index (equal to 1.5 for welded connections)

V_m = coefficient of variation of the material yield strength

V_P = coefficient of variation of the professional assumptions

V_F = coefficient of variation of the test/predicted results, the fabrication, or the manufacturing.

The value of R_m/R_n was calculated as the (J_u Test/J_u Predicted) /no. of test samples. The coefficient of variation of the material yield strength (V_m) was computed to be 0.078, V_P was assumed to be 0.05, and for V_F, the coefficient of variation for the particular strength equation was used.

Thus, for equation 3.1(b) the capacity reduction factor was computed as follows:

$$(J_u \text{ Test}/J_u \text{ Predicted})/61 = 1.02$$

$$V_R = \sqrt{(0.078)^2 + (0.05)^2 + (0.115)^2}$$

$$V_R = 0.148$$

and $\phi = 1.02e^{-(0.55)(0.148)(1.5)} = 0.903$

Similarly, the capacity reduction factor for equation 3.2(b) is

$$\phi = 1.01e^{-(0.55)(0.122)(1.5)}$$

$$\phi = 0.913$$

As both values are approximately 0.9, the capacity reduction factor for equations 3.1(b) and 3.2(b) can be taken as 0.9.